NUMERICAL MODELING AND PERFORMANCE ANALYSIS OF SOLAR-POWERED IDEAL ADSORPTION COOLING SYSTEMS

A THESIS SUBMITTED TO
THE GRADUATE SCHOOL OF NATURAL AND APPLIED SCIENCES
OF
MIDDLE EAST TECHNICAL UNIVERSITY

BY

ONUR TAYLAN

IN PARTIAL FULFILLMENT OF THE REQUIREMENTS
FOR
THE DEGREE OF MASTER OF SCIENCE
IN
MECHANICAL ENGINEERING

MAY 2010

Approval of the thesis:

NUMERICAL MODELING AND PERFORMANCE ANALYSIS OF SOLAR-POWERED IDEAL ADSORPTION COOLING SYSTEMS

submitted by **ONUR TAYLAN** in partial fulfillment of the requirements for the degree of **Master of Science in Mechanical Engineering Department, Middle East Technical University** by,

Prof. Dr. Canan Özgen _____
Dean, Graduate School of **Natural and Applied Sciences**

Prof. Dr. Suha Oral _____
Head of Department, **Mechanical Engineering**

Assoc. Prof. Dr. Derek K. Baker _____
Supervisor, **Mechanical Engineering Dept., METU**

Prof. Dr. Bilgin Kaftanoğlu _____
Co-supervisor, **Manufacturing Engineering Dept., Atılım University**

Examining Committee Members:

Assist. Prof. Dr. İlker Tarı _____
Mechanical Engineering Dept., METU

Assoc. Prof. Dr. Derek K. Baker _____
Mechanical Engineering Dept., METU

Prof. Dr. Bilgin Kaftanoğlu _____
Manufacturing Engineering Dept., Atılım University

Assist. Prof. Dr. Ahmet Yozgatlıgil _____
Mechanical Engineering Dept., METU

Assist. Prof. Dr. Eray Uzgören _____
Mechanical Engineering Dept., METU Northern Cyprus Campus

Date: _____

I hereby declare that all information in this document has been obtained and presented in accordance with academic rules and ethical conduct. I also declare that, as required by these rules and conduct, I have fully cited and referenced all material and results that are not original to this work.

Name, Last name : Onur TAYLAN

Signature :

ABSTRACT

NUMERICAL MODELING AND PERFORMANCE ANALYSIS OF SOLAR-POWERED IDEAL ADSORPTION COOLING SYSTEMS

Taylan, Onur
M.S., Department of Mechanical Engineering
Supervisor : Assoc. Prof. Dr. Derek K. Baker
Co-Supervisor: Prof. Dr. Bilgin Kaftanoğlu

May 2010, 139 pages

Energy consumption is continuously increasing around the world and this situation yields research to find sustainable energy solutions. Demand for cooling is one of the reasons of increasing energy demand. This research is focused on one of the sustainable ways to decrease energy demand for cooling which is the solar-powered adsorption cooling system. In this study, general theoretical performance trends of a solar-powered adsorption cooling system are investigated using TRNSYS and MATLAB. Effects of different cycle enhancements, working pairs, operating and design conditions on the performance are analyzed through a series of steady and seasonal-transient simulations. Additionally, a normalized model is presented to investigate the effects of size of the system, need for backup power, collector area and mass of adsorbent. Results are presented in terms of values and ratios of cooling capacity weighted COP. For the conditions explored, the thermal wave cycle, wet cooling towers, high evaporation temperatures and evacuated tube collectors produced the highest COP values. Moreover, the heat capacity of the adsorbent bed and its shell should be low for the simple and heat recovery cycles and the adsorbent bed should be cooled down to the condensation temperature for all cases to achieve the highest possible COP. The selection of working pair should depend on the temperature of the available heat source (solar energy in this study) since each working pair has a dis-

tinct operating temperature range. Furthermore, there is always a need for backup power for the analyzed location and the system.

Keywords: Adsorption, Cooling, Modeling, Simulation, Solar

ÖZ

GÜNEŞ ENERJİSİ DESTEKLİ ADSORPSİYONLU İDEAL SOĞUTMA SİSTEMLERİNİN SAYISAL MODELLENMESİ VE BAŞARIM İNCELEMESİ

Taylan, Onur
Yüksek Lisans, Makina Mühendisliği Bölümü
Tez Yöneticisi : Doç. Dr. Derek K. Baker
Ortak Tez Yöneticisi: Prof. Dr. Bilgin Kaftanoğlu

Mayıs 2010, 139 sayfa

Bütün dünyada enerji tüketimi gün geçtikçe artmakta ve bu durum araştırmacıları sürdürülebilir çözümler bulmaya sevk etmektedir. Soğutmaya olan talep de artan enerji talebinin nedenlerinden biridir. Bu araştırma soğutma için artan enerji talebini azaltmanın sürdürülebilir yollarından biri olan güneş enerjisi destekli soğutma sistemleri üzerinde yoğunlaşmıştır. Bu çalışmada güneş enerjisi destekli soğutma sistemlerinin genel teorik başarım eğilimleri TRNSYS ve MATLAB yazılımları kullanılarak incelenmiştir. Çeşitli döngü iyileştirmeleri, adsorban-soğutucu çifti, ortam ve tasarım koşullarının performans üzerindeki etkileri bir dizi zamandan bağımsız veya zamana bağlı benzetim yoluyla araştırılmıştır. Bu etkenlere ek olarak normalleştirilmiş bir model sunularak sistem boyutu, ek güç ihtiyacı, güneş toplaç alanı ve adsorban kütlesinin etkileri de incelenmiştir. Sonuçlar başarım katsayıları ve onların oranları şeklinde verilmiştir. İncelenen durumlara göre termik dalga döngüsü, yaş soğutma kulesi ve yüksek buharlaşma sıcaklığı yüksek başarım katsayı ortaya çıkarmıştır. Ayrıca basit ve ısıl kazanımlı döngü için ısı sığası düşük adsorban yatak ve kabuğu kullanmak ile her döngü için adsorban yatağı yoğunlaşma sıcaklığına düşürmek başarım katsayısını artırmıştır. Adsorban-soğutucu çifti seçimi ise her çiftin çalışma sıcaklığının farklı olmasından dolayı mevcut ısı kaynağının (bu

çalışma için güneş enerjisinin) ulaşabileceği sıcaklığa bağlıdır. Son olarak incelenen bölge ve her durum için daima bir ek güç ihtiyacı olduğu sonucuna varılmıştır.

Anahtar Kelimeler: Adsorpsiyon, Soğutma, Modelleme, Benzetim, Güneş Enerjisi

To Mom and Dad

ACKNOWLEDGEMENTS

Firstly, I would like to state my heartfelt appreciation to my supervisor Assoc. Prof. Dr. Derek K. Baker for his perceptive supervision, everlasting support and encouragement. I appreciate his continuous help inside and outside the academia within the last three years.

I also would like to thank my co-supervisor Prof. Dr. Bilgin Kaftanoğlu. I feel very privileged to have his precious advices, guidance and leadership.

Additionally, I would like to express my deepest feelings to my dearest parents for their full support on my decisions at every step of my life. At this point, it is so much momentous than ever to have them by my side. I am forever indebted to them.

I would like to show gratitude to my colleagues for their sincere friendships and technical support throughout the thesis period. Thesis period has become so much consequential with their harmony.

Finally, I would like to thank Assoc. Prof. Dr. Cemil Yamalı, Mr. İsmail Solmuş and Mr. Ahmet Çağlar for their insightful discussions and supports.

TABLE OF CONTENTS

LIST OF TABLES

TABLES

LIST OF FIGURES

FIGURES

LIST OF SYMBOLS

a, b, b_o	coefficients in adsorption capacity relation of zeolite NaX – water pair
c	specific heat of incompressible substance (kJ kg^{-1} K^{-1})
c_p	ideal gas specific heat at constant pressure (kJ kg^{-1} K^{-1})
d	a coefficient in adsorption capacity relation of zeolite NaX – water pair
d_o, d_1, d_2	performance coefficients in collector thermal efficiency equation
D	a coefficient in Dubinin – Astakhov equation
E	a coefficient in adsorption capacity relation of zeolite NaX – water pair
f	solar fraction (-)
G	solar radiation (W m^{-2})
h	specific enthalpy (kJ kg^{-1})
H	enthalpy (kJ)
h_{fg}	heat of vaporization / evaporation (kJ kg^{-1})
Δh_{ads}	heat of adsorption (kJ kg^{-1})
k	a coefficient in Dubinin – Astakhov equation
l	loss fraction (-)
m	mass (kg)
$\dot{m}$	mass flow rate (kg h^{-1})
n	exponent of Dubinin – Astakhov equation
ns	coefficients in adsorption capacity relation of zeolite NaX – water pair
P	pressure (kPa)
q	heat transfer per unit mass of adsorbent (kJ kg^{-1})
Q	heat transfer (kJ)
r	coefficient of performance ratio (-)
R	ratio of bed's design to inherent heat capacities (-)
S	user defined size of the cooling system (-)
t	time (min)
T	temperature (^oC)
T_{hot}	maximum bed temperature (^oC)
ΔT_{excess}	excess bed temperature ($T_o - T_{cond}$) (^oC)
u	specific internal energy (kJ kg^{-1})
U	internal energy (kJ)
X	adsorption capacity (kg_{ref} / kg_{ads})
ΔX	adsorption capacity change for a half cycle (kg_{ref} / kg_{ads})
y	thermal wave position (-)

Greek Symbol

ε	convergence criterion of numerical iteration scheme
η	thermal efficiency

Subscripts

a	common state after adiabatic mass recovery
ads	adsorbent / adsorption cycle
amb	ambient
b	back region of the bed
base	base case
bed	adsorbent bed
clg	cooling capacity
clr	cooler
coll	solar thermal collector
cond	condensation
evap	evaporation
f	front region of the bed
F	fuel
flow	flowing, not stagnant heat transfer fluid
hex	heat exchanger in solar thermal system
htf	heat transfer fluid
htr	heater
i	common state after isothermal mass recovery
in	inlet
liq	liquid refrigerant
load	cooling load
m	low-pressure adsorbent bed
max	maximum
min	minimum
n	high-pressure adsorbent bed
N	normalized
o	minimum of bed
out	exit / outlet
P	product
rec	heat recovery / recovered
ref	adsorbed refrigerant
rev	reversible
rfrc	reference
s	unspecified / unknown
sat	saturation
shell	adsorbent bed shell
sys	solar thermal system integrated adsorption cooling system
tot	total
v	refrigerant vapor
w	thermal wave
wb	wet bulb

Superscript

+	immediately after corresponding symbol

Abbreviations

AMR	adiabatic mass recovery
CA	activated carbon – ammonia pair
COP	coefficient of performance
CM	activated carbon – methanol pair
D-A	Dubinin – Astakhov equation
ET	evacuated tube solar thermal collector
FP, FPL	flat plate solar thermal collector
HRec	heat recovery cycle
HTF	heat transfer fluid
IAM	incidence angle modifiers
IMR	isothermal mass recovery
SG	silica gel – water pair
NMR	no mass recovery
TW	thermal wave cycle
WP	working pair
Z1	zeolite NaX – water pair
ZW	zeolite X13 – water pair

CHAPTER 1

INTRODUCTION

1.1 Background Information

"World marketed energy consumption is projected to increase by 44% from 2006 to 2030" according to the U.S. Energy Information Administration [1]. With the increasing trend in energy consumption and worldwide economic growth, the general trend in cooling and air conditioning requirements of industry and buildings is also increasing. To meet the demand in cooling, mechanical vapor-compression systems are commonly used which can be classified as conventional systems [2]. These systems are very popular due to their high coefficients of performance, small sizes and low weights. However, they also exhibit some disadvantages such as contributing to global warming and ozone layer depletion and high energy consumptions [3].

One of the disadvantages of conventional vapor-compression systems can be stated that these systems include refrigerants such as chlorofluorocarbon (CFC), hydrochlorofluorocarbon (HCFC) or hydrofluorocarbons (HFC) which have high global warming potential and ozone depletion potential [4-6]. Since the global warming problem is presently more critical, researchers are studying ways to reduce the emission of these greenhouse gases and overcome this significant disadvantage of conventional cooling systems, especially after the Montreal (1988) and Kyoto (1998) conventions. These conventions are held to force the participant countries to limit the greenhouse gas emissions. In Montreal protocol (1988), some severe regulations were agreed to reduce ozone layer depletion. In Kyoto protocol (1998), new regulations on the CFC, HCFC and HFC emissions have been agreed to reduce greenhouse gas emissions.

Another main disadvantage of conventional cooling systems is their large electricity consumption which causes a need for new investments and new infrastructure, such as new power plants, transmission and distribution lines on the electricity networks [6]. Although building new power plants seems to be a valid solution, each power plant requires fuels, and this requirement causes depletion in resources. In general, a rapid growth in energy consumption comes with a rapid depletion in resources. Therefore, the countries which do not have enough national resources start to import the necessitated resources or buy electricity directly from their neighbors which creates issues about national security and add extra load on economies, especially for countries like Turkey.

Turkey is a developing country and like other developing countries has a rapidly growing energy demand. According to statistical data of the Turkish Electricity Transmission Company (TEİAŞ), the average demand in electricity increased annually by 8.3% for the period of 1975-2008 [7]. In 2007, about 81% of the electricity demand of Turkey was met by thermal sources (coal, lignite, fuel oil, LPG and natural gas), of which 61.2% was natural gas which was mainly imported from nearby countries [8]. The remaining 19% of the electricity supply consisted of hydro dams, geothermal, wind, etc. According to TEİAŞ and under one scenario, electricity demand in Turkey will exceed the supply in 2016-2017 [9].

One of the main constituents of the increasing energy demand in Turkey is increasing cooling loads, especially on the Mediterranean coast of Turkey due to long and hot summers [10]. For instance, Antalya is situated on the Mediterranean coast of Turkey and has electricity shortages and blackouts in summer due to large air conditioning loads and consequent large loads on electricity networks. This city is also characterized by a large tourism industry. There are several top rated resorts, hotels, etc., and these centers use mainly conventional vapor-compression air conditioners to meet the cooling demand which also contributes to the significant load on the electricity networks. According to governor of Antalya, in 2007, daily peak electricity consumption of Antalya was around 18 million kWh, while the production in Antalya is

around 3 million kWh [11]. For all these reasons, Antalya needs to produce electricity or reduce its electricity demand.

As a result, both worldwide and nationwide, there is a strong need for alternative cooling technologies that use sustainable and renewable energy supplies. The proper technology should be environmentally benign and provide high performance so that it can be comparable with the conventional and commonly-used vapor-compression cooling systems.

1.2 Current Solar-Thermal Power Situation

According to United Nations' worldwide estimates, practical hydroelectric resources are less than 0.5 TW while tides and ocean movements can create cumulative power less than 2 TW. The geothermal energy of all continents is approximately 12 TW of which only a small amount of can be extracted. Additionally, potential wind power and other non-solar renewable energy sources are estimated as equivalent 2-4 TW. Among all discovered renewable energy sources, solar energy by far has the highest potential with an average of 120,000 TW that hits the earth's ground [12].

As all other renewable energy sources, usage of solar thermal energy is increasing. In 2006, there was an increase of 22% in new installations throughout the world when compared to the previous year according to the International Energy Agency's report of 2008 [13]. This increase corresponds to 18.3 GW of new capacity and 26.1 million square meters [13]. Especially, when flat plate and evacuated tube collectors are considered, China and Taiwan have the highest installed thermal collector area which corresponds to approximately 80 GW of thermal power whereas Turkey had approximately 7.1 MW of installed thermal collector power in 2007 [14].

As mentioned by Abu Hamdeh and Al-Muhtaseb, the Mediterranean countries may save 40-50% of their energy used for air-conditioning by implementing solar-driven air-conditioning systems [15]. Like other Mediterranean countries, Turkey has also a large opportunity for solar energy. The Mediterranean coast of Turkey is a popular

place for summer vacations due to its long, hot and sunny summer season. Antalya is situated on the Mediterranean coast of Turkey and is well-known for its luxury hotels. These hotels often use conventional vapor compression air-conditioning systems that require electricity and contribute to Antalya's annual peak electrical demand occurring during the summer [16]. Therefore, it is essential to reduce the electricity load on the network, especially summer cooling loads.

1.3 Overview of Adsorption Cooling Systems

One way to decrease electricity demand due to cooling is to use environmentally benign, thermally-powered cooling systems such as adsorption systems where the term "adsorption" in this study refers to solid physical sorption, not chemical sorption. Basically, in an adsorption cooling cycle (or heat pump), the mechanical compressor in the well-known conventional vapor-compression air conditioners that is generally powered by electricity is replaced with a thermal compressor that is driven by low grade thermal energy like solar energy or waste heat, and they do not require electricity, except for circulation pumps. Although adsorption cooling systems are not widely available in the market, these systems are proposed as a promising technology that deserves further research since they do not include rotating compressor parts [17-19].

Some of the advantages of adsorption cooling systems relative to conventional vapor-compression systems can be listed as [17-19]:

- Environmentally benign
- Can be operated with low-grade thermal energy such as solar, geothermal and waste heat
- Thermal energy storage possible
- Does not have moving parts, therefore long lifetime without noise and vibration
- Simple control and maintenance

Nevertheless, there are also some disadvantages of adsorption cooling systems compared with the conventional vapor-compression systems that can be listed as [17-19]:

- Low coefficient of performance
- Intermittent (not continuous) cooling
- System has to be operated under vacuum conditions and it is hard to maintain this vacuum
- Larger volume and weight

1.4 Motivation of the Present Study

The general goal is to find a solution to meet the rapidly growing demand for energy through an alternative cooling technology, specifically, adsorption cooling systems. This study, in particular, looks at the general performance trends of the adsorption cooling systems coupled with solar thermal systems, which are referred to as solar-thermal powered adsorption cooling systems, as operating conditions and several design parameters are varied. By common use of the adsorption cooling systems, it is believed that it would be possible to reduce the electricity demand due to cooling in areas like the Mediterranean coast of Turkey. Like other Mediterranean cities of Turkey, Antalya has large opportunities for solar energy. Systems like solar-powered adsorption cooling cycles can be used to reduce the load on electrical power by making the air conditioning independent of electricity. This study also investigates the suitability of the adsorption systems for the cities on the Mediterranean coast of Turkey, specifically Antalya. This study is done to assess the feasibility using solar energy for thermally-driven adsorption cooling systems.

Additionally, this study not only provides general guidelines to improve the performances of the adsorption cooling systems, it also reduces the time and cost of experiments by providing broad directions to pursue. This study foresees the difficulties and complexities of the experimental work by comparing and contrasting several cases by means of simulations.

Within this study, background information on the current energy situation, solar applications and adsorption systems are introduced in Chapter 1. In Chapter 2, an overview of refrigeration cycles and the completed studies on adsorption cooling systems are given. Newly introduced models are presented in Chapter 3 with the corresponding mathematical derivations. In Chapter 4, analyzed cases and model verifications are given. Detailed results of the analyzed cases are presented in Chapter 5 while the discussions on these results are given in Chapter 6. Finally, conclusions are presented in Chapter 7, and some suggestions as future work are provided in Chapter 8.

CHAPTER 2

SURVEY OF LITERATURE AND OBJECTIVES

2.1 Overview of Cooling Cycles

The adsorption cooling cycle is just one of many cooling cycles. To put this study into a broader context, a brief overview of the main refrigerant cycles except for the adsorption cycle is provided, while a more detailed description of the adsorption cycle is given in Section 2.2. The cooling cycles presented in this section are vapor-compression, absorption cycles and desiccant cooling cycles.

2.1.1 Vapor-Compression Cooling Cycle

As stated before and according to Moran and Shapiro, vapor-compression cooling cycles are the most commonly used cooling cycles [20]. A vapor-compression cycle works between two thermal reservoirs: one reservoir can be considered as the cold reservoir (or the space to be cooled) and the other as the hot reservoir (or the surroundings). A refrigerant is circulated within the system whose components are given in a schematic in Figure 2.1. As shown in this figure, this cooling cycle consists of a mechanically-driven compressor, a condenser, an evaporator and an expansion valve. The compressor in the vapor-compression cooling cycle is mechanically driven so that it should be operated externally by means of an electric motor or similar. In general, the ideal vapor-compression cooling cycles follow the following four processes as shown in Figure 2.1 [20, 21]:

- Process 1→2: The refrigerant at a saturated vapor phase enters the compressor and undergoes an adiabatic compression process where work input is necessary.

- Process 2→3: The refrigerant at a superheated vapor state undergoes an isobaric condensation process where heat is transferred from the condenser to the high temperature reservoir.
- Process 3→4: The saturated liquid refrigerant is throttled in an isenthalpic expansion process.
- Process 4→1: The refrigerant at a two-phase liquid-vapor mixture state undergoes an isobaric evaporation process where heat transfer from the cold reservoir occurs to the evaporator.

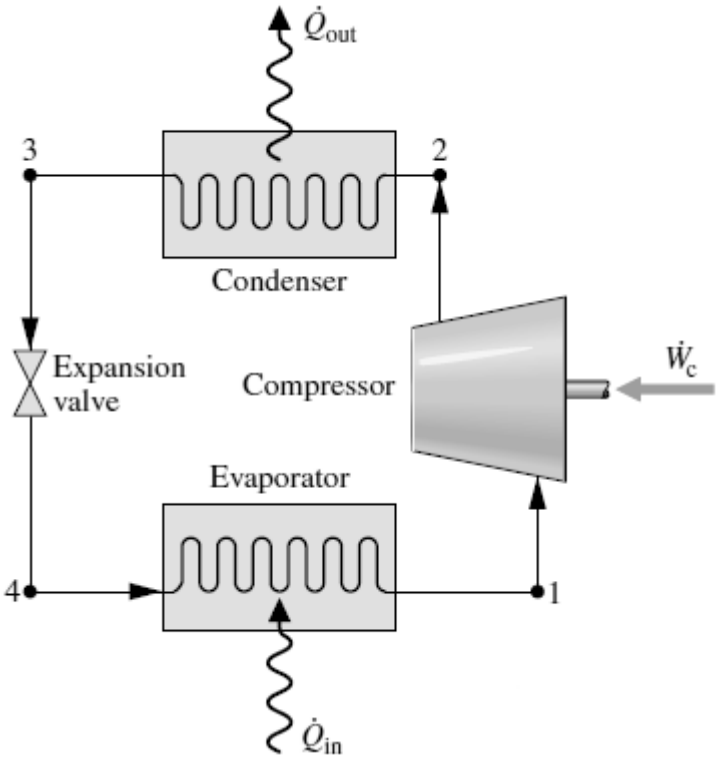

Figure 2.1. Vapor-compression cooling system [20].

One of the main advantages of the vapor-compression cycle is that this cycle can be used for freezing purposes since the refrigerants can be operated at temperatures below their freezing points. Another main advantage of this cycle is its high coefficient of performance as stated in Section 1.1. The actual vapor-compression cooling cycle

may deviate from the actual cycle by having the refrigerant at state 1 as a superheated vapor, heat transfer from the refrigerant in the compressor, pressure drop in the condenser, sub-cooled refrigerant at state 3, more heat transfer to the refrigerant in the evaporator, etc. For more information, interested readers are referred to Moran and Shapiro [20] and Sonntag et al. [21].

2.1.2 Absorption Cooling Cycles

Absorption cycles are also referred as liquid sorption cycles since absorbent is in the liquid phase in the absorbent bed (or absorber). Additionally, like adsorption cooling cycles, absorption cooling cycles are heat-powered cooling cycles and do not require mechanical compressors that have moving components. Unlike conventional vapor-compression cycles which operate between two thermal reservoirs, absorption cooling cycles operate between three thermal reservoirs: one reservoir is the cold reservoir (or the space to be cooled), the second reservoir is at the temperature of the available heat source and the last reservoir is the surroundings (or the reservoir to which heat is rejected from the condenser). Another difference between vapor-compression and absorption cooling cycles is that in vapor-compression cycles, refrigerant vapor is compressed in the mechanically-driven compressor, which reduces the specific volume of the refrigerant significantly and therefore requires a large amount of work. Conversely, in absorption cooling cycles, refrigerant in the liquid phase undergoes a compression process and the required amount of work is considerably reduced [22]. However, the overall energy used to generate refrigerant in the absorption cooling cycle is higher than the energy used in the vapor-compression cycle, so that the coefficient of performance of absorption cooling cycle is smaller [23]. Additionally, absorption systems are not suitable for mobile applications since they involve liquid absorbents, and these systems are susceptible to corrosion if they are operated under high temperatures (above 200^{o}C for instance) [24]. According to Meunier, another disadvantage of absorption cooling cycles is their high initial costs and they also require wet cooling towers (or low temperatures for the condenser) [25].

Two well-known absorbent – refrigerant (working) pairs are lithium bromide (LiBr) – water (H_2O) and ammonia (NH_3) – water (H_2O) pairs. A schematic of a simple (without enhancements) absorption cooling cycle is given in Figure 2.2, and the details of this cycle can be found in the books of Trott and Welch [23], Alefeld and Radermacher [26] and Herold et al. [27]. Basically, refrigerant at low pressure is absorbed and forms a strong liquor (or solution) before it is directed to the generator. After the liquor leaves the absorber, pressure is increased by a pump and refrigerant vapor is generated from liquor in the generator through heat transfer. Subsequently, the refrigerant vapor undergoes the common cooling cycle (condenser, throttling valve and evaporator) while the weak solution is directed to the absorber again.

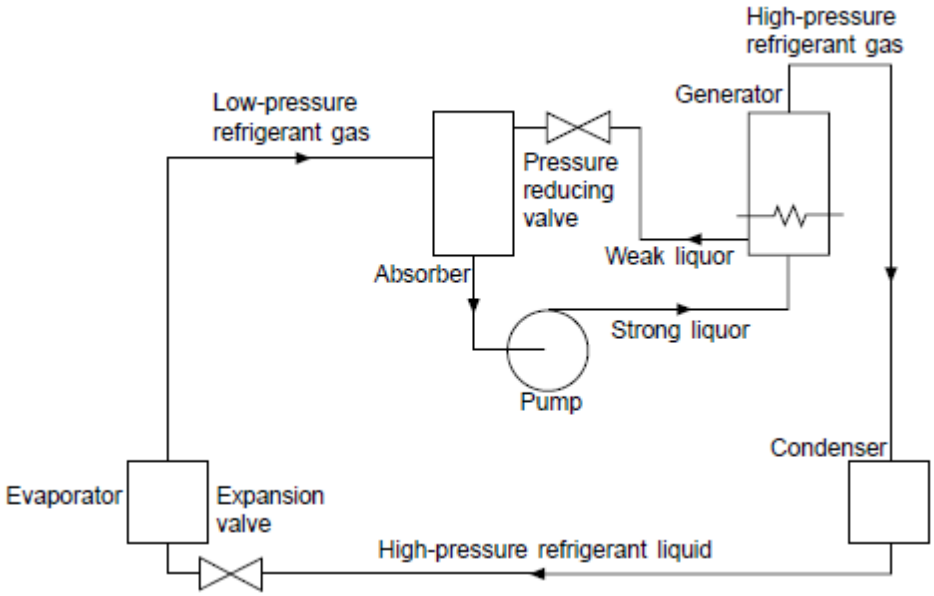

Figure 2.2. Simple absorption cooling cycle [23].

Moreover, absorbent pairs generally have lower temperature swing than adsorbent pairs, and absorption cooling necessitates use of liquid-gas heat exchangers rather than solid-gas heat exchangers found in adsorption cooling [25].

2.1.3 Desiccant Cooling

Another alternate cooling cycle that can be run with a low-grade thermal energy source is desiccant cooling. In desiccant cooling cycles, desiccants are used to dehumidify the air. The weight of the "wetted" commercial desiccants can reach up to 11 times their dry weights [28]. By heating the saturated desiccant, moisture can be removed thereby regenerating the desiccant.

The main advantages of desiccant cooling cycles over conventional vapor-compression cycles are the use of a low-grade energy source so that exergy consumption is lowered, no greenhouse gases are emitted and indoor air quality is improved through ventilation. Additionally, desiccant cooling cycles can operate with air as refrigerant and water for evaporative cooling.

The desiccant cooling cycles can be categorized into solid and liquid, or open and closed desiccant cooling cycles. In open desiccant cooling cycles, the ambient air enters the cycle and is then dehumidified by a desiccant (e.g., a bed packed with desiccants) as shown in Figure 2.3.

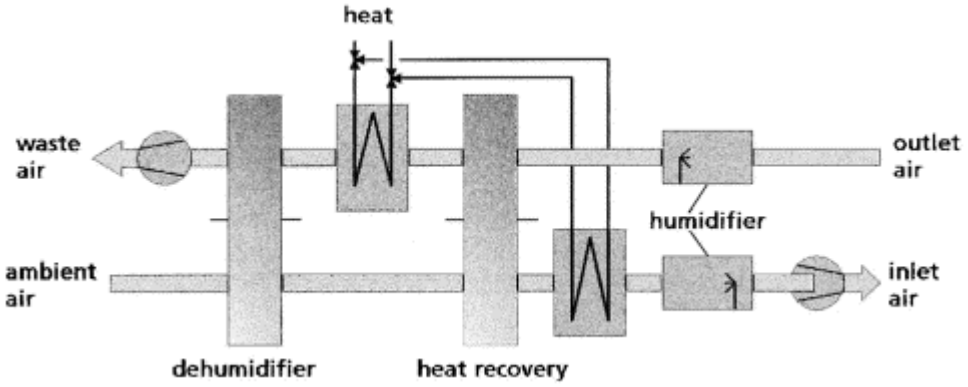

Figure 2.3. Basic desiccant cooling cycle [29].

The moisture (water vapor) is adsorbed (for solid desiccant cooling cycles) or absorbed (for liquid desiccant cooling cycles) in the desiccant. There occurs a temperature rise due to adsorption/absorption, and then sensible cooling occurs in a heat exchanger (heat recovery as labeled in Figure 2.3). Before entering the room to be cooled (or ventilated), the air is subjected to evaporative cooling through humidifiers. Simultaneously, the warm air to be exhausted is cooled evaporatively, and then it passes through a sensible heat exchanger as it recovers some amount of the heat of the inlet stream. Finally, the exhaust stream is heated by a low-grade thermal energy before regenerating the desiccant in the wheel. Alternatively, the air can be circulated between the inlet stream and the exhaust stream to form a closed desiccant cooling cycle. More details can be found in Waugaman et al. [28], Henning et al. [29], Daou et al. [30] and ASHRAE's publication [31].

2.2 Adsorption Cooling Cycles

Although the main attention in this study is given to the cooling cycles, the definitions in this section are also valid for other adsorption cycles (heat pumps, ice-making, etc.) as well.

2.2.1 Definitions

In the literature, the adsorption cooling cycle is well-established and several review papers have been published (e.g., [17, 19, 32-34]) describing the cycles in this section.

a. Simple adsorption cooling cycle

As mentioned previously, in an adsorption cooling cycle, the mechanical compressor in the well-known vapor compression cooling cycle that is generally powered by electricity is replaced with a thermal compressor that can be driven using low grade thermal energy like solar energy or waste heat. Simple (adsorption) cycle herein refers to an adsorption cycle with a spatially, but not temporally isothermal and isobar-

ic adsorbent bed. In the literature, the term "simple" is generally omitted or instead the term "intermittent" is used. A schematic of an ideal simple adsorption cycle is shown in Figure 2.4. The cycle is characterized by temporal variations in the refrigerant's vapor pressure and the adsorbent's temperature and adsorption capacity (X), which is defined as the ratio of adsorbed refrigerant mass to adsorbent mass. The ideal simple cycle is composed of four processes as shown in Figure 2.4.

- Process 1→2: Isosteric (constant X) heating
- Process 2→3: Isobaric heating and desorption
- Process 3→4: Isosteric (constant X) cooling
- Process 4→1: Isobaric cooling and adsorption

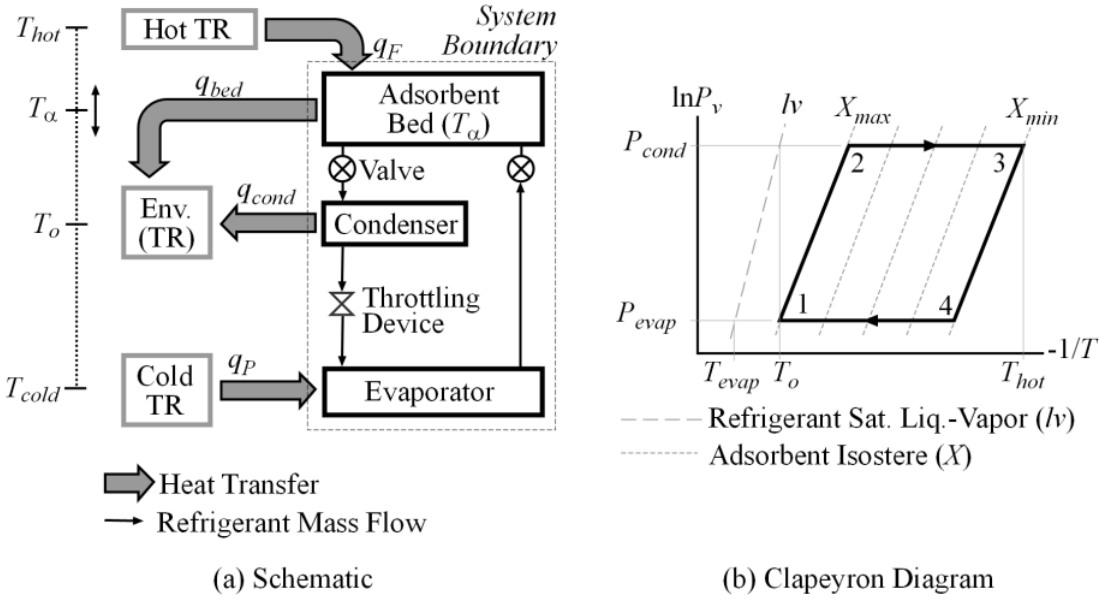

Figure 2.4. (a) Schematic and (b) Clapeyron diagram for an ideal simple adsorption cycle [35].

At the beginning of the adsorption cycle, the maximum amount of refrigerant is adsorbed on the adsorbent (X_{max}) in the adsorbent bed which is at the minimum bed temperature (T_o) and evaporator pressure (P_{evap}) (state 1). Additionally, all valves are

closed. In process 1→2, the adsorbent bed is heated by the driving heat transfer (q_F) from a hot thermal reservoir. The vapor pressure increases while the adsorption capacity essentially remains constant at the maximum adsorption capacity (isosteric process, dX = 0). Process 1→2 ends when the adsorbent bed reaches the condensation pressure (P_{cond}) (state 2).

At the state 2, the valve connecting the adsorbent bed to the condenser that is shown in Figure 2.4 is opened allowing desorbed refrigerant to flow to the condenser. For process 2→3 the bed continues to be heated using q_F and desorption and condensation occur isobarically at P_{cond}. Heat transfer occurs from the condenser to the environment. Process 2→3 ends when the bed reaches its maximum temperature (T_{hot}) and minimum adsorption capacity (X_{min}) (state 3).

Afterwards, the valve between the bed and the condenser is closed and the bed is brought into thermal communication with the environment allowing heat transfer from the adsorbent bed to the environment (q_{bed}) to occur. The bed cools isosterically for process 3→4 until the pressure inside the bed decreases to P_{evap} (state 4).

The valve connecting the evaporator to the bed is opened and the bed continues to be cooled to T_o at constant P_{evap} causing refrigerant to be adsorbed. This adsorption process pulls saturated liquid refrigerant from the condenser through the throttling device and evaporator creating the cooling by means of the product heat transfer (q_P) to the evaporator. The process ends (and the cycle is complete) when the adsorbent bed reaches T_o (state 1).

b. Adsorption cooling cycle with heat recovery

Heat recovery cycle herein refers to an adsorption cooling cycle with two spatially isothermal beds and ideal heat recovery. Each bed follows the same four processes (1→2→3→4→1) given in Figure 2.4b, and these two beds are operated out of phase by 180^o. Therefore, while one bed is being heated from T_o to T_{hot}, the other adsorbent bed is being cooled from T_{hot} to T_o. When these two beds are thermally connected to

each other, they can reach thermal equilibrium at a common temperature (T_{rec}) through q_{rec} that is heat transfer from the bed that is being cooled (process 3→1 in Figure 2.4b) to the bed that is being heated (process 1→3 in Figure 2.4b). Therefore, the total required q_F is decreased by q_{rec} and COP_{ads} of the cycle is increased compared to the simple cycle that is operating under same conditions (T_{hot}, T_{cond}, T_{evap}, etc).

In the design of heat recovery cycles, differences in sensible and latent heat capacities between the two analyzed adsorbent beds limit the possible thermal regeneration. The effect of these differences become more apparent when the heat recovery process is divided into four distinct sorption regimes [36]. These sorption regimes are defined based on the common bed temperature, T_{rec}.

- **Only Adsorption Regime** occurs when $T_1 \leq T_{rec} < T_2$. The adsorbent bed that is being heated is in the isosteric heating process (process 1→2 with $dX = 0$) while the adsorbent bed that is being cooled is in the isobaric cooling and adsorption process (process 4→1 with $dX > 0$).
- **Only Desorption Regime** occurs when $T_4 \leq T_{rec} < T_3$. The adsorbent bed that is being heated is in the isobaric heating and desorption process (process 2→3 with $dX < 0$) while the adsorbent bed that is being cooled is in the isosteric cooling process (process 3→4 with $dX = 0$).
- **Paired Sorption Regime** occurs when $T_2 \leq T_{rec} \leq T_4$. The adsorbent bed that is being heated is in the isobaric heating and desorption process (process 2→3 with $dX < 0$) while the adsorbent bed that is being cooled is in the isobaric cooling and desorption process (process 4→1 with $dX > 0$).
- **No Sorption Regime** occurs when $T_4 \leq T_{rec} \leq T_2$. The adsorbent bed that is being heated is in the isosteric heating process (process 1→2 with $dX = 0$) while the adsorbent bed that is being cooled is in the isosteric cooling process (process 3→4 with $dX = 0$).

Note that the paired sorption regime can occur only for the adsorbent bed pairs with $T_2 < T_4$, and no sorption regime can occur only for the adsorbent bed pairs with $T_4 <$

T_2. Among the described four sorption regimes, the most suitable regime for heat recovery is the paired sorption regime since the differences in heat capacities of the adsorbent beds are similar in this regime. More details can be found in [37-39].

Heat recovery processes are also applied to multi-stage and cascading adsorption cooling systems. These systems work under different temperature and/or pressure levels which make it possible to recover heat. In multi-stage systems, the same working pair is used with several temperature and/or pressure levels and the heat of adsorption or heat transfer from the condenser can be recovered in the same system. Alternatively, in cascading systems, different working pairs are used to recover heat. Cascading systems are especially advantageous over multi-stage systems if the operating temperature and/or pressure ranges of the working pairs are large [17].

c. Adsorption cooling cycle with mass recovery

Mass recovery can be classified as an enhancement process which is applied to the simple adsorption cycles or before the heat recovery process in heat recovery adsorption cycles. The main purpose of the mass recovery is to ease the pressurization and depressurization processes of the adsorbent beds. In two-bed adsorption cycles, one adsorbent bed at state 1 and the other adsorbent bed at state 3 are physically connected to each other through a pipe to let the mass recovery process occur. The adsorbent bed at state 3 is at high pressure and refrigerant vapor within this adsorbent bed leaves and enters the other adsorbent bed at state 1 whose vapor pressure is lower. This vapor refrigerant transfer between two adsorbent beds is referred to as a mass recovery process, and ideally the mass recovery process ends when the two adsorbent beds reach the same pressure level. As a result, a portion of the pressurization (process 1→2) and depressurization (process 3→4) processes are completed without any external source. Additionally, Clapeyron diagram changes slightly for cycles with mass recovery as shown in Figure 2.5. Note that the adsorption swing also increases with mass recovery. More information on mass recovery schemes can be found in [37, 38, 40, 41].

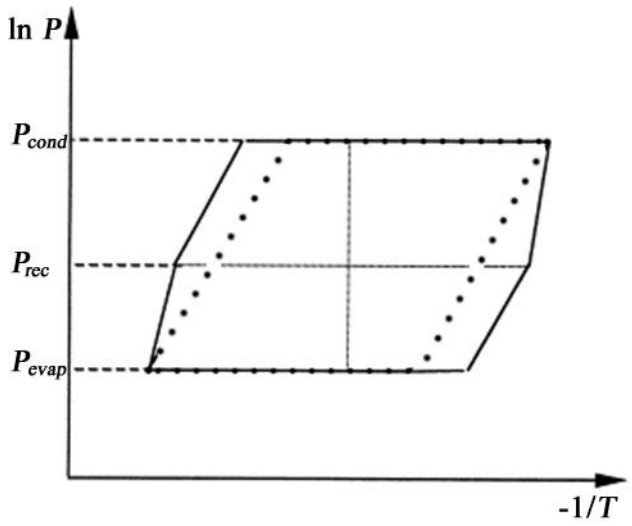

Figure 2.5. Clapeyron diagram for mass recovery cycle (Legend: solid lines for mass recovery cycle, dotted lines for simple cycle) (adapted from [37]).

d. Adsorption cooling cycle with thermal regeneration

Another commonly cited cycle enhancement scheme is thermal regeneration. Adsorption cooling cycles with thermal regeneration can be divided into three main types: thermal wave and convective thermal wave cycles and cycles with rotary adsorbent beds.

In thermal wave adsorption cooling cycles, two adsorbent beds are thermally connected to each other with the help of a heat transfer fluid (HTF). The heat transfer fluid passes through each adsorbent bed and creates a temperature variation (wave) inside the adsorbent beds. Due to the presence of this temperature wave inside the bed, this cycle is referred to as a thermal wave (adsorption cooling) cycle. A temperature schematic of the HTF loop for an ideal thermal wave cycle is shown in Figure 2.6 where the vertical position of the heat transfer fluid corresponds to its temperature. HTF that is heated to the maximum bed temperature (T_{hot}) in a heater enters the adsorbent bed that is to be heated and creates a temperature wave inside the adsorbent bed. Similarly, HTF that is cooled to the minimum bed temperature (T_o) enters the adsorbent bed which is being cooled and also creates a temperature wave inside

the adsorbent bed. The heater and cooler exit temperatures are fixed at T_{hot} and T_o. As the cycle proceeds, sorption processes cause the beds' exit temperatures to deviate from T_{hot} and T_o as shown in Figure 2.6 (as δT_1 and δT_2). These temperature deviations result in the need for the heater and cooler. Each adsorbent bed basically follows the same processes as the adsorbent beds in the simple adsorption cycle follow, except the adsorbent beds in thermal wave cycle are not spatially isothermal. The detailed information about each process in thermal wave adsorption cycle is given in Section 2.2.3.d with its mathematical model. Thermal wave adsorption cycle was first designed and patented by Shelton [42, 43].

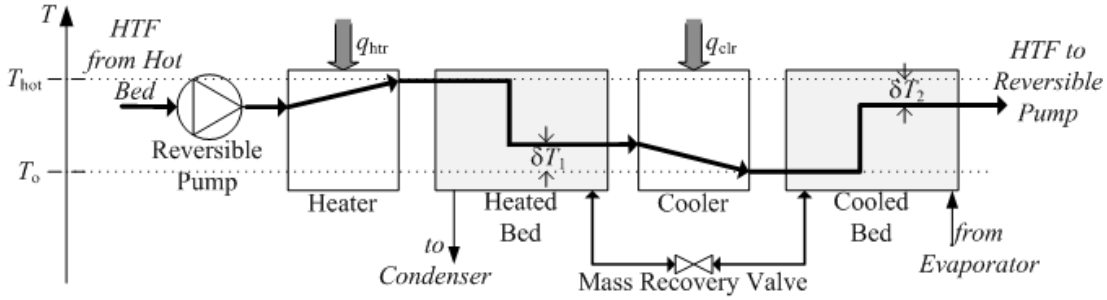

Figure 2.6. Schematic of the heat transfer fluid (HTF) flow for a half cycle in a thermal wave cycle [44].

Another regenerative adsorption cooling cycle is the convective thermal wave cycle proposed by Critoph [45] and patented by Sanburn [46]. In a convective thermal wave cycle, instead of using an external HTF loop, refrigerant is used for the same purpose. A schematic representation of the convective thermal wave cycle is given in Figure 2.7. As can be observed from Figure 2.7, in addition to the adsorbent beds, there are two inert beds that are packed with steel balls. These steel balls are used to recover heat, storing the heat of adsorption when the adsorbent bed is in the adsorption process (processes 3→4→1) and this stored heat can be used when the adsorbent bed is in desorption process (processes 1→2→3). The operation principle of the remaining part of the cycle is the same as in the thermal wave cycle.

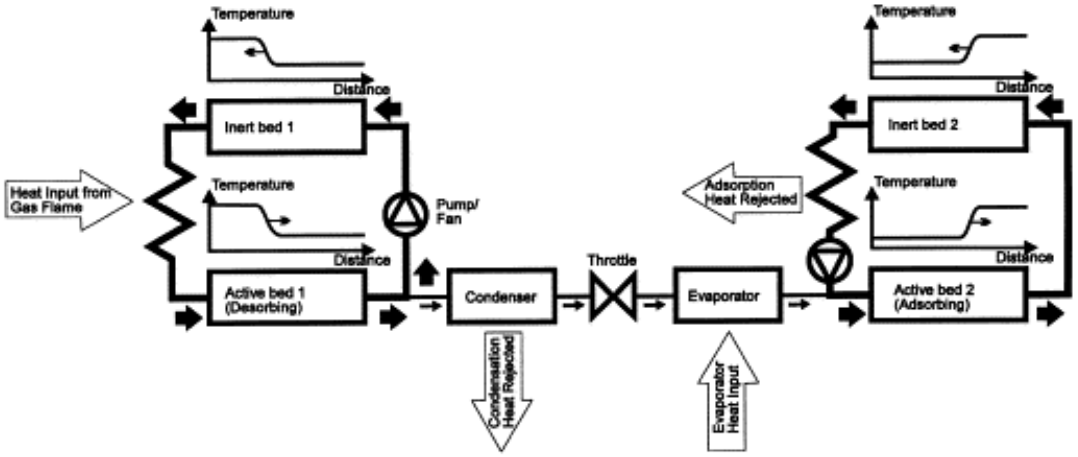

Figure 2.7. Schematic presentation of the convective thermal wave cycle [45].

A different regeneration method is achieved by rotating the adsorbent beds. This cycle is referred to as an adsorption (cooling) cycle with rotary beds. These rotary adsorbent beds are coupled with condensers and evaporators, and this novel design was suggested by Maier-Laxhuber and Kaubek [47] and further developed by Erickson [48] and Ebbeson [49]. With this regenerative design, the aim is to provide continuous cooling by having different temperature zones within the adsorbent bed and simplify the process management in the regenerative adsorption cooling cycles. Therefore, within a single adsorbent bed there are a number of sections at different temperature levels. As the adsorbent bed rotates, each section of the bed undergoes the processes one by one (from desorption to adsorption or vice versa). Within the rotary adsorbent bed, air as a heat transfer fluid is passed through channels to supply or remove the required heat transfers. The main concern of this design is the proper adjustments of rotation speed and flow rates of the heat transfer fluid. More detailed explanations can be found in [50-53].

2.2.2 Previous Experimental Studies

In the literature, there are many experimental studies on adsorption systems. Only the studies that are related to the present study are chronologically summarized here for

brevity. Interested readers may refer to the provided references for more information for each study.

One of the earliest studies which can be accessible on solar adsorption systems was performed by Pons and Guilleminot in 1986 [54]. A solar powered adsorption ice making system was analyzed from the fall 1984 to the end of summer 1985. Activated carbon – methanol pair was selected, the maximum bed temperature was 95^{o}C and the evaporation temperature varied between -5^{o}C and -10^{o}C. A maximum COP of 0.15 for the system was obtained.

Another study was performed by Wang et al. in 1998 [55]. As stated in this study, the most important parameters that affect the cycle performance are the cycle time and maximum bed temperature for a simple adsorption cycle. This study investigated these two parameters and compared experimental values with the simulated model results. According to the experimental results, as the maximum bed temperature increased, COP decreased and cooling power increased for activated carbon – methanol pair. Additionally, in this study, a new factor, packing coefficient, was defined to incorporate the high difference between theoretical and experimental results.

Different sorption systems were compared thermodynamically by Pons et al. in 1999 in terms of COP using different working pairs [56]. The results stated that absorption systems had higher COP values than adsorption systems and when cooling tower types were compared, wet cooling towers increased the system performance compared to dry cooling towers. Additionally, it was not possible to use water for ice making (which required temperatures below 0^{o}C) and results with methanol were not available for deep freezing purposes. The maximum COP values of the cycle were reported as 1.6 for cooling and 2.63 for heating purposes.

A prototype of a regenerative two-bed adsorption cooling cycle was designed and experimentally tested by Critoph et al. in 2000 [57]. Activated carbon – ammonia as the working pair and water as the heat transfer fluid were selected. The results of this study showed that with a maximum bed temperature of 140^{o}C, condensation temper-

ature of 32^{o}C, evaporation temperature of 7.5^{o}C and half cycle time as 620s the obtained COP value of the cycle was 0.44 and specific cooling power was approximately 0.18kW/kg.

A new design for two-stage adsorption cooling systems with two adsorbent beds was analyzed by Saha et al. in 2001 [58]. In this two-stage system, the pressurization (or depressurization) was completed in two progressive stages as the name implies. To achieve this aim, each adsorbent bed was divided into two parts, and as one part was being heated, the other part was being cooled. More details can be found in the related article. Silica gel – water was selected as the adsorbent – refrigerant (working) pair for the maximum bed temperature range of 40-75^{o}C. With a maximum temperature of 55^{o}C and condensation temperature of 30^{o}C, the COP of this cycle was reported as 0.36.

Wang in 2001 investigated the effects of heat and mass recovery on the simple cycle with two adsorbent beds and activated carbon – methanol pair [38]. The experimental results stated with the addition of heat recovery, the COP values increased by approximately 25%. Implementing mass recovery before heat recovery added 10% to the COP value of a simple cycle with heat recovery. Results also showed that with the mass recovery after heat recovery, COP reached 0.5 for a maximum bed temperature of 100^{o}C, condensation temperature of 24^{o}C, evaporation temperature of 10^{o}C and heat capacity ratio of 1.85. Heat capacity ratio is defined as the ratio of the bed's design to inherent heat capacities (R), i.e., ratio of heat capacities of adsorbent bed's shell and heat transfer fluid to heat capacity of adsorbent inside the bed. The results were also verified by theoretical analyses.

A prototype of a solar powered simple adsorption cooling system was built in Nigeria by Anyanwu and Ezekwe in 2003 [59]. This designed system was tested with activated carbon – methanol pair in November and December 1995. Therefore, the collector efficiencies were low and the obtained COP of the cooling cycle was around 0.31-0.35.

Additionally, experimental studies were done by Wang et al. in 2003 to investigate the effects of heat and mass recovery [60, 61]. In these studies, two beds with activated carbon – methanol pair were used with maximum bed temperatures lower than 120^{o}C and evaporation temperature at 10^{o}C. According to the results, implementing mass recovery to the adsorption cycle increased the cycle's cooling power up to 11% where the maximum COP was 0.115. The maximum COP value increased to 0.125 with the implementation of both heat and mass recovery processes. Additionally, results showed that heat recovery processes can decrease the total required heat transfer to drive the cycle by 20-30%.

Another design which was a simple adsorption cooling cycle with a binary working medium was proposed by Wang and Zhu in 2004 [62]. Instead of a cycle which worked with a zeolite – water pair, the authors suggested using a zeolite – ammonia – water working media. Therefore, the cycle would work with a significantly larger pressure swing than a cycle with a zeolite – water pair. This cycle is actually a combination of adsorption and absorption cooling cycles. The test results showed that the COP increased considerably, but COP values were dependent on the concentration of ammonia in the working medium. Additionally, this new system was more responsive to temperature changes. A maximum COP value of 0.48 was obtained when the maximum bed temperature was 120^{o}C.

A simple adsorption cooling cycle was also developed by Chang et al. in 2007 using a silica gel – water pair [63]. With a novel design of the adsorbent bed, a COP of 0.53 was obtained for the test conditions of maximum bed temperature of 80^{o}C, condensation temperature of 30^{o}C and evaporation temperature of 14^{o}C. The results also showed that the COP value of the cycle decreased as the maximum bed and evaporation temperatures decreased and condensation temperature increased. Within this study, effects of mass flow rate in the condenser and cycle time on the cycle's COP values were also investigated.

A solar powered adsorption cooling system was developed by Zhai and Wang in 2009 for the green house in Shanghai Jiao Tong University [64]. They provided 10^{o}C

of evaporation temperature using a maximum bed temperature of 85^{o}C and condensation temperature of 32^{o}C for a silica gel – water pair. They designed this simple adsorption system with evacuated tube collectors and wet cooling towers, and experimental COP values were within 0.29-0.32. Economic analyses were also done for this system and the corresponding results showed that the payback period for this solar-powered adsorption cooling system coupled with heating and hot water applications was approximately 3 years.

An adsorption cooling cycle with activated carbon – HFC 134a pair was experimentally investigated by Banker et al. in 2010 [65]. They worked with maximum bed temperatures between 73-93^{o}C, condensation temperatures between 28-32^{o}C and evaporation temperatures between 5-18^{o}C. Their study included steady and transient results and their aim was to cool down some electronic components. However, they could only test their model up to 5W cooling loads and COP values obtained in this study were below 0.04 for all investigated configurations.

Grisel et al. in 2010 constructed a heat recovery adsorption cooling system with a two-bed silica gel – water pair and analyzed its performance experimentally [66]. They tested the system at maximum temperatures between 73-91^{o}C, condensation temperatures between 22-43^{o}C and evaporation temperatures between 6-20^{o}C. When heat recovery was considered, the maximum COP value of the cycle was approximately 0.85.

2.2.3 Previously Developed Numerical Modeling

a. Simple adsorption cooling cycle

A description of the operating principles and processes of the simple adsorption cycle are given in Section 2.2.1.a and a thermodynamic model of the simple adsorption cycle is presented in this section. The thermodynamic model presented here was previously developed by Baker and Kaftanoğlu [35, 36, 67].

The main goal of the model is to predict the coefficient of performance of the adsorption cycle (COP_{ads}). In order to predict COP_{ads}, heat transfer values for each process have to be calculated. The required heat transfer to the adsorbent bed for process 1→2 ($Q_{F,1\text{-}2}$) can be found using the 1st Law of Thermodynamics as,

$$\mathrm{d}Q_{F,1\to 2} = \mathrm{d}U_{ads} + \mathrm{d}U_{shell} + \mathrm{d}U_{HTF} + \mathrm{d}U_{ref} \tag{2.1}$$

$$\mathrm{d}Q_{F,1\to 2} = \mathrm{d}\left(m\cdot u\right)_{ads} + \mathrm{d}\left(m\cdot u\right)_{shell} + \mathrm{d}\left(m\cdot u\right)_{HTF} + \mathrm{d}\left(m\cdot u\right)_{ref} \tag{2.2}$$

$$\mathrm{d}Q_{F,1\to 2} = m_{ads}\mathrm{d}u_{ads} + m_{shell}\mathrm{d}u_{shell} + m_{HTF}\mathrm{d}u_{HTF} + m_{ref}\mathrm{d}u_{ref} + u_{ref}\mathrm{d}m_{ref} \tag{2.3}$$

Note that $\mathrm{d}m_{ads} = \mathrm{d}m_{shell} = \mathrm{d}m_{HTF} = 0$ and the mass of vapor refrigerant is neglected (therefore, no change in adsorbed refrigerant, $\mathrm{d}m_{ref} = 0$). Assuming constant specific heats,

$$\mathrm{d}q_{F,1\to 2} = \frac{\mathrm{d}Q_{F,1\to 2}}{m_{ads}} = c_{ads}\mathrm{d}T + \frac{m_{shell}c_{shell} + m_{HTF}c_{HTF}}{m_{ads}c_{ads}}c_{ads}\mathrm{d}T + \frac{m_{ref}}{m_{ads}}c_{ref}\mathrm{d}T \tag{2.4}$$

Using the definition of adsorption capacity (X) and defining the ratio of the adsorbent bed's design to inherent heat capacities (R) as $R = \left(m_{shell}c_{shell} + m_{HTF}c_{HTF}\right)\left(m_{ads}c_{ads}\right)^{-1}$ where $\left(m_{shell}c_{shell} + m_{HTF}c_{HTF}\right)$ is the design heat capacity and $\left(m_{ads}c_{ads}\right)$ is the inherent heat capacity,

$$\mathrm{d}q_{F,1\to 2} = \left(R+1\right)c_{ads}\mathrm{d}T + X_1 c_{ref}\mathrm{d}T \tag{2.5}$$

Therefore, the required heat transfer for process 1→2 can be found by integrating Equation (2.5). The required heat transfer for process 2→3 can be calculated using a similar approach to that given in Equations (2.1) through (2.5), except the refrigerant vapor leaves the adsorbent bed (i.e., $\mathrm{d}m_{ref} \neq 0$) for process 2→3. Therefore,

$$\mathrm{d}Q_{F,2\to3} + \mathrm{d}H_v = \mathrm{d}U_{ads} + \mathrm{d}U_{shell} + \mathrm{d}U_{HTF} + \mathrm{d}U_{ref} \tag{2.6}$$

$$\mathrm{d}Q_{F,2\to3} + \mathrm{d}\left(m\cdot h\right)_v = \mathrm{d}\left(m\cdot u\right)_{ads} + \mathrm{d}\left(m\cdot u\right)_{shell} + \mathrm{d}\left(m\cdot u\right)_{HTF} + \mathrm{d}\left(m\cdot u\right)_{ref} \tag{2.7}$$

$$\mathrm{d}Q_{F,2\to3} + h_v\mathrm{d}m_v = m_{ads}\mathrm{d}u_{ads} + m_{shell}\mathrm{d}u_{shell} + m_{HTF}\mathrm{d}u_{HTF} + m_{ref}\mathrm{d}u_{ref} + u_{ref}\mathrm{d}m_{ref} \tag{2.8}$$

Similar to Equations (2.4) and (2.5) with $\mathrm{d}m_{ads} = \mathrm{d}m_{shell} = \mathrm{d}m_{HTF} = 0$ and $\mathrm{d}m_{ref} = \mathrm{d}m_v \neq 0$,

$$\mathrm{d}Q_{F,2\to3} = m_{ads}\mathrm{d}u_{ads} + m_{shell}\mathrm{d}u_{shell} + m_{HTF}\mathrm{d}u_{HTF} + m_{ref}\mathrm{d}u_{ref} + \left(u_{ref} - h_v\right)\mathrm{d}m_{ref} \tag{2.9}$$

Defining a constant heat of adsorption as $\Delta h_{ads} = u_{ads} - h_v$,

$$\mathrm{d}q_{F,2\to3} = \left(R+1\right)c_{ads}\mathrm{d}T + X\cdot c_{ref}\mathrm{d}T + \Delta h_{ads}\mathrm{d}X \tag{2.10}$$

The required heat transfer for process 2→3 can be found by integrating Equation (2.10). Modeling process 3→4 is similar to modeling process 1→2, except that the adsorbent bed cools down for process 3→4. Therefore, the heat transfer from the adsorbent bed to the environment can be calculated similar to Equation (2.5) as,

$$\mathrm{d}q_{bed,3\to4} = \left(R+1\right)c_{ads}\mathrm{d}T + X_3 c_{ref}\mathrm{d}T \tag{2.11}$$

The heat transfer from the adsorbent bed for process 4→1 can be calculated using Equation (2.10) with refrigerant vapor entering the adsorbent bed at the evaporation temperature (T_{evap}).

Heat transfers from the condenser and the evaporator per unit mass of adsorbent can also be calculated, respectively, as,

$$q_{cond} = \left[\mathrm{h_v}\left(T_o\right) - \mathrm{h_{liq}}\left(T_o\right)\right]\left(X_3 - X_1\right) \tag{2.12}$$

$$q_P = \left[\mathrm{h_v}\left(T_{evap}\right) - \mathrm{h_{liq}}\left(T_o\right) \right]\left(X_3 - X_1\right) \tag{2.13}$$

where $X_3 - X_1$ is described as the adsorption capacity swing of the cycle, ΔX_{cycle}. The energy performance of the adsorption cycle is defined as the coefficient of performance of the adsorption cycle (COP_{ads}), which is also one of the main parameters examined in this study.

$$COP_{ads} = \frac{q_P}{q_{F,1\to2} + q_{F,2\to3}} = \frac{q_P}{q_F} \tag{2.14}$$

b. Heat recovery

The mathematical model is constructed for heat recovery cycle which is described in Section 2.2.1.b using equations similar to Equations (2.1)-(2.14). Heat transfer that is being transferred between the two adsorbent beds during heat recovery (q_{rec}) is calculated considering the corresponding sorption regime (sorption regimes are described in Section 2.2.1.b) for each simulated case. The COP_{ads} of heat recovery cycle is calculated similarly with COP_{ads} of the simple cycle given in Equation (2.14), where $q_{F,HRec} = q_{F,Simple} - q_{rec}$. Details are given in [35, 67].

c. Mass recovery

The mass recovery model does not require any special mathematical formulation beyond the simple adsorption cycle's relations. The two beds at the end of their adsorption/desorption processes are brought into mechanical equilibrium until the two adsorbent beds have the same pressure. As suggested by Qu et al. [37], for ideal mass recovery process and for simplicity, the adsorption capacity (X) changes of the two adsorbent beds over the mass recovery process are also assumed to be identical. Details are given by Qu et al. [37].

d. Thermal wave adsorption cooling cycle

Thermal wave adsorption cooling cycle is introduced briefly in Section 2.2.1.d. In this section, a thermodynamic model of thermal wave adsorption cooling cycle that was developed by Baker and Kaftanoğlu [35] and re-evaluated by Taylan et al. [44] is given in detail for comprehensiveness of the present study.

To explore thermodynamic limits to and trends for COP_{ads} for the thermal wave adsorption cooling cycle, the following assumptions are made. Each bed is spatially (but not temporally) isobaric and the only heat exchange is with the heat transfer fluid (HTF). An ideal square thermal wave divides each adsorption bed into a *back* region behind the wave and a *front* region in front of the wave. Each region is isothermal and isosteric with the back region at $T_b \equiv T_{HTF,in}$ and X_b, and the front region at $T_f \equiv T_{HTF,out}$ and X_f. Sorption at the thermal wave occurs at the average wave temperature, $T_w = (T_b + T_f)/2$. Each bed has a normalized length of 1 and the position of the moving thermal wave is $0 \leq y_w \leq 1$. The adsorbent and adsorbed refrigerant masses for the back and front regions are given mathematically in Table 2.1.

Table 2.1. Adsorbent and adsorbed refrigerant masses for the back and front regions of the bed [44].

	Back region at T_b & X_b	Front region at T_f & X_f
Mass of adsorbent (m_{ads})	$y_w \cdot m_{ads}$	$(1-y_w) \cdot m_{ads}$
Mass of adsorbed refrigerant (m_{ref})	$y_w \cdot m_{ads} \cdot X_b$	$(1-y_w) \cdot m_{ads} \cdot X_f$

A half-cycle is completed when the waves reach the right sides of the beds in Figure 2.6. The cycle is completed by reversing the direction of the HTF flow via a reversible pump, thereby reversing the direction of the thermal wave. At state 1, $y_{w,1} = 0$, $T_{b,1} = T_{f,1} = T_o$, $P_1 = P_{evap}$ and all valves are closed. A heat capacity ratio, R, analogous to that introduced in Equation (2.5) is defined as the ratio of the design to the

inherent heat capacities [38, 67]. The model is developed for the left bed undergoing a complete cycle in Figure 2.6 and initially uniformly at the minimum bed temperature (T_o).

Process 1→2: The heat transfer fluid starts to circulate at T_{hot} through the bed initiating the thermal wave. At the wave the refrigerant desorbs at T_w causing the vapor pressure to increase, which in turn causes refrigerant vapor to be re-adsorbed in the front and back regions. For simplicity, the heat of adsorption released in the back region is assumed to be transferred to the thermal wave, such that $T_b \equiv T_{hot}$ and $\mathrm{d}T_b = 0$. In reality, the re-adsorption of refrigerant vapor occurring behind the wave likely causes the temperature behind the wave to vary spatially and temporally. However, modeling these temperature variation increases the complexity and computational time of the model significantly. Since one of the goals of the present work is to use fast models to perform a large number of parametric studies, as a first case approximation the effect of these spatial and temporal variations is assumed small and is neglected. Conversely, in the front region the heat of adsorption causes the temperature to increase ($\mathrm{d}T_f > 0$). To find T_f and the vapor pressure inside the bed, a control volume at an unspecified position, y_s, in front of the wave is considered ($y_w < y_s < 1$). The control volume is spatially both isothermal ($T_s = T_f$) and isosteric ($X_s = X_f$). Some net amount of refrigerant vapor entering the control volume is adsorbed ($\mathrm{d}m_{v,in} = \mathrm{d}m_{ref,s}$), while the rest passes through the control volume. An energy balance can be obtained similar to Equation (2.5),

$$h_{v,in}\mathrm{d}m_{v,in} = (R+1)\,\mathrm{d}\left(m_{ads,s}u_{ads,s}\right) + \mathrm{d}\left(m_{ref,s}u_{ref,s}\right) \tag{2.15}$$

Rearranging the terms in Equation (2.15) yields,

$$h_{v,in}\mathrm{d}m_{ref,s} = (R+1)\,m_{ads,s}\mathrm{d}u_{ads,s} + m_{ref,s}\mathrm{d}u_{ref,s} + u_{ref,s}\mathrm{d}m_{ref,s} \tag{2.16}$$

Using the relations in Table 2.1 and noting that $\mathrm{d}m_{ads,s} = 0$,

$$h_{v,in} m_{ads,s} \mathrm{d}X_s = (R+1)\, m_{ads,s} \mathrm{d}u_{ads,s} + X_s m_{ads,s} \mathrm{d}u_{ref,s} + m_{ads,s} u_{ref,s} \mathrm{d}X_s \qquad (2.17)$$

Canceling out $m_{ads,s}$ in all the terms,

$$h_{v,in} \mathrm{d}X_s = (R+1)\, \mathrm{d}u_{ads,s} + X_s \mathrm{d}u_{ref,s} + u_{ref,s} \mathrm{d}X_s \qquad (2.18)$$

Rearranging the terms in Equation (2.18) yields,

$$(R+1)\, \mathrm{d}u_{ads,f} + X_f \mathrm{d}u_{ref,f} + (u_{ref,f} - h_{v,in}) \mathrm{d}X_f = 0 \qquad (2.19)$$

Using constant specific heats and adding $\pm h_{v,f} \mathrm{d}X_f$ to the right hand side of Equation (2.19),

$$(R+1) c_{ads} \mathrm{d}T_f + X_f c_{ref} \mathrm{d}T_f + (u_{ref,f} - h_{v,f} + h_{v,f} - h_{v,in}) \mathrm{d}X_f = 0 \qquad (2.20)$$

Applying constant specific heats and rearranging terms yield,

$$\left[(R+1) c_{ads} + X_f c_{ref}\right] \mathrm{d}T_f + (u_{ref,f} - h_{v,f}) \mathrm{d}X_f + c_p (T_f - T_{in}) \mathrm{d}X_f = 0 \qquad (2.21)$$

A more detailed and complete presentation of Equation (2.21) that explicitly shows the dependence of u_{ref} and h_v on temperature is,

$$\left[(R+1) c_{ads} + X_f c_{ref}\right] \mathrm{d}T_f + \left[\mathrm{u_{ref}}(T_f) - \mathrm{h_v}(T_f) + c_p (T_f - T_{in})\right] \mathrm{d}X_f = 0 \qquad (2.22)$$

Equation (2.22) is independent of y_s and is valid for the entire front part of the bed. Assuming the desorbed refrigerant vapor enters the control volume at $T_{in} = T_w$ and constant heat of adsorption [68], Equation (2.22) becomes,

$$\left[(R+1) c_{ads} + X_f c_{ref}\right] \mathrm{d}T_f + \left[\Delta h_{ads} + c_p (T_f - T_w)\right] \mathrm{d}X_f = 0 \qquad (2.23)$$

From Equation (2.23) it is possible to find T_f implicitly for a specified vapor pressure. To find the position of the thermal wave, y_w, conservation of refrigerant mass can be applied to the adsorbent bed.

$$m_{ref} = m_{ref,b} + m_{ref,f} \tag{2.24}$$

Since no refrigerant leaves the bed during the process 1→2, $dm_{ref} = 0$. Therefore, m_{ref} in Equation (2.24) is constant during this process. Using the relations in Table 2.1,

$$m_{ads} X_{min} = y_w m_{ads} X_b + (1 - y_w) m_{ads} X_f \tag{2.25}$$

where $X_b = X(T_{hot}, P_v)$, $X_f = X(T_f, P_v)$ and $X_{min} = X(T_o, P_{evap})$. Therefore, the position of the thermal wave, y_w, can be found using,

$$y_w = \frac{X_{min} - X_f}{X_b - X_f} = \frac{X(T_o, P_{evap}) - X(T_f, P_v)}{X(T_{hot}, P_v) - X(T_f, P_v)} \tag{2.26}$$

An energy balance on the entire bed for $dm_{HTF,flow}$ yields,

$$(h_{HTF,in} - h_{HTF,out})\, dm_{HTF,flow} = (R+1)\, d(m_{ads,b} u_{ads,b} + m_{ads,f} u_{ads,f}) + d(m_{ref,b} u_{ref,b} + m_{ref,f} u_{ref,f}) \tag{2.27}$$

Note that $T_b = T_{hot}$ and T_{hot} is fixed, therefore $du_{ads,b} = du_{ref,b} = 0$. Conservation of mass necessitates $dm_{ads,b} + dm_{ads,f} = 0$ and $dm_{ref,b} + dm_{ref,f} = 0$ with $dm_{ads,b} \neq 0$, $dm_{ads,f} \neq 0$, $dm_{ref,f} \neq 0$ and $dm_{ref,b} \neq 0$. Therefore, Equation (2.27) becomes,

$$\begin{aligned}(h_{HTF,in} - h_{HTF,out})\, dm_{HTF,flow} = (R+1)\Big[&(u_{ads,b} - u_{ads,f})\, dm_{ads,b} + m_{ads,f}\, du_{ads,f}\Big] \\ &+ (u_{ref,b} - u_{ref,f})\, dm_{ref,b} + m_{ref,f}\, du_{ref,f}\end{aligned} \tag{2.28}$$

Using constant specific heats,

$$c_{HTF}\left(T_{in}-T_{out}\right)\mathrm{d}m_{HTF,flow}=\left(R+1\right)\left[c_{ads}\left(T_b-T_f\right)\mathrm{d}m_{ads,b}+m_{ads,f}c_{ads}\mathrm{d}T_f\right]+c_{ref}\left(T_b-T_f\right)\mathrm{d}m_{ref,b}+m_{ref,f}c_{ref}\mathrm{d}T_f \quad (2.29)$$

Using Table 2.1, Equation (2.29) becomes,

$$c_{HTF}\left(T_b-T_f\right)\mathrm{d}m_{HTF,flow}=\left(R+1\right)m_{ads}c_{ads}\left[\left(T_b-T_f\right)\mathrm{d}y_w+\left(1-y_w\right)\mathrm{d}T_f\right]+m_{ads}c_{ref}\left(T_b-T_f\right)X_b\mathrm{d}y_w+m_{ads}c_{ref}\left(T_b-T_f\right)y_w\mathrm{d}X_b+\left(1-y_w\right)m_{ads}c_{ref}X_f\mathrm{d}T_f \quad (2.30)$$

Rearranging terms in Equation (2.30) yields,

$$c_{HTF}\left(T_{hot}-T_f\right)\frac{\mathrm{d}m_{HTF,flow}}{m_{ads}}=\left(1-y_w\right)\left[c_{ads}\left(R+1\right)+c_{ref}X_f\right]\mathrm{d}T_f+\left(T_{hot}-T_f\right)\left\{\left[c_{ads}\left(R+1\right)+c_{ref}X_b\right]\mathrm{d}y_w+c_{ref}y_w\mathrm{d}X_b\right\} \quad (2.31)$$

For fixed P_v, T_f and y_w, Equation (2.31) can be solved for d$m_{HTF,flow}$. Process 1→2 ends when $P_v = P_{cond}$.

Process 2→3: The valve between the bed and the condenser is opened, and the wave continues to progress through the bed. The desorbed refrigerant leaves the bed and is condensed in the condenser, resulting in a temporally isobaric process inside the bed at P_{cond}. An energy balance on the entire bed yields,

$$\left(h_{HTF,in}-h_{HTF,out}\right)\mathrm{d}m_{HTF,flow}-h_{v,out}\mathrm{d}m_{v,out}=\left(R+1\right)\mathrm{d}\left(m_{ads,b}u_{ads,b}+m_{ads,f}u_{ads,f}\right)+\mathrm{d}\left(m_{ref,b}u_{ref,b}+m_{ref,f}u_{ref,f}\right) \quad (2.32)$$

Since all desorbed refrigerant leaves the bed, dT_f = dT_b = 0. From conservation of mass, d$m_{ads,b}$ = -d$m_{ads,f}$ = m_{ads}dy_w and d$m_{v,out}$ = -d$m_{ref,b}$ – d$m_{ref,f}$, where $m_{v,out}$ is the mass of refrigerant vapor exiting the bed. Assuming the refrigerant leaves the bed at T_w and using Table 2.1 and a similar methodology as to obtain Equation (2.31) from Equation (2.27),

$$\frac{c_{HTF}\left(T_{hot}-T_f\right)}{m_{ads}}\frac{\mathrm{d}m_{HTF,flow}}{\mathrm{d}y_w}=\Delta h_{ads}\left(X_b-X_f\right)+\left(R+1\right)c_{ads}\left(T_{hot}-T_f\right)+c_p\left[X_b\left(T_{hot}-T_w\right)-X_f\left(T_f-T_w\right)\right] \tag{2.33}$$

Integrating Equation (2.33) yields,

$$\frac{c_{HTF}\left(T_{hot}-T_{f,2}\right)}{1-y_{w,2}}\frac{m_{HTF,flow,2\to3}}{m_{ads}}=\Delta h_{ads}\left(X_{b,2}-X_{f,2}\right)+\left(R+1\right)c_{ads}\left(T_{hot}-T_{f,2}\right)+c_p\left[X_{b,2}\left(T_{hot}-T_w\right)-X_{f,2}\left(T_{f,2}-T_w\right)\right] \tag{2.34}$$

Equation (2.34) fixes $m_{HTF,flow,2\text{-}3}$. Process 2→3 ends when $y_w = 1$ and the bed is uniformly at T_{hot} and P_{cond}.

Process 3→4: The valve between the bed and the condenser is closed, the direction of the heat transfer fluid flow reversed, and the heat transfer fluid now enters the bed at T_o. The process is essentially the reverse of process 1→2 and described by a set of equations parallel to Equations (2.15)-(2.31). Equations (2.23) and (2.31) is valid with $T_w = T_{evap}$ and $T_b = T_o$ and Equation (2.26) becomes,

$$y_w=\frac{X_{max}-X_f}{X_b-X_f}=\frac{\mathrm{X}\left(T_{hot},P_{cond}\right)-\mathrm{X}\left(T_f,P_v\right)}{\mathrm{X}\left(T_o,P_v\right)-\mathrm{X}\left(T_f,P_v\right)} \tag{2.35}$$

Process 4→1: The valve between the bed and the evaporator is opened, and the wave continues to progress through the bed. The process is essentially the reverse of process 2→3 with the exception that evaporated refrigerant enters the bed at T_{evap}. Equations parallel to Equations (2.32) and (2.34) describe this process as,

$$\frac{c_{HTF}\left(T_o-T_{f,4}\right)}{1-y_{w,4}}\frac{m_{HTF,flow,4\to1}}{m_{ads}}=\Delta h_{ads}\left(X_{b,4}-X_{f,4}\right)+\left(R+1\right)c_{ads}\left(T_o-T_{f,4}\right)+c_p\left[X_{b,4}\left(T_o-T_{evap}\right)-X_{f,4}\left(T_{f,4}-T_{evap}\right)\right] \tag{2.36}$$

q_{htr} and q_{clr}: For the processes 1→2→3, the total mass of heat transfer fluid that passes through the bed is,

$$\frac{m_{HTF,flow,1\to3}}{m_{ads}} = \int_1^2 \frac{\mathrm{d}m_{HTF,flow}}{m_{ads}} + \frac{m_{HTF,flow,2\to3}}{m_{ads}} \tag{2.37}$$

Similarly, for processes 3→4→1,

$$\frac{m_{HTF,flow,3\to1}}{m_{ads}} = \int_3^4 \frac{\mathrm{d}m_{HTF,flow}}{m_{ads}} + \frac{m_{HTF,flow,4\to1}}{m_{ads}} \tag{2.38}$$

Significantly, $m_{HTF,flow,1\text{-}3} < m_{HTF,flow,3\text{-}1}$ since the adsorption capacities are different for processes 1→2 and 3→4, resulting in different sensible loads [42]. This difference in $m_{HTF,flow}$ yields two possible thermal wave cycle models: without bypass and with bypass.

In the thermal wave cycle without bypass model, all $m_{HTF,flow,3\text{-}1}$ passes through both the heater and cooler. Therefore, the total heat transfers per unit mass of adsorbent to the heater and from the cooler are,

$$\frac{m_{ads}q_{htr}}{c_{HTF}} = \int_3^4 \left(T_{hot} - T_f\right)\mathrm{d}m_{HTF,flow} + m_{HTF,flow,4\to1}\left(T_{hot} - T_{f,4}\right) \tag{2.39}$$

$$\begin{aligned}\frac{m_{ads}q_{clr}}{c_{HTF}} = &\int_1^2 \left(T_f - T_o\right)\mathrm{d}m_{HTF,flow} + m_{HTF,flow,2\to3}\left(T_{f,2} - T_o\right) \\ &+ \left(m_{HTF,flow,3\to1} - m_{HTF,flow,1\to3}\right)\left(T_{hot} - T_o\right)\end{aligned} \tag{2.40}$$

In the thermal wave cycle with bypass model, $m_{htf,flow,1\text{-}3}$ passes through the heater while $m_{htf,flow,3\text{-}1} - m_{htf,flow,1\text{-}3}$ bypasses the heater and the heated bed. Therefore, only $m_{htf,flow,1\text{-}3}$ needs to be heated to T_{hot} resulting in,

$$\frac{m_{ads}q_{htr}}{c_{HTF}} = \int_{3}^{4}\left(T_{hot} - T_f\right)\mathrm{d}m_{HTF,flow} + \left(m_{HTF,flow,1\to3} - m_{HTF,flow,3\to4}\right)\left(T_{hot} - T_{f,4}\right) \quad (2.41)$$

Since all $m_{htf,flow,3\text{-}1}$ needs to be cooled to T_o,

$$\begin{aligned}\frac{m_{ads}q_{clr}}{c_{HTF}} = &\int_{1}^{2}\left(T_f - T_o\right)\mathrm{d}m_{HTF,flow} + m_{HTF,flow,2\to3}\left(T_{f,2} - T_o\right)\\ &+\left(m_{HTF,flow,3\to1} - m_{HTF,flow,1\to3}\right)\left(T_{f,4} - T_o\right)\end{aligned} \quad (2.42)$$

Note that while q_{clr} given in Equations (2.40) and (2.42) is not needed for COP_{ads} calculations, it is used in a global energy balance to check the 1st Law consistency of the overall model.

e. Reversible cycle

In the all adsorption cycles described in Sections 2.2.3.a through 2.2.3.d, irreversibilities occur due to heat transfers across finite temperature differences and throttling. In order to have the maximum possible thermodynamic performance, a reversible cycle is modeled. One completely reversible cycle between the three thermal reservoirs shown in Figure 2.4 is a combination of a Carnot refrigerator operating between T_o and T_{evap} that is driven by a Carnot power cycle operating between T_{hot} and T_o. Therefore, COP_{ads} of the reversible cycle is given in [69] as,

$$COP_{ads,rev} = \frac{1 - \frac{T_o}{T_{hot}}}{\frac{T_o}{T_{evap}} - 1} \quad (2.43)$$

The reversible cycle has the maximum theoretically possible COP_{ads} and COP_{ads} of reversible cycle does not depend on the components or the processes of the cycles. For this reason, the reversible cycle is a base case with which to compare all the adsorption cycles described in Sections 2.2.3.a through 2.2.3.d.

2.2.4 Previous Theoretical Studies

Theoretical models of adsorption systems with their mathematical explanations can be widely found in literature. For brevity, only a number of the relevant studies are chronologically summarized in this study. As before, more information can be found in the references provided for each study.

Douss et al. in 1988 developed a numerical model for simple and heat and mass recovery cycles [70]. Heat pumps with zeolite NaX – water pair were considered and analyzed in this theoretical study. The numerical model was supported by some experimental study. According to the results, the simple cycle could reach COP of 1.38 whereas heat and mass recovery cycle could reach 1.56. The results also stated that condensation and evaporation pressures had the largest effect on the COP values among bed temperatures and other components' design parameters (such as heat transfer coefficients).

Effects of operating conditions on a heat recovery adsorption heat pump were investigated by Zheng et al in 1995 [71]. In this study, activated carbon – ammonia pair was selected and two adsorbent beds were used. Conditions like maximum bed temperature and ambient temperature were analyzed. The results showed that increasing maximum bed temperature from 180 to 250^{o}C increased the COP by 20%. Additionally, as the ambient temperature (which ideally is equal to the condensation temperature if a dry cooling tower is used) increased, COP decreased.

Another theoretical study was conducted by Zheng et al. in 1995 [72]. They analyzed a two-bed adsorption heat pump with heat regeneration was analyzed, and an activated carbon – ammonia pair was used. Effects of several parameters related to cycle time and heat transfer coefficients on the cycle performance were investigated, but the related part of this study is the effect of the dead mass within the adsorbent bed. According to the results, increasing the adsorbent bed shell's mass (i.e., heat capacity) decreased the COP and cooling capacity of the cycle whereas increasing the mass

of heat transfer fluid within the adsorbent bed increases COP slightly, but decreases cooling capacity considerably.

Another model was developed for simple and heat recovery cycle by Teng et al. in 1997 [73]. In this study, effects of the parameters (coefficients and exponent) in Dubinin – Astakhov (D-A) equation on cycle performance were investigated. More information on D-A equation can be found in Section 2.3. Additionally, effects of maximum bed temperature, evaporation temperature and heat capacity ratio were analyzed. As predicted, the adsorption cycle with regeneration gave higher COP values than the simple cycle. Additionally, COP values of the adsorption heat pump with activated carbon – methanol pair increased by increasing the maximum bed temperature (varied between 90 – 140^{o}C) and evaporation temperature (varied between -20 – 15^{o}C) or decreasing heat capacity ratio (varied between 0 – 50). The maximum COP value reported was approximately 1.5.

A thermal wave adsorption heat pump model with only heat transfer equations (i.e., excluding mass transfer) was developed by Sun et al. in 1997 [74]. Zeolite NaX – ammonia pair was selected with constant heat of adsorption value for analyses. The model considered two-dimensional heat transfer within the adsorbent bed: axial for heat transfer fluid only (excluding axial heat transfer for adsorbent) and radial heat transfer. This two-dimensional model was solved using ordinary differential equations (one dimensional) with a number of assumptions. As a result, the authors reported a maximum COP of 0.87 for the following condition: maximum bed temperature at 260^{o}C, condensation temperature at 40^{o}C, evaporation temperature at 5^{o}C and ambient temperature at 20^{o}C.

Pons and Poyelle in 1999 investigated the heat recovery and thermal wave adsorption cycles numerically [75]. These cycles were coupled with mass recovery, and two types of working pair were selected: activated carbon – methanol and zeolite NaX – water. Additionally, effects of cooling tower type on the system performance were investigated. The COP values of the cycle obtained in this study are given in Table 2.2.

Table 2.2. COP comparison of adsorption systems with different configurations [75].

	Heat and Mass Recovery Cycle				**Thermal Wave Cycle with Mass Recovery**			
	Zeolite NaX – Water		**Activated Carbon – Methanol**		**Zeolite NaX – Water**		**Activated Carbon – Methanol**	
Cooling Tower	**Dry**	**Wet**	**Dry**	**Wet**	**Dry**	**Wet**	**Dry**	**Wet**
Cooling	0.63	0.68	0.52	0.55	0.70	0.92	-	0.61
Ice Making	-	-	0.33	0.42	-	-	-	0.31
Heat Pump	1.6	1.7	1.45	1.6	1.7	2.0	-	-

According to the results, the thermal wave cycle gave higher COP values than heat recovery cycle (except for ice-making) and wet cooling tower was advantageous over dry cooling tower in terms of COP. Note that ice making results for zeolite NaX – water pair are not available since water cannot be run below 0^{o}C (which is the freezing temperature of water) in adsorption cooling cycles. When the authors compared these results with the previous studies, they claimed that adding mass recovery enhanced the COP values.

A numerical model for thermal wave adsorption cycle with zeolite NaX – water pair was developed by Sward et al. in 2000 [76]. The effects of maximum bed temperature (varied between 100^{o}C and 120^{o}C) and condensation temperature (varied between 30^{o}C and 40^{o}C) on COP values were analyzed. For the selected base case where maximum bed temperature was 120^{o}C, condensation temperature was 30^{o}C and evaporation temperature was 5^{o}C, a COP of 1.24 was reported. Additionally, as the maximum bed temperature increased and as the condensation temperature decreased, COP values of the cycle was increased.

Wang et al. in 2000 [77] predicted the performance of solar powered ice maker coupled with water heater through energy analysis. Activated carbon – methanol pair was selected as working pair and simulations were performed for a complete year. The results showed that the maximum COP of the refrigeration cycle was 0.51 for the period from October to December which resulted according to the simulated operating conditions. The simulation results were higher than the experimental results in which the COP was 0.386 in two days in December 1998.

Effects of heat transfer fluid in a thermal wave adsorption cooling cycle with two beds were investigated numerically through thermodynamic models by Pons and Szarzynski in 2000 [78]. Zeolite – water pair was used, and heat transfer fluid with constant density and specific heat was compared with heat transfer fluid with temperature dependent density and specific heat. According to the simulation results, assuming constant density did not affect the performance of the cycle whereas results with constant specific heat assumption over-predicted the cycle performance.

Chua et al. in 2001 investigated the differences in performance of the adsorption cooling cycles as the number of adsorbent beds was varied [51]. When two, four and six adsorbent beds were compared in a heat recovery adsorption cooling cycle, heat recovered increased by 70% switching from two beds to four beds and by 40% switching from four beds to six beds. Silica gel – water pair was considered in this study with the base case as a maximum bed temperature at 85.7^{o}C and condensation temperature at 31^{o}C.

Two and three-bed adsorption cycles with heat recovery and silica gel – water pair were compared by Saha et al. in 2003 [79]. The results stated that with three adsorbent beds it was possible to increase the recovered heat transfer by 35% compared to system with two adsorbent beds. The parametric results showed that the maximum COP value (0.43) was achieved when the maximum bed temperature was between 80^{o}C and 90^{o}C if the condensation temperature was 30^{o}C. COP increased with increasing maximum bed temperature and with decreasing condensation temperature.

A theroretical study of the previously developed two-stage adsorption cooling cycle [58] was accomplished using a theoretical model of the system by Alam et al. in 2004 [80]. Silica gel – water pair was selected as in the experimental study, and effects of cycle time, maximum bed and condensation temperature and mass of adsorbent on the system performance were investigated. According to the results, COP values increased, achieved a peak value and then decreased as the maximum bed temperature increased. Cooling capacity increased with decreasing cycle time and increasing mass of adsorbent, while with longer cycle times better COP values could be attained. Finally, as the condensation temperature decreased, both COP and cooling capacity increased.

Wang et al. in 2005 developed an analytical model for a two-bed adsorption cooling cycle with silica gel – water pair [81]. Effects of heat and mass recovery and operating temperatures on the system performance were investigated. The highest COP was obtained when the maximum bed temperature was 80-85^{o}C for the investigated 65-85^{o}C range. However, mass recovery enhancement was more effective at low maximum bed temperatures. When the condensation temperature was 20^{o}C, the maximum predicted COP of the cycle was 0.65.

Another theoretical model for a solar-powered regenerative adsorption heat pump was developed by Lambert in 2007 [82]. The author suggested using activated carbon – ammonia pair with $CaCl_2$ additions. Therefore, within the system physical adsorption could be supported by chemical adsorption. As a result, the adsorption capacity of the pair increased by 35% on average. Detailed design parameters and corresponding mathematical model are presented in the provided reference. According to the results, a maximum COP of 1.604 was reported. Additionally, different types of solar collectors (single or double-glazed flat plate with or without coating, evacuated tube and parabolic concentrator) were compared under certain conditions and the highest solar thermal efficiency was obtained from evacuated tube collector while parabolic concentrator had second highest solar thermal efficiency.

Liu and Leong claimed that the condensation pressure is not constant as time progresses for the process 2→3 due to heat transfer limitations which were not included in previous studies. A numerical two-dimensional heat and mass transfer model that accounted for heat transfer limitations was developed by Liu and Leong in 2008 for a transient simple adsorption cooling cycle [83]. Contradictory to the authors' claim, the simulations results showed that the pressure in the condenser does not change significantly for the simple adsorption cycle and COP increases as mass flow rate within the condenser increases (in this model, systems with wet cooling tower was simulated).

A new design called an adsorption tube was developed by Wang and Zhang in 2009 [84]. An adsorption tube is actually an adsorption cooling (or heating) system that consists of an adsorbent bed, a condenser and an evaporator in a single tubular housing. In order to verify the accuracy of this new design, the authors analyzed the system with a numerical model. Although the system was small in size compared with the previous studies, the COP of the cycle for silica gel – water pair was approximately 0.5. The authors predicted that one of the main concerns would arise in the manufacturing process since a thin walled housing with low heat capacity is necessary in order to decrease the cycle time.

A solar-powered two-bed adsorption cooling cycle with heat and mass recovery was modeled for silica gel – water pair by Luo et al. in 2010 [85]. The COP values were predicted using energy balances with a maximum bed temperature range of 55-90^{o}C. The results predicted that a COP of the system higher than 0.25 can be achieved under fair solar radiation and with an evacuated tube collector. Results also stated that the evacuated tube collector always has higher thermal efficiencies than the flat plate collector for the investigated cases.

2.3 Adsorption Capacity Models

Adsorption capacity (X) models of adsorbent – refrigerant (working) pairs were developed and presented in the literature. More information on working pairs and the

properties of adsorbents and refrigerants can also be found in these review papers [24, 32, 33, 86, 87]. Only the final governing equations for these models are presented here for completeness and brevity.

In general, adsorption capacity (X) is characterized by temperature (T) and pressure (P) and given in form of Dubinin – Astakhov (D-A) equations [88]. There are two main D-A equations, Equations (2.44) and (2.45), to describe the adsorption capacity (X) as a function of temperature and pressure.

$$\mathrm{X}\left(T,P\right)=X_o\exp\left[-k\left(\frac{T}{\mathrm{T_{sat}}\left(P\right)}-1\right)^n\right] \tag{2.44}$$

$$\mathrm{X}\left(T,P\right)=X_o\exp\left[-D\left(T\ln\frac{P}{\mathrm{P_{sat}}\left(T\right)}\right)^n\right] \tag{2.45}$$

Working pairs which have been widely investigated and are well-established are chosen for the present study. Investigated pairs and their corresponding coefficients for D-A equations are given in Table 2.3.

Table 2.3. Coefficients for D-A equations [89].

Adsorbent – Refrigerant Pair	X_o	k	D	n
Zeolite NaX – Water (Z1) [90]	-	-	-	-
Zeolite X13 – Water (ZW) [24, 91]	0.261	5.36	-	1.73
Silica Gel – Water (SG) [24, 92]	0.350	-	6×10^{-6}	1.70
Activated Carbon – Ammonia (CA) [24, 93]	0.290	3.57	-	1.38
Activated Carbon – Methanol (CM) [24, 93]	0.450	13.38	-	1.50

One exception to using the D-A equation is for the zeolite NaX – water (Z1) pair. Its adsorption capacity model is presented in a different form and details are given in [90, 94]. The adsorption capacity model for zeolite NaX – water (Z1) pair is described with Equations (2.46) through (2.49).

$$ns_j = a_{1,j} + \frac{a_{2,j}}{T} + \frac{a_{3,j}}{T^2} + \frac{a_{4,j}}{T^3} \quad , \quad for \quad j = 1,2 \tag{2.46}$$

$$ns_3 = d - ns_1 - ns_2 \tag{2.47}$$

$$b_j = b_{o,j} \exp\left(\frac{E_j}{T}\right) \quad , \quad for \quad j = 1,2,3 \tag{2.48}$$

$$X = \sum_{j=1}^{3} ns_j b_j \frac{P}{1 + b_j P} \tag{2.49}$$

The constants in Equations (2.46)-(2.49) are given in Table 2.4.

Table 2.4. Coefficients for adsorption capacity model of zeolite NaX – water pair [90, 94].

j	***a₁***	***a₂***	***a₃***	***a₄***	***b₀***	***E***	***d***
1	0.070	-119.9	63690	-8450000	1.508×10^{-10}	7726	0.267
2	-0.687	775.7	-254200	27750000	5.407×10^{-10}	6075	
3	-	-	-	-	1.708×10^{-10}	5392	

In the adsorption cycle models, there are several other constants that are specific to the adsorbent – refrigerant pair. These constants are heat of adsorption (Δh_{ads}) [87, 95], specific heats of adsorbent (c_{ads}) and refrigerant vapor (c_p) and the enthalpy of vaporization (h_{fg}) and are given in Table 2.5.

Table 2.5. Constants for adsorption cycle models [89].

Adsorbent – Refrigerant Pair	Δh_{ads} **[kJ/kg]**	c_{ads} **[kJ/kg·K]**	c_{liq} **[kJ/kg·K]**	c_p **[kJ/kg·K]**	h_{fg} **[kJ/kg]**
Activated Carbon – Ammonia (CA) [24, 93]	1900	0.930	4.84	2.13	1225.03
Activated Carbon – Methanol (CM) [24, 93]	1900	0.930	1.405	1.405	1200
Silica Gel – Water (SG) [24, 92]	2500	1.000	4.2	1.8644	2476.9
Zeolite NaX – Water (Z1) [90]	3200	0.836	4.2	1.8644	2476.9
Zeolite X13 – Water (ZW) [24, 91]	3750	0.836	4.2	1.8644	2476.9

The working pairs given in Table 2.3 and the zeolite NaX – water pair are embedded in the adsorption cycle models stated in Sections 2.2.3 and 3.1.

2.3.1 Previous Studies on Working Pair Comparison

A number of studies on working pair comparison are presented in the literature. In this section, some of the results from those papers are given chronologically. As before, more explanations about each paper can be found in the provided references.

Performance of simple and heat recovery adsorption cycles are simulated by Wang et al. in 1997 for granular and activated carbon fiber – methanol pairs [96]. According to the results, COP was increased by almost 20% with the addition of heat recovery with two adsorbent beds, and COP values of systems with activated carbon fiber were 15% higher on average than systems with granular activated carbon.

Effects of adding salts such as $CaCl_2$, LiBr, LiCl, $MgCl_2$ into the well-established adsorbents such as silica gel, activated carbon, zeolite on the performance of simple cycle were analyzed by Restuccia et al. in 2004 [97]. The experimental results were also supported by a theoretical study, and as a result, addition of salts improved the COP values of the simple adsorption cycle by 30% for cooling and 60% for heating cycles when zeolite 4A – water and silica gel – water pairs were considered at the same conditions.

The previous approach was also experimentally analyzed by Wang et al. in 2004 [98]. They suggested adding activated carbon to $CaCl_2$ to form a new hybrid adsorbent for ice-making in adsorption refrigeration cycle where ammonia was selected as refrigerant. As the experimental results showed, addition of activated carbon to $CaCl_2$ increased the adsorption capacity until a maximum value. Therefore, there was an optimum addition level of activated carbon to obtain the best performance among the investigated conditions. The authors stated that adding activated carbon increased the mass transfer inside the adsorbent bed.

Cui et al. in 2005 compared several adsorbent – refrigerant pairs, with adsorbents as zeolite 13X, silica gel, activated carbon and composite adsorbents developed by the authors (NA and NB) and refrigerants as water and ethanol [99]. Adsorption and cooling capacities of these working pairs were tested experimentally where cooling capacity was defined as the adsorption swing of the adsorption capacity times the latent heat of adsorbent. The result of this study stated that NA – water pair had almost 2.5 times higher adsorption capacity as zeolite 13X – water pair had. Similarly, NB – ethanol pair had 3 times higher adsorption capacity than activated carbon – ethanol pair. These results are also valid for cooling capacities.

A numerical study of adsorption refrigeration cycles with two types of activated carbon fiber – methanol pairs were done by Hamamoto et al. in 2006 [100]. Specific cooling effects and coefficient of performances for simple adsorption cycle with two adsorbent beds were compared within two activated carbon fiber – methanol pairs and also with silica gel – methanol pair. The results stated that activated carbon fiber

– methanol and silica gel – methanol pairs have distinct ranges of operating conditions ranges where COP values of one pair is higher than others.

Saha et al. in 2006 investigated the adsorption performances of silica gel – water, activated carbon – ethanol and activated carbon – HFC 134a [101]. The conditions were selected as evaporation temperature at 7^{o}C, condensation temperature at 30^{o}C and the maximum bed temperature range between 50-90^{o}C. Results are given in terms of isentropic efficiency and uptake efficiency which is a function of adsorption capacity. According to the results, isentropic efficiency decreases as the maximum bed temperature increases.

Different activated carbon types with ethanol as refrigerant were experimentally tested by El-Sharkawy et al. in 2008 [102]. As a result, correlations for adsorption capacities for these pairs were obtained using D-A equations. Clapeyron diagrams were also obtained for the investigated working pairs.

Loh et al. in 2009 analyzed six different pairs theoretically for simple adsorption cycles [103]. These pairs included two different activated carbon fiber – ethanol, chemviron – R134a, fluka – R134a and maxsorbll – R134a. According to this study's results, as the maximum bed temperature increases, the COP values of the simple cycle also increases. For the investigated two activated carbon fiber – ethanol pairs, maximum COP values were 0.56 and 0.68 where the maximum bed temperature was 85^{o}C. For the silica gel – water pair, the maximum COP value at 85^{o}C maximum bed temperature was 0.68. Results also showed that activated carbon – ethanol pair has the highest specific cooling power while silica gel – water pair gives the highest cooling effect per unit volume of adsorbent.

2.4 TRNSYS Software

TRNSYS is a FORTRAN-based simulation software that is used throughout the present study. The name TRNSYS stands for the Transient Energy System Simulation tool [104]. This software is commercially available since 1975 and developed by the

members of Solar Energy Laboratory at the University of Wisconsin – Madison. However, the foundation of the software was a joint project between the University of Wisconsin – Madison and the University of Colorado [105].

In general, TRNSYS is a tool that is used to simulate the performance of transient energy systems, especially thermal systems. TRNSYS includes several built-in components which can be used for constructing the desired systems with ease. These components generally include algebraic or differential equations which are also solved numerically within the software. One of the strengths of this software is that other companies (such as TESS – Thermal Energy System Specialists, Inc. [106]) also develop other components which are not available in the default library of the software as it is purchased. Additionally, users can develop their own components with the provided source codes. Using this software, the users are able to;

- display the simulation results as the simulation continues so that users do not have to wait for the whole simulation to be completed,
- provide inputs to the software with simple text files and get the outputs as formatted spreadsheets,
- form complex user graphical interfaces which allow users to enter inputs and get the predefined outputs,
- finalize the model with executable files
- call some other software, such as MATLAB, Fluent and Excel, within TRNSYS.

More details on this software can be found on these websites [105-107].

2.5 Objectives of the Present Study

Models for the ideal simple adsorption cycle, the ideal heat recovery adsorption cycle with two spatially isothermal beds and ideal thermal wave model exist in the literature with corresponding analyses. The present study builds on these aforementioned existing works by:

- Implementing the existing adsorption cycle models into a TRNSYS-compatible environment via MATLAB
- Extending the thermal wave model to include adiabatic and isothermal mass recovery with or without by-pass line
- Modeling the following commonly-used adsorbent – refrigerant (working) pairs using MATLAB
    - Zeolite NaX – Water
    - Zeolite X13 – Water
    - Silica Gel – Water
    - Activated Carbon – Ammonia
    - Activated Carbon – Methanol
- Constructing a solar thermal system model within TRNSYS that can be used both for steady and seasonal-transient simulations
- Integrating three (two flat plate and one evacuated tube) commercial collector models with the solar thermal system
- Developing a normalized seasonal model where solar and loss fractions, collector area and mass of adsorbent can be analyzed
- Linking the adsorption cycle models with working pair models and the solar thermal system to construct solar-thermal-powered adsorption cooling system
- Running steady and seasonal-transient simulations
- Investigating basic trends in the cycle and system performances as the following parameters are varied
    - Maximum bed temperature
    - Condensation temperature
    - Evaporation temperature
    - Heat capacity ratio
    - Excess bed temperature

CHAPTER 3

MODELS

The models presented in this chapter are extensions of models previously published or under revision by Taylan, Baker and Kaftanoğlu [44, 89, 108] and build on the models presented in Chapter 2.

3.1 Modifications on Thermal Wave Adsorption Cooling Cycle Model

In this section, definitions and thermodynamic models of analyzed adsorption cycles are given. In all models, the following assumptions are considered.

- Constant specific heat and heat of adsorption
- Refrigerant vapor as an ideal gas
- Mass of refrigerant vapor in the adsorbent bed is negligible relative to that in the liquid and adsorbed phrases.
- The modeled adsorbent beds are assumed to be spatially isobaric.
- Enthalpy change in throttling is neglected.
- Specific heat of adsorbed refrigerant is assumed to be equal to the specific heat of refrigerant vapor to be consistent with the 1st Law of Thermodynamics [90].

Three thermal wave cycles are considered within this study: (1) no mass recovery (NMR); (2) adiabatic mass recovery (AMR); and, (3) isothermal mass recovery (IMR). For the no mass recovery thermal wave cycle (NMR), the vapor line and mass recovery valve connecting the two beds in Figure 2.6 do not exist. For the mass recovery cycles, mass recovery occurs at the end of each half cycle when the hot,

high-pressure bed is at T_{hot} and P_{cond}, and the cold, low-pressure bed is at T_o and $P_{evap} < P_{cond}$. During the mass recovery process, the two beds are isolated from the condenser and evaporator, and the mass recovery valve is opened. Refrigerant vapor flows from the hot, high-pressure bed to the cold, low-pressure bed until the two reach the same pressure. Adiabatic mass recovery (AMR) and isothermal mass recovery (IMR) thermal wave cycles represent two limiting cases. For AMR, each bed undergoes an adiabatic mass recovery process, which is equivalent to the heat transfer fluid (HTF) pump being turned off. For IMR, each bed undergoes an isothermal mass recovery process, which is equivalent to the HTF pump being left on. Clapeyron diagrams for both back and front regions of NMR, AMR and IMR are given in Figure 3.1 and Figure 3.2, respectively.

3.1.1 Thermal Wave Adsorption Cooling Cycle with Adiabatic Mass Recovery (AMR)

For the mass recovery cycles, at the end of the half cycles (states 1 and 3) the valves connecting the beds to the condenser and evaporator are closed, and the mass recovery valve connecting the beds is opened to allow refrigerant vapor to flow from the high pressure to the low pressure bed. For AMR, the beds are assumed adiabatic throughout the mass recovery process, and therefore, there is no heat exchange with the HTF. For the back region, as shown in Figure 3.1, the processes 1→2 and 3→4 in NMR are divided into the two processes 1→a1→a1$^+$→2 and 3→a3→a3$^+$→4. Similarly, for the front region the corresponding processes and states for AMR are 1→a1→a2 and 3→a3→a4 as shown in Figure 3.2.

For the processes 1→a1 and 3→a3 (i.e., the mass recovery processes), assuming that all the refrigerant desorbed in the high-pressure bed will be adsorbed by the low-pressure bed as suggested by [37],

$$\Delta X_m = \left| X_m - X_{min} \right| = \left| X_n - X_{max} \right| = \Delta X_n \tag{3.1}$$

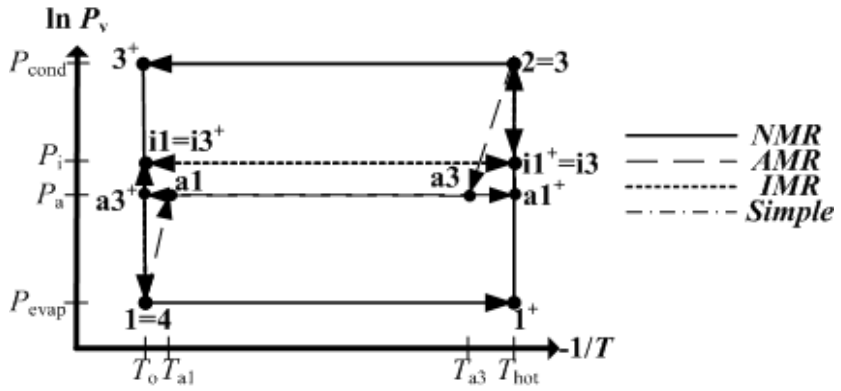

Figure 3.1. Clapeyron diagram for back region of thermal wave adsorption cycles (Notation for States: # = NMR, a# = AMR, i# = IMR, s# = Simple Cycle, while $a\#^+$ and $i\#^+$ occur immediately after corresponding a# and i#) [44].

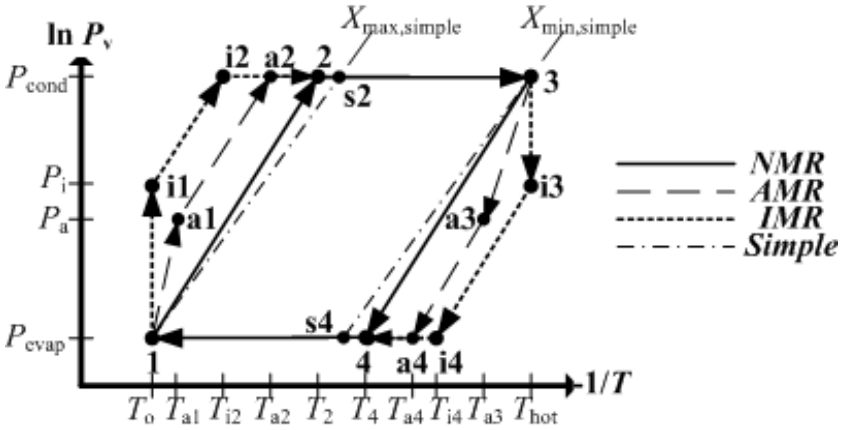

Figure 3.2. Clapeyron diagram for front region of thermal wave adsorption cycles (Notation for States: # = NMR, a# = AMR, i# = IMR, s# = Simple Cycle) [44].

where subscripts *m* and *n* denote the low-pressure and high-pressure beds, respectively.

Defining the final common pressure as $P_a = P_{a1} = P_{a3}$, and referring to Figure 3.1 and Figure 3.2, yields,

$$\mathrm{X}\left(T_{a1}, P_a\right) - \mathrm{X}\left(T_o, P_{evap}\right) = \mathrm{X}\left(T_{hot}, P_{cond}\right) - \mathrm{X}\left(T_{a2}, P_a\right) \tag{3.2}$$

The exact path for the mass recovery process is defined by assuming the refrigerant vapor entering the low-pressure bed is at the same temperature as the high-pressure bed,

$$h_v \mathrm{d}m_v = \left(R+1\right)\mathrm{d}\left(m_{ads}u_{ads}\right) + \mathrm{d}\left(u_{ref}m_{ref}\right) \tag{3.3}$$

Note that the masses of adsorbent in both beds are constant, i.e., dm_{ads} = 0. Using the definition of adsorption capacity, X,

$$h_v m_{ads}\mathrm{d}X_m = \left(R+1\right)m_{ads}\mathrm{d}u_{ads} + m_{ads}X_m\mathrm{d}u_{ref} + m_{ads}u_{ref}\mathrm{d}X_m \tag{3.4}$$

Canceling out m_{ads} in all terms and rearranging Equation (3.4),

$$\left(R+1\right)\mathrm{d}u_{ads} + X_m\mathrm{d}u_{ref} + \left[\mathrm{u}_{\mathrm{ref}}\left(T_m\right) - \mathrm{h}_{\mathrm{v}}\left(T_n\right)\right]\mathrm{d}X_m = 0 \tag{3.5}$$

Note that the refrigerant vapor enters the low-pressure bed at T_n, while the adsorbent bed itself is at T_m. Adding $\pm\mathrm{h}_{\mathrm{v}}\left(T_m\right)\mathrm{d}X_m$ to Equation (3.5) yields,

$$\left(R+1\right)\mathrm{d}u_{ads} + X_m\mathrm{d}u_{ref} + \left[\mathrm{u}_{\mathrm{ref}}\left(T_m\right) - \mathrm{h}_{\mathrm{v}}\left(T_m\right) + \mathrm{h}_{\mathrm{v}}\left(T_m\right) - \mathrm{h}_{\mathrm{v}}\left(T_n\right)\right]\mathrm{d}X_m = 0 \tag{3.6}$$

Applying constant specific heats to Equation (3.6) gives,

$$\left(R+1\right)c_{ads}\mathrm{d}T_m + X_m c_{ref}\mathrm{d}T_m + \left[\Delta h_{ads} + c_p\left(T_m - T_n\right)\right]\mathrm{d}X_m = 0 \tag{3.7}$$

Arranging terms in Equation (3.7) yields,

$$\left[\left(R+1\right)c_{ads} + c_p X_m\right]\mathrm{d}T_m + \left[\Delta h_{ads} + c_p\left(T_m - T_n\right)\right]\mathrm{d}X_m = 0 \tag{3.8}$$

A parallel set of equations similar to Equations (3.3)-(3.8) can be derived for the high-pressure bed, except for the high-pressure bed the refrigerant vapor leaves the adsorbent bed at T_n,

$$\left[c_{ads}\left(R+1\right)+c_p X_n\right]\mathrm{d}T_n+\Delta h_{ads}\mathrm{d}X_n=0 \tag{3.9}$$

The processes a1→a1$^+$→2, a3→a3$^+$→4, a1→a2 and a3→a4 in Figure 3.1 and Figure 3.2 are identical to processes 1→2 and 3→4 of NMR, except they start at T_{a1} and P_a, and T_{a3} and P_a. Therefore, the model for these processes is parallel to Equations (2.15)-(2.42).

3.1.2 Thermal Wave Adsorption Cooling Cycle with Isothermal Mass Recovery (IMR)

Modeling the mass recovery processes for IMR is similar to that with AMR except the adsorbent beds are assumed isothermal through heat exchange with the HTF. Therefore, the model is parallel to Equations (2.15)-(2.42) except the adsorbent beds are kept both spatially and temporally isothermal during the mass recovery process. Unlike AMR, to keep both beds at constant temperatures requires heat transfer to occur to the hot bed and from the cold bed during the mass recovery process. The heat transfer per unit mass of adsorbent can be calculated for the low-pressure bed similar to Equation (3.8) as,

$$\frac{q_{bed,1\to i1}}{m_{ads}}=\int_1^{\mathrm{i1}}\left[\Delta h_{ads}+c_p\left(T_o-T_{hot}\right)\right]\mathrm{d}X \tag{3.10}$$

since the refrigerant enters the low-pressure bed at T_{hot} = T_3. Similar to Equations (3.9) and (3.10), for the high-pressure bed,

$$\frac{q_{bed,3\to i3}}{m_{ads}}=\int_3^{\mathrm{i3}}\Delta h_{ads}\mathrm{d}X \tag{3.11}$$

The processes i1→i1^{+}→2, i3→i3^{+}→4, i1→i2 and i3→i4 in Figure 3.1 and Figure 3.2 are parallel to processes 1→2 and 3→4 of NMR, except the processes start at $T_{i1} = T_1$ and P_i, and $T_{i3} = T_3$ and P_i, respectively.

3.2 Solar Thermal System Model

The solar thermal system consists of a solar thermal collector, a heat exchanger, a circulation pump and a control unit. Details of each component are given in the following subsections. The solar thermal system is modeled in TRNSYS, and built-in types of TRNSYS are used to model these components. The schematic presentation of the solar thermal system is given in Figure 3.3.

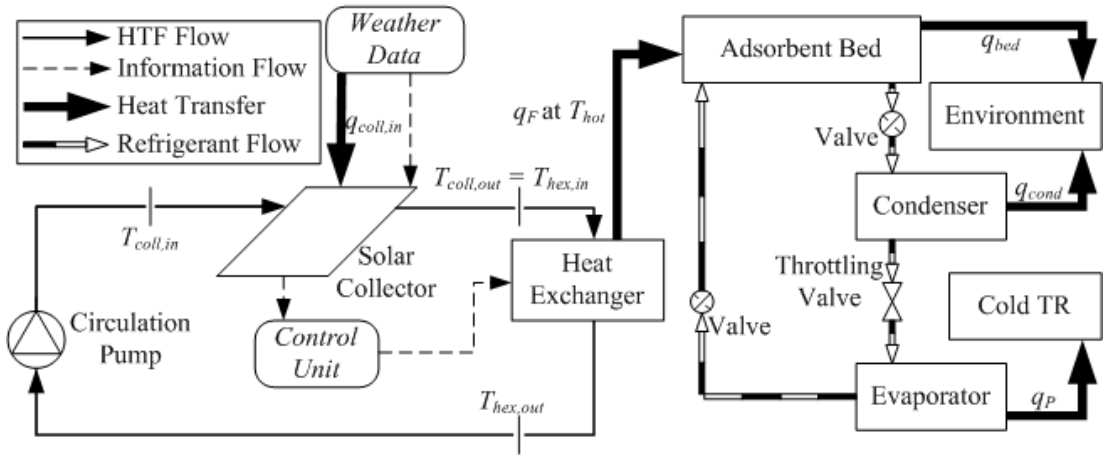

Figure 3.3. Solar thermal system and its integration with the adsorption cycle [89].

A TRNSYS screen capture of the solar thermal system is also given in Figure 3.4. In Figure 3.4, the solid lines represent the flow loop of the working fluid and the dashed lines represent the information flow between the TRNSYS components.

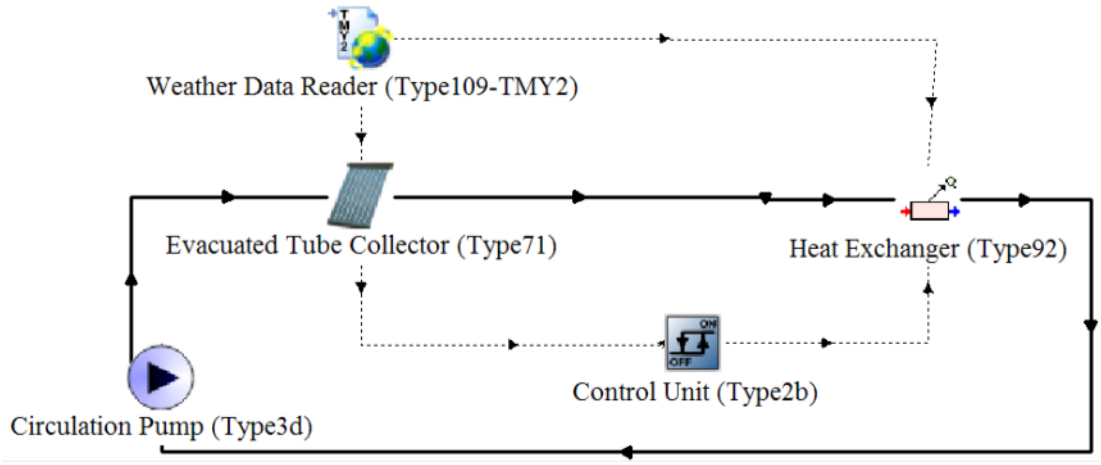

Figure 3.4. TRNSYS screen capture of the solar thermal system.

3.2.1 Solar Thermal Collectors

The solar thermal collector is one of the essential components of the solar thermal powered adsorption cooling system. Two flat plate collectors (coded as FPL and FP) and one evacuated tube collector (coded as ET) are modeled using built-in TRNSYS types. The collectors' corresponding performance parameters are obtained from commercial solar thermal collectors and these parameters are given in the following two subsections. The manufacturers of these collectors are not provided so as not to commercialize the present study.

a. Flat plate solar collectors

TRNSYS built-in component Type 1c is used to model the flat plate collectors. This component is based on the second order efficiency formula which is given in Equation (3.12). The form of this equation is based on ASHRAE 93-77 and 96-1980 standards and most of the collector manufacturers use this form of the efficiency relation to get solar certification for their collectors [109].

$$\eta_{coll} = d_0 - d_1 \frac{T_{mean} - T_{amb}}{G} - d_2 \frac{\left(T_{mean} - T_{amb}\right)^2}{G} \tag{3.12}$$

η_{coll} is the thermal efficiency of the solar collector, T_{mean} (^{o}C) is the mean temperature of the inlet and outlet temperatures of the solar collector, T_{amb} (^{o}C) is the ambient temperature, G (W/m^2) is the solar radiation on the solar collector and d_0, d_1 and d_2 are performance coefficients that are given for a specific solar collector. The performance coefficients that are used in modeling are given in Table 3.1.

Table 3.1. Performance coefficients for the flat plate solar collectors.

Collector Code	FPL	FP
Conversion Coefficient $d_0\,(-)$	0.780	0.751
Loss Coefficient $d_1\left(\mathrm{W}/\mathrm{m}^2\cdot\mathrm{K}\right)$	3.591	4.999
Loss Coefficient $d_2\left(\mathrm{W}/\mathrm{m}^2\cdot\mathrm{K}^2\right)$	0.0199	0.000

The other parameters that are required to model flat plate solar collectors are given in Table 3.2.

Table 3.2. Other necessary parameters for the flat plate solar collectors.

Collector Code	FPL	FP
Collector Area $\left(\mathrm{m}^2\right)$	1.912	1.620
Specific Heat of Working Fluid $\left(\mathrm{kJ}/\mathrm{kg}\cdot\mathrm{K}\right)$	4.190	4.190
Tested Flow Rate $\left(\mathrm{kg}/\mathrm{h}\cdot\mathrm{m}^2\right)$	74.791	53.500

The final parameters required to model the flat plate collectors using TRNSYS Type 1c are the Incidence Angle Modifiers (IAM). The Incidence Angle Modifiers define the fraction of radiation incident on the collector cover that reaches the absorber of the collector. The modifier is one when the collector cover transmits all solar radiation, and it is zero when the collector cover does not transmit any solar radiation. According to ASHRAE standards, incidence angle modifiers include both direct and diffuse light modifiers [109]. The IAM values that are used in modeled flat plate collectors are given in Table 3.3.

Table 3.3. Incidence angle modifiers for the flat plate collectors.

Collector Code	FPL							
Incidence Angle	0^o			50^o			90^o	
IAM	1.000			0.865			0.000	
Collector Code	FP							
Incidence Angle	0^o	20^o	30^o	40^o	50^o	60^o	70^o	90^o
IAM	1.000	0.983	0.958	0.918	0.851	0.732	0.484	0.000

b. Evacuated tube solar collector

TRNSYS built-in component Type 71 is used to model an evacuated tube collector. This component also uses the second order efficiency formula as given in Equation (3.12). One of the main differences between the flat plat collector and evacuated tube collector models is the Incidence Angle Modifiers (IAM). Evacuated tube collectors require biaxial (both longitudinal and transverse) IAM values while flat plate collectors require only one dimensional IAM values. The parameters that are used to model the commercial evacuated tube solar collector in TRNSYS Type 71 are given in Table 3.4.

Table 3.4. Parameters for the evacuated tube solar collector.

Collector Code	ET
Conversion Coefficient $d_0\,(-)$	0.825
Loss Coefficient $d_1\left(\mathrm{W}/\mathrm{m^2\cdot K}\right)$	1.190
Loss Coefficient $d_2\left(\mathrm{W}/\mathrm{m^2\cdot K^2}\right)$	0.009
Collector Areas $\left(\mathrm{m^2}\right)$	2.000
Specific Heat of Working Fluid $\left(\mathrm{kJ}/\mathrm{kg\cdot K}\right)$	4.190
Tested Flow Rate $\left(\mathrm{kg}/\mathrm{h\cdot m^2}\right)$	3.0 (TRNSYS Default Value)

3.2.2 Heat Exchanger

TRNSYS built-in component Type 92 is used to model the heat exchanger shown in Figure 3.3. The main purpose of using this heat exchanger in the solar thermal system is to provide the heat transfer that is required to drive the adsorption cooling cycle (q_F). The hot working fluid that exits the solar collector provides the required q_F as shown in Figure 3.3. TRNSYS Type 92 also has an internal on-off controller whose control signal can be sent externally, and this signal is sent by the control unit as shown in Figure 3.3. The parameters of the modeled heat exchanger are given in Table 3.5. Note that in order to analyze the limits of solar thermal system, the maximum capacity of the heat exchanger is chosen as a very large value and all the losses in heat exchanger are neglected.

Table 3.5. Parameters for the heat exchanger.

Maximum Capacity $\left(\frac{kJ}{h}\right)$	100,000
Specific Heat of Working Fluid $\left(\frac{kJ}{kg \cdot K}\right)$	4.190
Loss Coefficient $\left(\frac{kJ}{h \cdot K}\right)$	0.000
Heat Exchanger Efficiency (-)	1.000

3.2.3 Circulation Pump

TRNSYS built-in component Type 3d is used to model the circulation pump in Figure 3.3. Although this component has the capability to vary the flow rate of the working fluid that is circulating in the loop shown in Figure 3.3, in this solar thermal system the flow rate is kept constant. As in the heat exchanger, all the losses in the circulation pump are neglected. The parameters that are used to model the circulation pump are given in Table 3.6.

Table 3.6. Parameters for the circulation pump.

Maximum Flow Rate $\left(\frac{kg}{h}\right)$	100
Specific Heat of Working Fluid $\left(\frac{kJ}{kg \cdot K}\right)$	4.190
Maximum Power $\left(\frac{kJ}{h}\right)$	60
Loss Coefficient (-)	0

3.2.4 Control Unit

TRNSYS built-in component Type 2b is used to model the control unit shown in Figure 3.3. This control unit is added to the solar thermal system to fix the temperature at which the heat transfer that is required to drive the adsorption cooling cycle (q_F) occurs since in the modeled ideal adsorption cooling system this temperature is kept constant at the maximum bed temperature (T_{hot}).

The operating principle of this control unit is as follows: If the outlet temperature of the solar collector is higher than the initially set T_{hot}, the control unit turns on the heat exchanger and the outlet temperature of the heat exchanger becomes the set T_{hot}. On the other hand, if the outlet temperature of the solar collector is lower than the initially set T_{hot}, the control unit turns off the heat exchanger and the adsorption cycle does not operate until the outlet temperature of the solar collector reaches T_{hot}.

3.2.5 Weather Data

In addition to the units that are described in the preceding subsections, another TRNSYS built-in component Type 109-TMY is used to obtain the meteorological data (for instance, ambient temperature and solar radiation). TMY stands for Typical Meteorological Year, and all the meteorological data that are in TMY format can be read by TRNSYS Type 109-TMY.

3.2.6 Integration of Solar Thermal System with Adsorption Cycle Models

As mentioned in the preceding sections, adsorption cooling cycles are modeled in MATLAB and the solar thermal system is modeled in TRNSYS. The TRNSYS screen of the integration of the solar thermal system and adsorption cooling cycle models is given in Figure 3.5. In Figure 3.5, Macro is the solar thermal system as shown in Figure 3.4, Type 155 is the component that is used to run MATLAB commands, Equa includes the cells to enter the inputs to the system, Equa-2 has the formulation to calculate the system efficiency, Type 65d shows the requested outputs to

show on the screen and Type 25c writes all the outputs to a specified Microsoft Excel file. A sample TRNSYS deck (input) file for a solar system integrated thermal wave cycle with evacuated tube collector is given in Appendix A and TRNSYS Studio Report that shows the relations between the TRNSYS components is given in Appendix B for the same system.

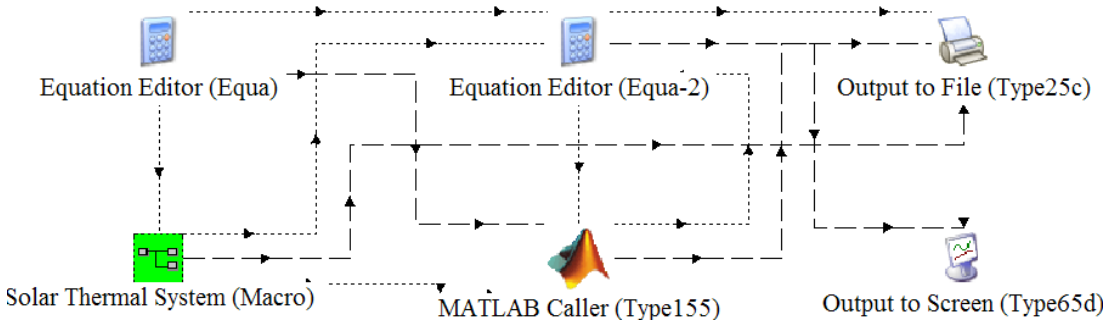

Figure 3.5. Integration of solar thermal system with adsorption cycle in TRNSYS.

As mentioned in Appendix B, the inputs for the integrated TRNSYS model are,

- Adsorbent – refrigerant pair
- Minimum adsorbent bed temperature (T_o)
- Maximum adsorbent bed temperature (T_{hot})
- Condensation temperature (T_{cond})
- Evaporation temperature (T_{evap})
- Ratio of bed's design to inherent heat capacities (R) defined as

$$R = \left(m_{shell}c_{shell} + m_{HTF}c_{HTF}\right)\left(m_{ads}c_{ads}\right)^{-1}$$

The coefficient of performance of the adsorption cooling cycle (COP_{ads}) and the efficiency of the solar thermal collector (η_{coll}) are obtained as outputs of the integrated TRNSYS model, and the overall system efficiency (COP_{sys}) is calculated by multiplying the coefficient of performance of adsorption cooling cycle (COP_{ads}) by the efficiency of solar thermal collector (η_{coll}).

3.3 Normalized Model

A new normalized model is developed for post-processing of the simulation results. The normalized model is used to investigate how the size of the cooling system, amount of storage, and coincidence between the solar-supplied cooling and cooling demand affects the system's seasonal energy performance. In all cases this normalized model stresses simplicity over detail to quickly identify the most promising directions for more detailed research.

Several normalized transient parameters are defined at each time step (t_i). A normalized cooling load ($q_{load,N}$) is defined as being proportional to the temperature difference between T_{amb} and a reference temperature (T_{rfrc}).

$$\mathrm{q}_{\mathrm{load,N}}\left(t_i\right) = \frac{\mathrm{T}_{\mathrm{amb}}\left(t_i\right) - T_{rfrc}}{\mathrm{Max}\left(T_{amb} - T_{rfrc}\right)} \tag{3.13}$$

Here Max($T_{amb} - T_{rfrc}$) corresponds to the time interval during the simulation with the highest T_{amb}, and therefore maximum cooling load, and $0 \le q_{load,N} \le 1$. A normalized cooling capacity ($q_{clg,N}$) is defined as,

$$\mathrm{q}_{\mathrm{clg,N}}\left(t_i\right) = S\,\frac{\mathrm{q}_{\mathrm{F}}\left(t_i\right)\mathrm{COP}_{\mathrm{ads}}\left(t_i\right)}{\mathrm{Max}\left(q_F COP_{ads}\right)} \tag{3.14}$$

where S is a user defined size of the cooling system and $0 \le q_{clg,N} \le S$. Additionally, the required heat transfer is calculated using $q_F = \dot{m}_{HTF} c_{p,HTF}\left(T_{hex,in} - T_{hex,out}\right)$ where HTF is the heat transfer fluid of the solar thermal system as shown in Figure 3.3. By definition, one unit of normalized load is equal to one unit of normalized cooling capacity and $S > 1$ corresponds to the common case where the maximum output of the cooling system is larger than the maximum cooling load, which allows for storage. At each time step, the transient parameter $q_{Match,N}$ is used to quantify the differences in the magnitudes of the normalized load and normalized cooling capacity as,

$$q_{\text{Match,N}}(t_i) = q_{\text{clg,N}}(t_i) - q_{\text{load,N}}(t_i) \tag{3.15}$$

Thus $q_{Match,N} < 0$ indicates the case where backup cooling or storage is needed to meet the cooling load while $q_{Match,N} > 0$ indicates an opportunity for storage. Three normalized parameters are defined to investigate how the amount of storage affects broad trends in the system's seasonal energy performance. To keep the model as simple as possible, only the storage magnitude and not type (hot/cold storage, building thermal mass, etc.) is specified. The user inputted normalized storage magnitude, $q_{Storage,max}$, is defined such that one unit of normalized storage ($q_{Storage,N}$) is equal to one unit of normalized cooling load (and capacity). At the start of each simulation the storage is assumed empty; i.e., $q_{\text{Storage,N}}(t=0) = 0$. A normalized loss, $q_{Loss,N}$, quantifies the solar-supplied cooling lost to the environment when $q_{clg,N} > q_{load,N}$ and the storage is full. The normalized backup power, $q_{Backup,N}$, quantifies the backup cooling power required when $q_{clg,N} < q_{load,N}$ and $q_{Storage,N} = 0$.

For each simulation, solar and loss fractions are defined as additional seasonal energy performance parameters. The solar fraction (f) is the normalized load met by solar energy.

$$f = \frac{q_{clg,tot}}{q_{load,tot}} = \frac{\sum_i q_{\text{clg,N}}(t_i)}{\sum_i q_{\text{load,N}}(t_i)} \tag{3.16}$$

The loss fraction, l, is defined as,

$$l = \frac{q_{Loss,tot}}{q_{load,tot}} = \frac{\sum_i q_{\text{Loss,N}}(t_i)}{\sum_i q_{\text{load,N}}(t_i)} \tag{3.17}$$

Similar to the transient and seasonal energy performance parameters, two normalized size parameters for collector area and mass of adsorbent are also defined. A normalized collector area ($A_{coll,N}$) is defined as,

$$A_{coll,N} = \frac{\mathrm{q}_{\mathrm{clg,N}}(t_i)}{\mathrm{G}_{\mathrm{N}}(t_i)\mathrm{COP}_{\mathrm{sys}}(t_i)} \tag{3.18}$$

where $\mathrm{G}_{\mathrm{N}}(t_i) = \mathrm{G}(t_i)/G_{rfrc}$ is the normalized solar radiation and G_{rfrc} is a reference solar radiation level. Therefore, one unit of normalized collector area supplies one unit of normalized cooling capacity when both G_N and COP_{sys} are one. As a normalized area, $A_{coll,N}$ can be used to compare the relative required collector area to meet the cooling load for different cases. $A_{coll,N}$ is constant in each individual case but varies among the investigated cases.

Similar to the normalized collector area, a normalized mass of adsorbent ($m_{ads,N}$) is defined. As an intermittent cooling cycle, the required $m_{ads,N}$ decreases with decreasing cycle time. For simplicity in these analyses all cycle times are assumed equal. The required $m_{ads,N}$ is inversely proportional to maximum change in adsorption capacity of the adsorbent over the half cycle ($\Delta X = X_{max} - X_{min}$) during the simulation relative to that for a base case (ΔX_{base}).

$$m_{ads,N} = \left[\frac{\mathrm{Max}(\Delta X)}{\Delta X_{base}}\right]^{-1} \tag{3.19}$$

CHAPTER 4

ANALYSES AND VERIFICATION

The information presented in this chapter is an extension of that previously published or under revision by Taylan, Baker and Kaftanoğlu [44, 89, 108].

4.1 Analyses

A number of steady and seasonal-transient simulations are run using the modeled system described in detail in Section 2.2.3 and Chapter 3 to investigate general energy performance trends while several parameters are varied. Seasonal transient simulations are run with 15-minute time intervals over an entire summer from June 1 to September 30 using hourly weather data for Antalya, a city on Turkey's Mediterranean coast, using the typical meteorological year format as described in Section 3.2.5. In all simulations, liquid water is used as heat transfer fluid (HTF), and its properties are taken from [21, 110].

As pointed out in previous studies [44, 108], system performance depends on several parameters in addition to the working pair. In all simulations, the energy performance characteristics of either a flat plate or evacuated tube non-tracking solar collector located on the roof of the Mechanical Engineering Department at the Middle East Technical University are used. The energy performance characteristics for these collectors obtained from their manufacturers are given in Section 3.2.1. Another investigated parameter is the condensation temperature (T_{cond}) (or cooling tower type). The effect of using a dry rather than wet cooling tower due to concerns over water consumption is investigated through the condensation temperature. The condensation temperature is set equal to either ambient temperature (which corresponds to using an ideal dry cooling tower) or wet bulb temperature (which corresponds to using an

ideal wet cooling tower). Evaporation temperature (T_{evap}) is also investigated, and it is fixed by the application of the cooling system (i.e., the required temperature for cooling). The investigated values of the heat capacity ratio of the adsorbent bed (R) correspond to the theoretical limit (R = 0), state-of-the-art design (R = 3) and typical design (R = 10) [38]. Minimum and maximum bed temperatures are also investigated. It is theoretically possible to cool down the adsorbent bed to the condensation temperature. However, in reality due to the heat capacities of the system and some other design restrictions, the possible lowest temperature of the adsorbent bed (T_o) may be larger than the condensation temperature (T_{cond}). In order to consider this condition, ΔT_{excess} is defined as $\Delta T_{excess} = T_o - T_{cond}$. Maximum bed temperature (T_{hot}) is dependent on the working pair. Analyzed values for these parameters with the investigated working pairs are summarized in Table 4.1.

In order to determine T_{hot} ranges for a specific working pair, two main criteria are applied to the adsorption capacity models of the pairs given in Table 4.1. One criterion is based on a minimum adsorption capacity swing for a half cycle, $\mathrm{Min}\left(\Delta X_{cycle}\right) = X_{max} - X_{min} = 0.03$, since cooling capacity is directly proportional to ΔX, and operating the cycle with low ΔX values will not be advantageous. The other criterion is applied to X_{min}. X_{min} values that are lower than 0.03 are disregarded since adsorption capacities (X) approach to some value (in this study this value is chosen as 0.03) asymptotically (i.e., zero adsorption capacity is physically not possible) and very small X values require large increases in temperature. Additionally, in order to eliminate inconsistencies embedded in the adsorption capacity models, X_{max} values that are higher than $\mathrm{X}\left(T_o, P_{evap}\right) = \mathrm{X}\left(25^{\circ}\mathrm{C}, \mathrm{P_{sat}}\left(T_{evap} = 15^{\circ}\mathrm{C}\right)\right)$ are eliminated, as among the investigated conditions given in Table 4.1, the maximum X value can be obtained with $T_o = 25^{\circ}\mathrm{C}$ and $P_{evap} = \mathrm{P_{sat}}\left(T_{evap} = 15^{\circ}\mathrm{C}\right)$. All these criteria yield the T_{hot} ranges given in Table 4.2.

Table 4.1. Investigated conditions.

Parameter Analyzed	**Values or Condition**
Adsorption Cycle Type	Reversible Ideal Simple Heat Recovery with Two Spatially Isothermal Beds Thermal Wave with No Mass Recovery (with by-pass line) Thermal Wave with No Mass Recovery (without by-pass line) Thermal Wave with Adiabatic Mass Recovery (with by-pass line) Thermal Wave with Adiabatic Mass Recovery (without by-pass line) Thermal Wave with Isothermal Mass Recovery (with by-pass line) Thermal Wave with Isothermal Mass Recovery (without by-pass line)
Adsorbent – Refrigerant (Working) Pair	Zeolite NaX – Water (Z1) Zeolite X13 – Water (ZW) Silica Gel – Water (SG) Activated Carbon – Ammonia (CA) Activated Carbon – Methanol (CM)
Cooling Tower Type	Dry, Wet
Condensation Temperature, T_{cond} (^{o}C)	25, 30, 35
Evaporator Temperature, T_{evap} (^{o}C)	5, 10, 15
Heat Capacity Ratio, R	0, 3, 10
Excess Bed Temperature, ΔT_{excess} (^{o}C)	0, 5, 10
Maximum Bed Temperature Range, T_{hot} (^{o}C)	50 – 250

Table 4.2. Analyzed maximum bed temperature ranges for each pair.

Adsorbent – Refrigerant Pair	T_{hot} **range (°C)**	T_{hot} **values (°C)**
Zeolite NaX – Water (Z1)	90 – 190	90, 120, 150, 180, 190
Zeolite X13 – Water (ZW)	80 – 160	80, 100, 120, 150, 160
Silica Gel – Water (SG)	80 – 100	80, 90, 100
Activated Carbon – Ammonia (CA)	80 – 150	80, 100, 120, 150
Activated Carbon – Methanol (CM)	80 – 100	80, 90, 100

For the thermal wave cycles with adiabatic (AMR) or isothermal (IMR) mass recovery, a finite difference method is applied to solve Equations (3.8)-(3.11). For AMR, mass recovery processes are divided into a series of steps with fixed ΔX increments and decrements. At each step, the bed temperature for the low-pressure bed (T_m) is found using Equation (3.8). A similar discretization scheme is used for IMR except since the temperatures are known at each step, the corresponding pressures (P_m and P_n) can be found iteratively from $X = X(T,P)$. Steps are continued to be taken until $P_n - P_m < 0$. Subsequently, linear interpolations between the last two steps are done for both beds until a convergence criterion ($|P_n - P_m| < \varepsilon$) is reached. When the convergence criterion is met, states a1 and a3 for AMR and i1 and i3 IMR are fixed.

To interpret the possible effects of the parameters given in Table 4.1 and Table 4.2 on each system's energy performance, cases are compared based on COP_{ads}, COP_{sys} and $COP_{sys,clg}$. COP_{ads} is given in Equation (4.1).

$$COP_{ads} = \frac{q_{evap}}{q_{htr} + q_{bed,3i3}} = \frac{\left(X_{max} - X_{min}\right)\left[\mathrm{h_v}\left(T_{evap}\right) - \mathrm{h_l}\left(T_{cond}\right)\right]}{q_{htr} + q_{bed,3i3}} \tag{4.1}$$

Note that for the simple and heat recovery cycles $q_{htr} = q_F$. For the simple and heat recovery cycles, and for the thermal wave cycles with no mass (NMR) and adiabatic mass recovery (AMR) $q_{bed,3i3} = 0$. COP_{ads} of the reversible cycle can be calculated using the information in Section 2.2.3.e and as given in Equation (2.43).

The systems' overall coefficient of performance can be calculated as,

$$COP_{sys} = COP_{ads} \cdot \eta_{coll} \tag{4.2}$$

where the definition of collector efficiency (η_{coll}) is given in Section 3.2.1.

A coefficient of performance of the integrated system (COP_{sys}) for steady simulations as given in Equation (4.2) and cooling capacity weighted COP_{sys} ($COP_{sys,clg}$) for seasonal-transient simulations are defined as performance parameters. The definition of $COP_{sys,clg}$ is given in Equation (4.3).

$$COP_{sys,clg} = \frac{\sum_i \left[\mathrm{COP}_{\mathrm{sys}}(t_i)\, \mathrm{q}_{\mathrm{clg,N}}(t_i) \right]}{\sum_i \mathrm{q}_{\mathrm{clg,N}}(t_i)} \tag{4.3}$$

To further compare the investigated parameters given in Table 4.1, $COP_{sys,clg}$ ratio (r_{sys}) is introduced such that,

$$\mathrm{r}_{\mathrm{sys,i}}(T_{hot}, WP) = \frac{\mathrm{COP}_{\mathrm{sys,clg,i}}(T_{hot}, WP) - \mathrm{COP}_{\mathrm{sys,clg,base}}(T_{hot}, WP)}{\mathrm{COP}_{\mathrm{sys,clg,base}}(T_{hot}, WP)} \tag{4.4}$$

where *i* represent any case, *WP* is the abbreviation of the working pair, and base case is selected with simple cycle, dry cooling tower, T_{evap} = 10°C, R = 10 and ΔT_{excess} = 0°C.

The constants in the normalized model described in Section 3.3 are as follows. To fix $A_{coll,N}$ in the normalized model, G_{rfrc} is chosen as 1,000 W/m^2 which is close to the maximum solar radiation level of Antalya, Turkey. Similarly, to calculate the cooling load ($q_{load,N}$), T_{rfrc} = 21°C is selected. For $m_{ads,N}$, ΔX_{base} is calculated assuming T_{hot} = 150°C, $T_o = T_{cond}$ = 30°C, $P_{cond} = \mathrm{P_{sat}}(T_{cond})$, and $P_{evap} = \mathrm{P_{sat}}(T_{evap})$ where P_{sat} indicates the saturation pressure as a function of temperature.

4.2 Error Quantification

The adsorption cycle models described in detail in Section 3.1 are checked for consistency using the 1st Law of Thermodynamics. For this reason, an energy balance is performed for the overall system. For the simple and heat recovery cycles, the system boundary is drawn around the adsorbent beds, condenser and evaporator.

$$Error = \frac{q_{htr} - q_{clr} - q_{bed}}{q_{htr}} \tag{4.5}$$

Similarly, another error is defined for the thermal wave cycles. The system boundary for the thermal wave cycles also includes the heater and the cooler as partially shown in Figure 2.6. The error for thermal wave cycles is given in Equation (4.6).

$$Error = \frac{q_{htr} - q_{clr} + q_{bed,1i1} + q_{bed,3i3} - c_p \left(X_{max} - X_{min} \right)\left(T_{w,2} - T_{evap} \right)}{q_{htr} + q_{bed,3i3}} \tag{4.6}$$

Note that for the thermal wave cycles with no (NMR) and adiabatic (AMR) mass recovery cycles, $q_{bed,1i1} = q_{bed,3i3} = 0$ in Equation (4.6).

Additional consistency checking for models is established through the 2nd Law of Thermodynamics. The adsorption models are empirical curve fits to experimental data and may not necessarily obey the 2nd Law of Thermodynamics. Therefore, the COP_{ads} values of the investigated pairs are compared with the reversible COP_{ads}, and cases with COP_{ads} higher than the reversible COP_{ads} are eliminated.

The assumption of constant specific heats is also investigated by comparing the model results with model results in which variable specific heat values are used. This verification is specifically done for working pairs with water as refrigerant since water properties are well established. Therefore, the adsorption cycle model for NMR (both with and without by-pass line) is modified and several cases are run using variable specific heats. Sample steady simulation durations and corresponding percent-

age errors using Equation (4.6) for NMR and by-pass line using T_{hot} = 150°C, T_{cond} = 30°C, T_{evap} = 10°C, ΔT_{excess} = 0°C, R = 10 are given in Table 4.3. In Table 4.3, the interval size refers to the number of steps between states 1 and 2 (and states 3 and 4) as shown in Figure 3.1 and Figure 3.2, which is used in the numerical solution of integrodifferential equations in Sections 2.2.3 and 3.1.

Table 4.3. Simulation durations and 1st Law error comparison of constant and variable specific heats (NMR cycle with by-pass line, T_{hot} = 150°C, T_{cond} = 30°C, T_{evap} = 10°C, ΔT_{excess} = 0°C and R = 10).

Interval Size	**Constant Specific Heat**		**Variable Specific Heat**	
	Duration (s)	**Error (%)**	**Duration (s)**	**Error (%)**
1000	5.185	0.17221	32.832	0.14605
5000	19.224	0.03442	147.265	0.01106
10000	35.990	0.01721	321.018	0.00580
50000	221.594	0.00344	1487.501	0.01929

The comparison results in Table 4.3 show that the simulation times increase significantly as the model switches from constant to variable specific heats while the percentage error that is described in Equation (4.6) decreases slightly. Therefore, constant specific heats are assumed to reduce simulation times and allow more simulations to be run. Additionally, using constant specific heat gives higher COP_{ads} values than variable specific heat, which is consistent with findings of Pons and Szarzynski [78]. For all analyzed cases, as the interval size of the finite-difference scheme is halved, the error is almost halved as can be interpreted from Table 4.3, suggesting that this error originates from the finite-difference method.

4.3 Solar Thermal Collector Model Verification

The solar thermal system is modeled as described in Section 3.2 and one of the main components of the solar thermal system is the solar thermal collectors. In order to verify the accuracy of the collector models, outlet temperatures of the modeled collectors are compared with experimental results. The experiments were conducted in the Mechanical Engineering Department at the Middle East Technical University in 2008 [111]. The experimental parameters such as the inlet temperature of the collector, solar radiation, ambient temperature and the flow rate of the working fluid are manually entered to the collector model, and the outlet temperatures of the actual and modeled collectors are compared.

In Table 4.4 and Table 4.5, verification results for commercially available flat plate solar collectors are given (FPL and FP). For each collector 10 cases are randomly selected from the experiments that were conducted in August 2008. Similarly, in Table 4.6, verification results are given for the modeled evacuated tube solar collector (ET). The corresponding experiments were conducted in October 2008.

Table 4.4. Solar collector verification results for FPL.

$G\left(\mathrm{W/m^2}\right)$	T_{amb} (^{o}C)	$\dot{m}\left(\mathrm{kg/h}\right)$	$T_{coll,in}$ (^{o}C)	$T_{coll,out}$ (^{o}C) **(Experiment)**	$T_{coll,out}$ (^{o}C) **(Model)**
873.9	27.18	135.81	70.48	75.71	76.20
977.3	25.31	136.82	64.25	70.37	71.15
966.9	24.16	143.05	61.00	66.89	67.63
1000.8	27.67	135.26	75.14	81.08	81.79
997.0	26.41	143.42	64.66	70.86	71.45
1004.9	25.93	138.60	60.66	67.40	67.97
975.8	28.84	132.36	74.42	80.69	81.10
936.3	28.66	140.58	56.31	62.59	63.31
973.8	23.22	137.92	56.30	62.92	63.46
952.0	28.91	134.28	80.14	85.16	86.13

Table 4.5. Solar collector verification results for FP.

$G\left(\mathrm{W/m^2}\right)$	T_{amb} (°C)	$\dot{m}\left(\mathrm{kg/h}\right)$	$T_{coll,in}$ (°C)	$T_{coll,out}$ (°C) **(Experiment)**	$T_{coll,out}$ (°C) **(Model)**
984.9	30.20	127.59	68.93	74.31	74.73
931.6	26.09	123.78	57.78	63.41	63.70
884.8	28.59	115.81	55.20	60.88	61.41
950.9	32.36	115.70	58.38	64.44	65.20
898.0	33.69	113.74	62.97	68.44	69.24
955.5	30.54	116.39	57.18	63.63	63.97
802.9	30.70	116.42	45.01	50.40	51.18
946.3	32.83	116.58	58.19	64.23	64.96
895.5	29.97	117.34	51.26	57.04	57.79
909.5	29.13	117.04	50.56	56.48	57.21

Table 4.6. Solar collector verification results for ET.

$G\left(\mathrm{W/m^2}\right)$	T_{amb} (°C)	$\dot{m}\left(\mathrm{kg/h}\right)$	$T_{coll,in}$ (°C)	$T_{coll,out}$ (°C) **(Experiment)**	$T_{coll,out}$ (°C) **(Model)**
722.1	16.35	143.42	74.14	79.42	80.13
899.0	16.85	139.51	73.85	80.83	81.84
852.9	21.05	140.50	84.61	91.22	91.91
889.8	18.72	140.60	70.83	77.76	78.80
903.3	16.71	142.54	75.08	82.12	82.91
929.3	16.97	144.18	50.35	57.63	58.94
960.2	15.19	143.81	42.66	50.42	51.57
892.8	16.13	144.01	46.64	53.88	54.82
933.6	16.44	143.75	45.88	53.52	54.50
771.1	13.79	152.56	46.82	52.82	53.38

For Table 4.4 through Table 4.6, G is solar radiation, T_{amb} is ambient temperature, $\dot{m}$ is mass flow rate of the working fluid, $T_{coll,in}$ is inlet temperature of the collector and $T_{coll,out}$ is outlet temperature of the collector. As can be seen from the results from Table 4.4 through Table 4.6, all the differences of the outlet temperatures are below 1.2^{o}C. Therefore, the collector model results are close to the actual results within acceptable limits and the models are verified. In addition, the second flat plate collector (FP) gives higher thermal efficiencies and has higher stagnation temperature than the first flat plate collector (FPL) as stated in the collectors' catalog. Therefore, the simulations are continued only using the second flat plate collector (FP).

CHAPTER 5

RESULTS

The information presented in this chapter is an extension of that previously published or under revision by Taylan, Baker and Kaftanoğlu [44, 89, 108].

Trends in COP_{ads} and COP_{sys} are investigated while varying the cycle type, adsorbent – refrigerant (working) pair and working conditions given in Table 4.1. Although it is possible to get errors that are defined in Equations (4.5) and (4.6) on the order of 10^{-8}, the errors are kept less than 3.5% so as not to increase the simulation times significantly. The relation between simulation times and the interval sizes of the finite difference solution can be observed in Table 4.3 to some extent. Furthermore, convergence criterion for the finite difference scheme is selected as 10^{-6}. The convergence criterion is described as the estimated absolute error, i.e., the absolute difference between the present result and corresponding result in the previous time step or attempt. More than 10,000 cases were investigated, and many of the investigated cases produced similar results and trends. For brevity and clarity, only the most significant results are presented and discussed in this chapter. Additionally, the presented trends are representative of the trends for all analyzed cases.

5.1 Adsorption Cooling Cycle Comparison

Trends in COP_{ads} for the thermal wave cycles with no mass recovery (NMR), adiabatic mass recovery (AMR) and isothermal mass recovery (IMR) are given in Figure 5.1. All thermal wave cycles are also presented with or without by-pass lines for zeolite NaX – water (Z1) pair. Also presented in this Figure are COP_{ads} values for the reversible cycle, simple cycle and heat recovery cycle with two isothermal beds. As required, in all cases COP_{ads} of the reversible cycle is the highest since the reversible

cycle is the thermodynamically limiting case. From Figure 5.1, it is observed that for the conditions explored the thermal wave cycles are superior to the simple and heat recovery cycles, especially when the maximum bed temperature (T_{hot}) is high. In other words, as T_{hot} increases, COP_{ads} trends of all the thermal wave cycles and simple or heat recovery cycles diverge. Although the differences between the thermal wave cycles with and without by-pass line among the investigated cases are very small, COP_{ads} values of the thermal wave cycles with by-pass line are slightly higher than the corresponding values for the thermal wave cycles without by-pass line.

The working pair in Figure 5.1 is zeolite NaX – water (Z1) and the corresponding COP_{ads} curves for NMR and AMR coincide while the COP_{ads} curves for IMR are slightly higher than the other thermal wave cycles' COP_{ads} curves. This result holds for both thermal wave cycles with and without by-pass lines.

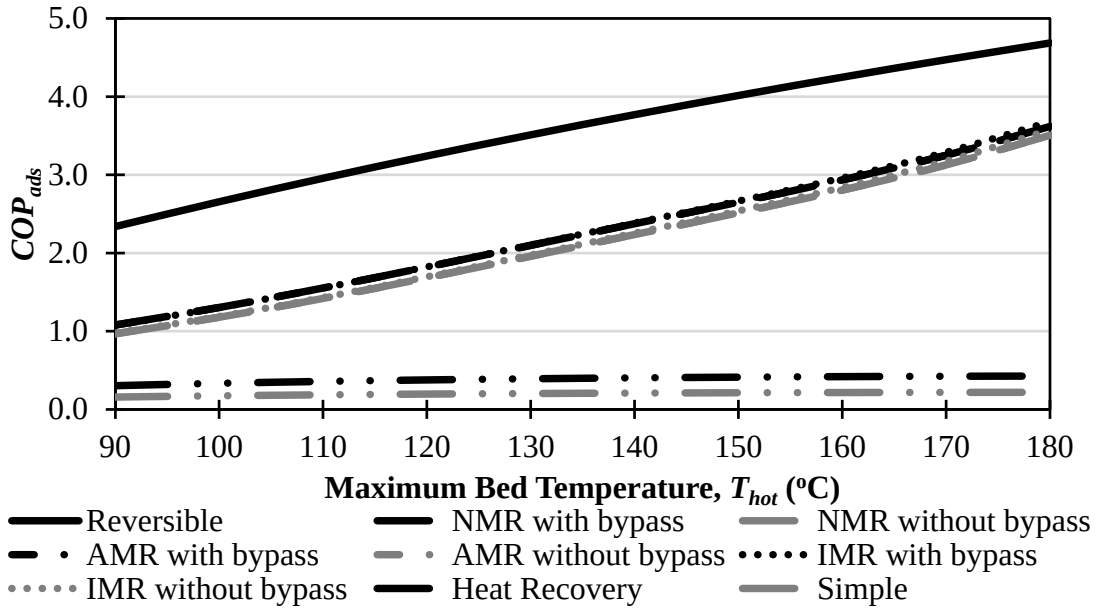

Figure 5.1. Comparison of different adsorption cycle types for Z1 pair, T_{cond} = 30°C, T_{evap} = 10°C, R = 10 and ΔT_{excess} = 0°C.

In addition to Figure 5.1, in Figure 5.2 the COP_{ads} trends for different adsorption cooling cycles are given for an activated carbon – ammonia (CA) working pair. Unlike the results for zeolite NaX – water (Z1) working pair given in Figure 5.1, COP_{ads} curves of AMR and NMR do not coincide. For maximum bed temperature lower than approximately 110°C (T_{hot} < ~110°C), COP_{ads} values of AMR are slightly higher than COP_{ads} values of NMR. For maximum bed temperatures higher than approximately 110°C (T_{hot} > ~110°C), COP_{ads} values of NMR are higher than COP_{ads} values of the AMR as shown in Figure 5.2. Considering all investigated cases, IMR gives higher COP_{ads} values than NMR and AMR.

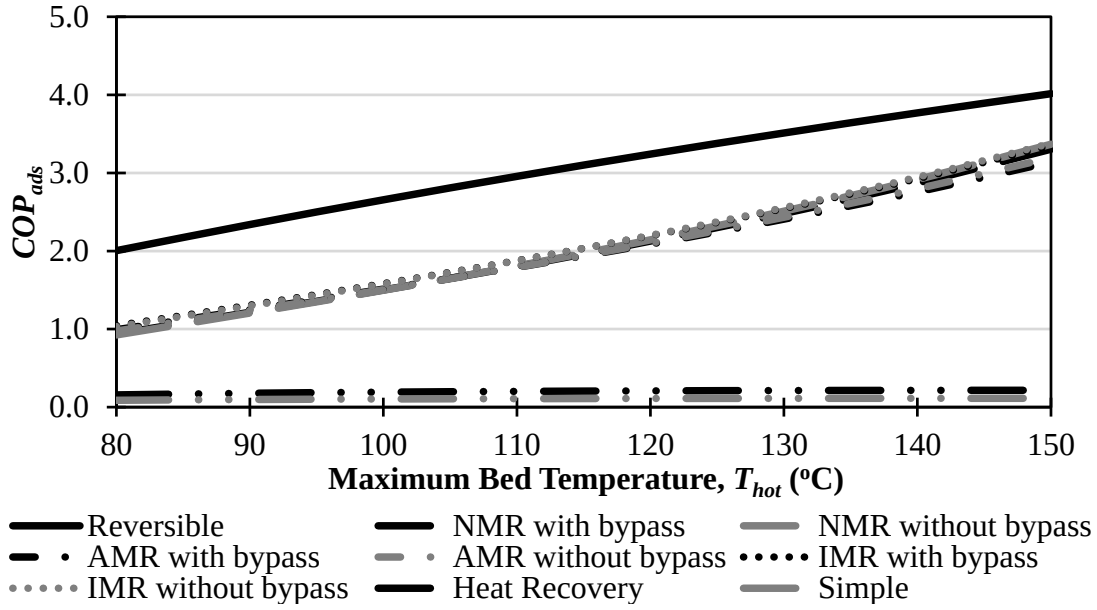

Figure 5.2. Comparison of different adsorption cycle types for CA pair, T_{cond} = 30°C, T_{evap} = 10°C, R = 10 and ΔT_{excess} = 0°C.

The relative difference of COP_{ads} between NMR and AMR for zeolite NaX – water varies as -0.01 < ($COP_{ads,AMR} - COP_{ads,NMR}$) / $COP_{ads,NMR}$ < 0.17 and is large only when T_{hot} is low. The relative difference of COP_{ads} between NMR and IMR for zeolite NaX – water varies as -0.01 < ($COP_{ads,IMR} - COP_{ads,NMR}$) / $COP_{ads,NMR}$ < 1.62 and is large when the condensation temperature (T_{cond}) is high and T_{hot} is low. Converse-

ly, the relative differences of COP_{ads} between all investigated thermal wave cycles are low when T_{cond} is low and T_{hot} is high.

5.2 Adsorbent – Refrigerant Pair Comparison

Clapeyron diagrams ($\ln(P_v)$ vs. $-1/T$) for different adsorbent – refrigerant (working) pairs are given in Figure 5.3 and Figure 5.4. As it can be observed from both figures, the activated carbon – ammonia (CA) pair works with the highest vapor pressure among the investigated working pairs given in Table 4.1, whereas activated carbon – methanol (CM) pair has the second highest vapor pressure. As is obvious from Section 3.1, vapor pressures are related with the saturation pressures of the corresponding refrigerants and the condensation and evaporation pressures. Maximum and minimum bed temperatures are independent of the working pairs, and they are fixed in each simulation by user/designer as shown in Figure 5.3 and Figure 5.4. For a certain case, bed temperatures at the end of Process 1→2 (state 2, end of the isosteric heating) and Process 3→4 (state 4, isobaric heating and desorption) differ slightly for each working pair. The pairs with water as refrigerant (SG, Z1 and ZW) can be listed with decreasing temperature at state 2 (T_2) as silica gel – water (SG), zeolite NaX – water (Z1) and zeolite X13 – water (ZW) and with decreasing temperature at state 4 (T_4) as zeolite X13 – water (ZW), silica gel – water (SG) and zeolite NaX – water (Z1). Similarly, the pairs with activated carbon as adsorbent can be listed with decreasing temperature at state 2 (T_2) as activated carbon – ammonia (CA) and activated carbon – methanol (CM) and with decreasing temperature at state 4 (T_4) as activated carbon – methanol (CM) and activated carbon – ammonia (CA).

In order to illustrate the sorption regimes described in Section 2.2.1.b, Figure 5.3 and Figure 5.4 can be compared. Note that in Figure 5.3, the temperature at state 4 (T_4) is higher than temperature at state 2 (T_2), i.e., $T_4 > T_2$. Therefore, the condition given in Figure 5.3 is suitable for *paired sorption* heat recovery. On the contrary, the temperature at state 4 (T_4) is lower than the temperature at state 2 (T_2), i.e., $T_4 < T_2$ in Figure 5.4. For the conditions given in Figure 5.4 the *no sorption regime* can occur, and as

explained in Section 2.2.1.b the illustrated condition in Figure 5.4 limits heat recovery.

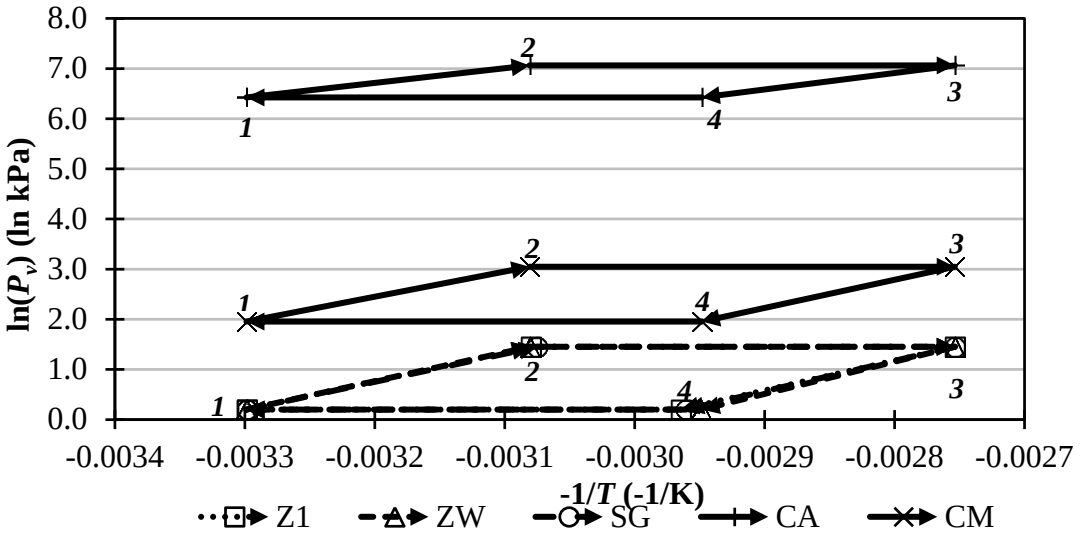

Figure 5.3. Clapeyron diagrams for different working pairs with T_{hot} = 90°C, T_{cond} = 30°C, T_{evap} = 10°C, R = 10 and ΔT_{excess} = 0°C. Numbers on plot area indicate the state numbers.

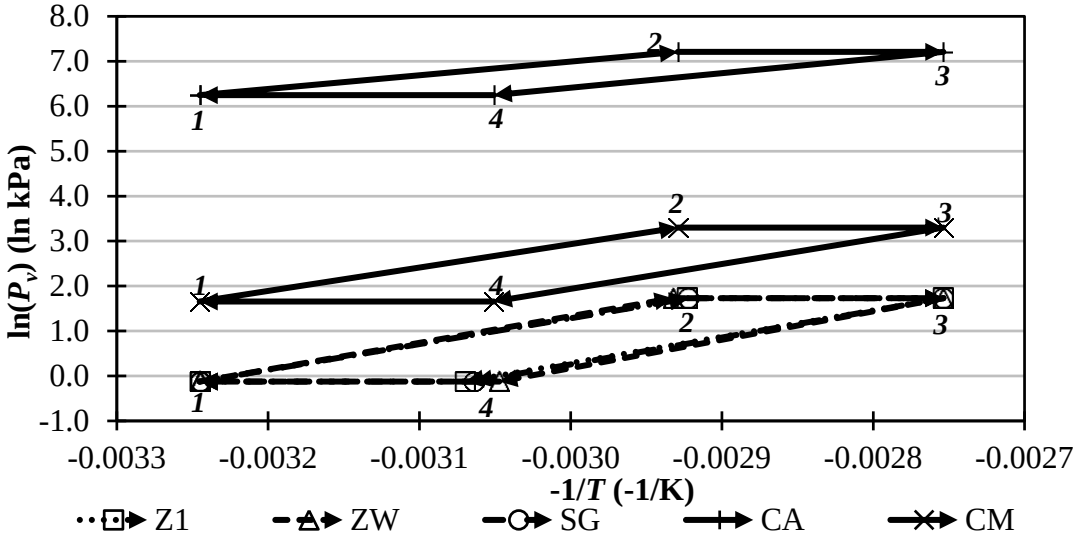

Figure 5.4. Clapeyron diagrams for different working pairs with T_{hot} = 90°C, T_{cond} = 35°C, T_{evap} = 5°C, R = 10 and ΔT_{excess} = 0°C. Numbers on plot area indicate the states.

Working pairs are compared in Figure 5.5 in terms of COP_{ads}. For thermal wave cycles, the trend in COP_{ads} for all working pairs is always increasing with increasing T_{hot} as shown in Figure 5.5. For heat recovery and simple cycles, the COP_{ads} curves increase for all working pairs and COP_{ads} asymptotically reach different values for different pairs as shown in Figure 5.5. The working pair with the highest COP_{ads} varies with T_{hot}. For the thermal wave cycles, silica gel – water (SG) pair has the highest COP_{ads} for the T_{hot} range of 80-100^{o}C, activated carbon – ammonia (CA) pair for 100-150^{o}C and zeolite NaX – water (Z1) pair for 150-190^{o}C. For the heat recovery and simple cycles, silica gel – water (SG) pair still has the highest $COP_{sys,clg}$ for the 80-100^{o}C range and zeolite X13 – water (ZW) pair has the highest $COP_{sys,clg}$ for the 100-160^{o}C region.

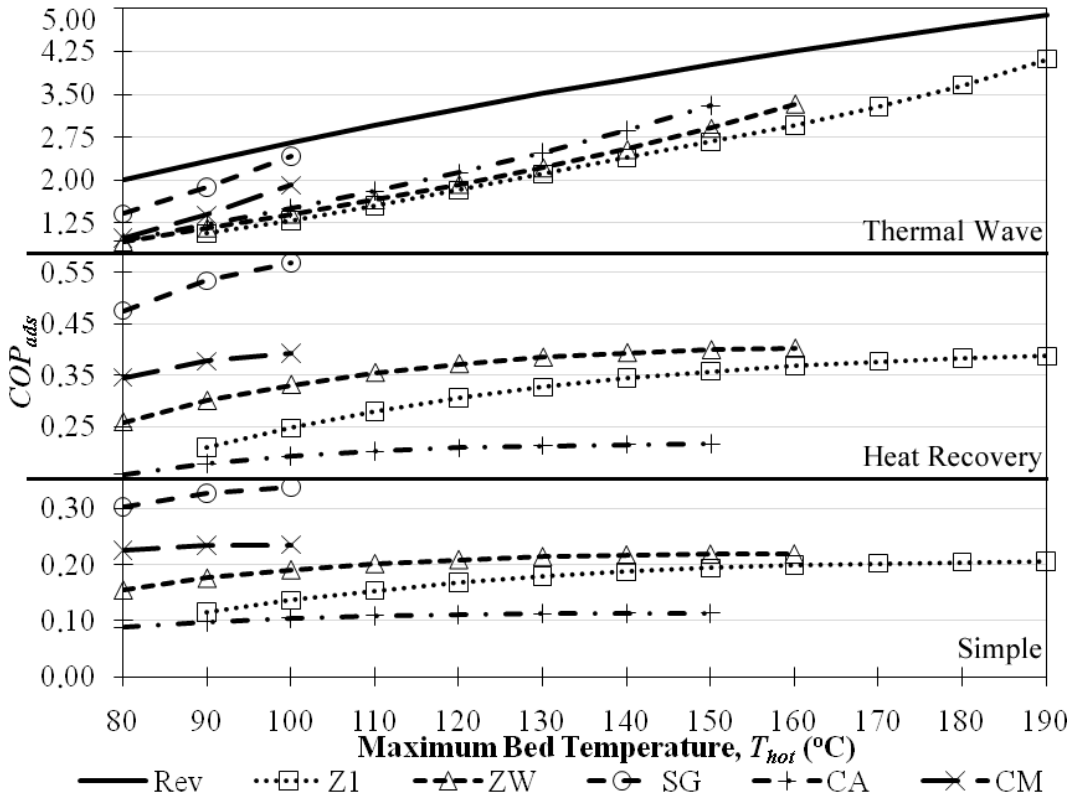

Figure 5.5. Working pair comparison using different adsorption cycle types with T_{cond} = 30^{o}C, T_{evap} = 10^{o}C, R = 10 and ΔT_{excess} = 0^{o}C.

In addition to Figure 5.5, the working pairs are also compared using seasonal-transient simulations. In Figure 5.6, the working pairs are compared in terms of $COP_{sys,clg}$. Similar to the results in Figure 5.5, the $COP_{sys,clg}$ trends of thermal wave cycles are to increase with increasing T_{hot} as shown in Figure 5.6. For the heat recovery and simple cycles, $COP_{sys,clg}$ values increase with increasing T_{hot}, achieve a peak and then decrease. For these cycles, working pairs have peak $COP_{sys,clg}$ values at different T_{hot} values. The peak $COP_{sys,clg}$ is at approximately 90°C for silica gel – water (SG) and activated carbon – methanol (CM) pairs, 100°C for activated carbon – ammonia (CA) and zeolite X13 – water (ZW) pairs, and 120°C for zeolite NaX – water (Z1) pair. As with the COP_{ads} results, $COP_{sys,clg}$ results also show that each pair achieves the highest $COP_{sys,clg}$ at a different T_{hot} as can be seen in Figure 5.6.

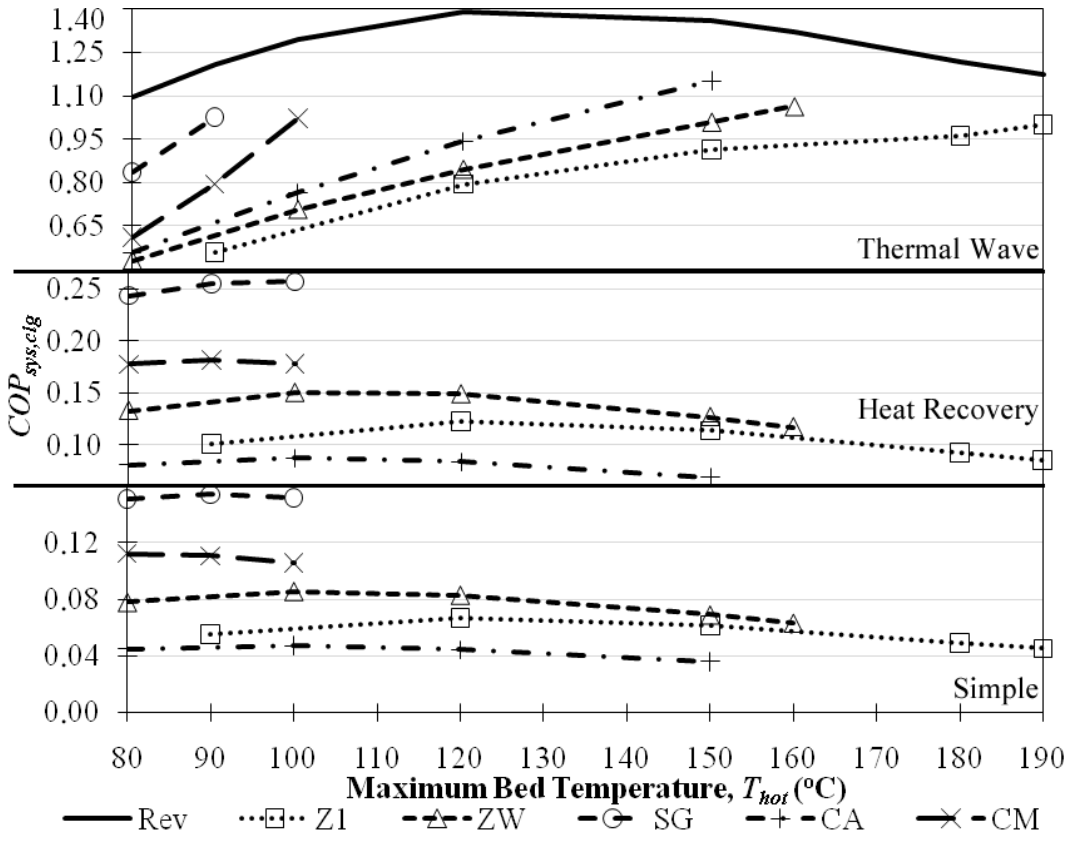

Figure 5.6. Working pair comparison using different adsorption cycle types with dry cooling tower, T_{evap} = 10°C, R = 10 and ΔT_{excess} = 0°C.

5.3 Design and Working Conditions Comparison

In this section, effects of the parameters that are given in Table 4.1 on performances of the adsorption cooling cycle (COP_{ads}) and the solar thermal integrated adsorption cooling system (in terms of COP_{sys} for steady simulations and $COP_{sys,clg}$ and $r_{sys,clg}$ for seasonal-transient simulations) are given in detail.

5.3.1 Effects of Collector Choice and Solar Radiation Level

As mentioned in Section 3.2.1, two types of solar thermal collectors are modeled: flat plate and evacuated tube collectors. Although the collector choice does not affect COP_{ads}, it affects COP_{sys} (and $COP_{sys,clg}$) since COP_{sys} is calculated using Equation (4.2). Meanwhile, solar radiation (G) level has a direct effect on the efficiencies of solar thermal collectors as can be seen from Equation (3.12).

In Figure 5.7, collector efficiencies and the simple adsorption cycle's COP_{ads} are given for steady simulations as G varies. As expected, the evacuated tube collector has higher thermal efficiency than the flat plate collector for all investigated cases. As can be seen from Figure 5.7, thermal efficiencies of the solar thermal collectors (η_{coll}) decrease with increasing T_{hot}, and under certain conditions (e.g., G = 500W/m^2, T_{cond} = 20^{o}C or 35^{o}C and T_{hot} > 110^{o}C for flat plate collector in Figure 5.7), the solar thermal collectors reach their stagnation temperature, defined as the maximum achievable collector temperature with a stagnated fluid [112, 113], and consequently collector efficiency becomes zero (η_{coll} = 0). As shown in Figure 5.7 (and Figure 5.8), the flat plate collector reaches zero thermal efficiency at lower temperatures than the evacuated tube collector, i.e., the flat plate collector has lower stagnation temperatures than the evacuated tube collector. Therefore, the modeled flat plate collector is not suitable for adsorption cooling cycles that require high (driving) temperatures. Additionally, as G level increases, η_{coll} and stagnation temperatures for both collectors increase.

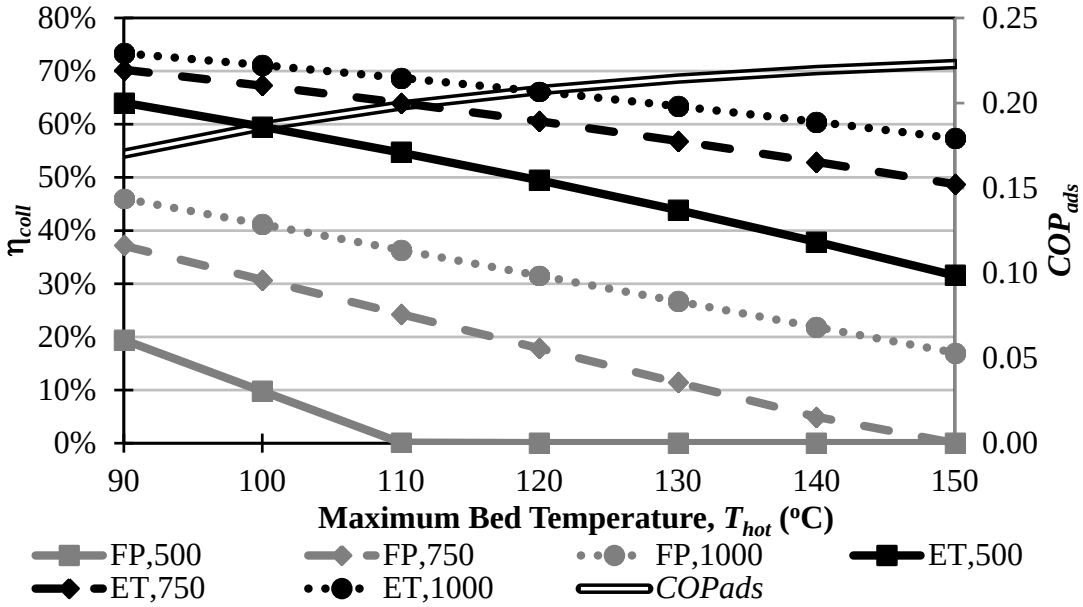

Figure 5.7. Collector and solar radiation level comparison for simple cycle, Z1 pair, T_{cond} = 20°C, T_{amb} = 35°C, T_{evap} = 10°C, R = 10 and ΔT_{excess} = 10°C (Legend: CC,GGG where CC = collector type: FP = flat plate; ET = evacuated tube; GGG=G (W/m^2)).

COP_{sys} changes with variations in T_{hot}, G and collector type are given in Figure 5.8. For the investigated T_{hot} range, systems with an evacuated tube collector (ET) have a peak COP_{sys} at different T_{hot} values depending on the working pair as mentioned in Section 5.2. As in Figure 5.7, stagnation temperature for flat plate collector and increasing stagnation temperature with increasing G can be observed in Figure 5.8. Moreover, COP_{sys} increases with increasing G.

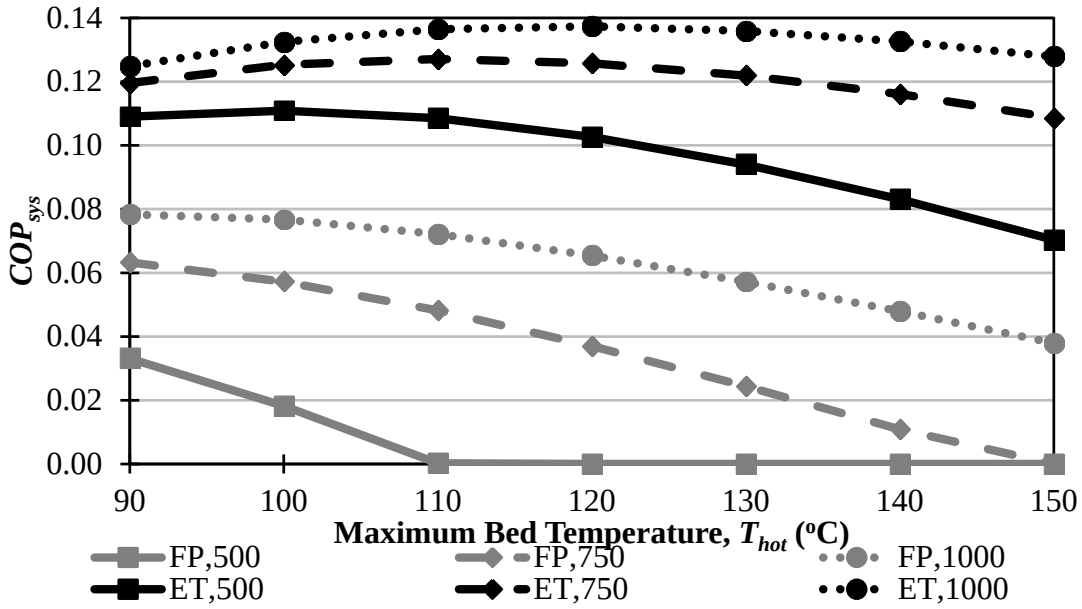

Figure 5.8. Collector and solar radiation level comparison for simple cycle, Z1 pair, T_{cond} = 20°C, T_{amb} = 35°C, T_{evap} = 10°C, R = 10 and ΔT_{excess} = 10°C (Legend: CC,GGG where CC = collector type: FP = flat plate; ET = evacuated tube; GGG=G (W/m^2)).

5.3.2 Effects of Condensation Temperature

Effects of T_{cond} on COP_{ads} are investigated through steady simulations, and representative results can be seen in Figure 5.9 for NMR with different working pairs. For all working pairs and working conditions, as T_{cond} increases, COP_{ads} decreases. Additionally, as T_{hot} increases, the differences in COP_{ads} due to changes in T_{cond} increase according to steady results as can be seen in Figure 5.9. For investigated working pairs and conditions the level of COP_{ads} increase when condensation temperature decreases from T_{cond} = 35°C to 30°C is smaller than the level of COP_{ads} decrease when condensation temperature decreases from T_{cond} = 30°C to 25°C, although the decrease in condensation temperature for each case is the same and 5°C.

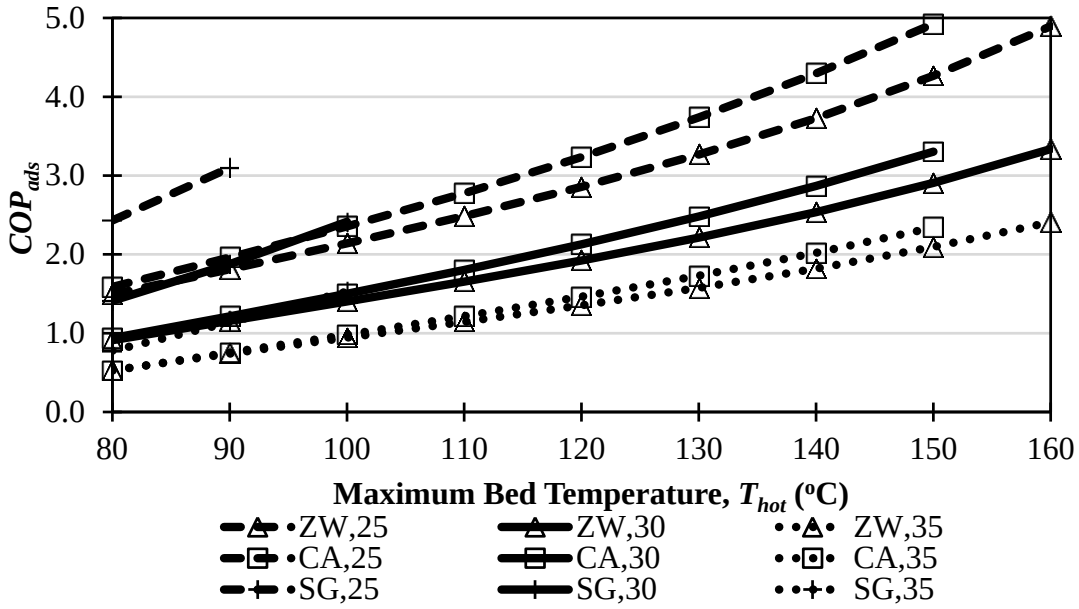

Figure 5.9. Condensation temperature comparison for different working pairs, NMR, T_{evap} = 10°C, R = 10 and ΔT_{excess} = 10°C (Legend shows working pair and T_{cond} (°C)).

The effect of using ideal dry ($T_{cond} = T_o$) versus ideal wet ($T_{cond} = T_{wb}$) cooling towers are analyzed through seasonal-transient simulations, and representative results are shown in Figure 5.10. In all investigated cases, systems with wet cooling towers have higher efficiencies than systems with dry cooling towers. Unlike the steady simulation results, the differences in $COP_{sys,clg}$ with varying T_{cond} diminish as T_{hot} increases for simple and heat recovery cycles. The difference in $COP_{sys,clg}$ curve still increases for thermal wave cycles. As mentioned in Sections 5.1 and 5.3.1, the systems with an evacuated tube collector and thermal wave cycle have the highest $COP_{sys,clg}$ values followed by systems with an evacuated tube collector and heat recovery cycle. Systems with a flat plate collector and simple cycle have the lowest $COP_{sys,clg}$ values.

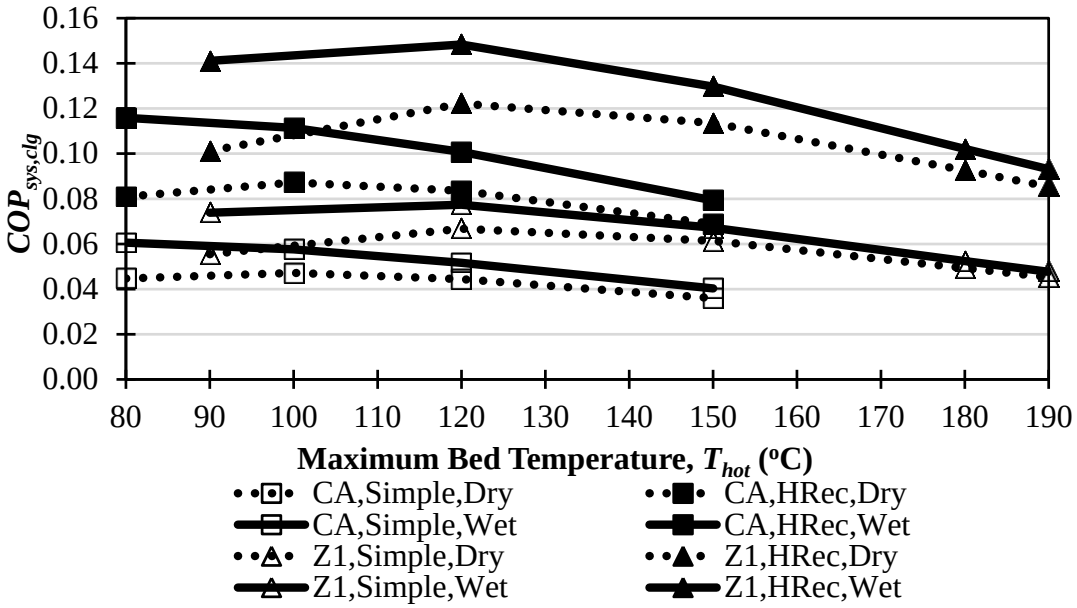

Figure 5.10. Cooling tower comparison for CA and Z1 pairs, simple and heat recovery cycles, T_{evap} = 10°C, R = 10 and ΔT_{excess} = 10°C (Legend shows the working pair, cycle type and cooling tower type).

In addition to the $COP_{sys,clg}$ results that are obtained through seasonal-transient simulations, effects of cooling tower type on $COP_{sys,clg}$ ratios (r_{sys}) are also investigated and results are presented in Figure 5.11. As for the results with $COP_{sys,clg}$, using a wet cooling tower increases r_{sys} for all working pairs, cycle types and operating conditions. As T_{hot} increases, r_{sys} continuously increases for the thermal wave cycles while r_{sys} asymptotically approaches to approximately 1 for the heat recovery cycle. Additionally, r_{sys} approach to zero for the simple cycle since r_{sys} definition is based on simple cycle of the base case and dry cooling tower is selected for the base case. Hence, $COP_{sys,clg}$ of simple cycles approaches to their corresponding $COP_{sys,clg}$ of the base cases as T_{hot} increases as can be derived using Equation (4.4).

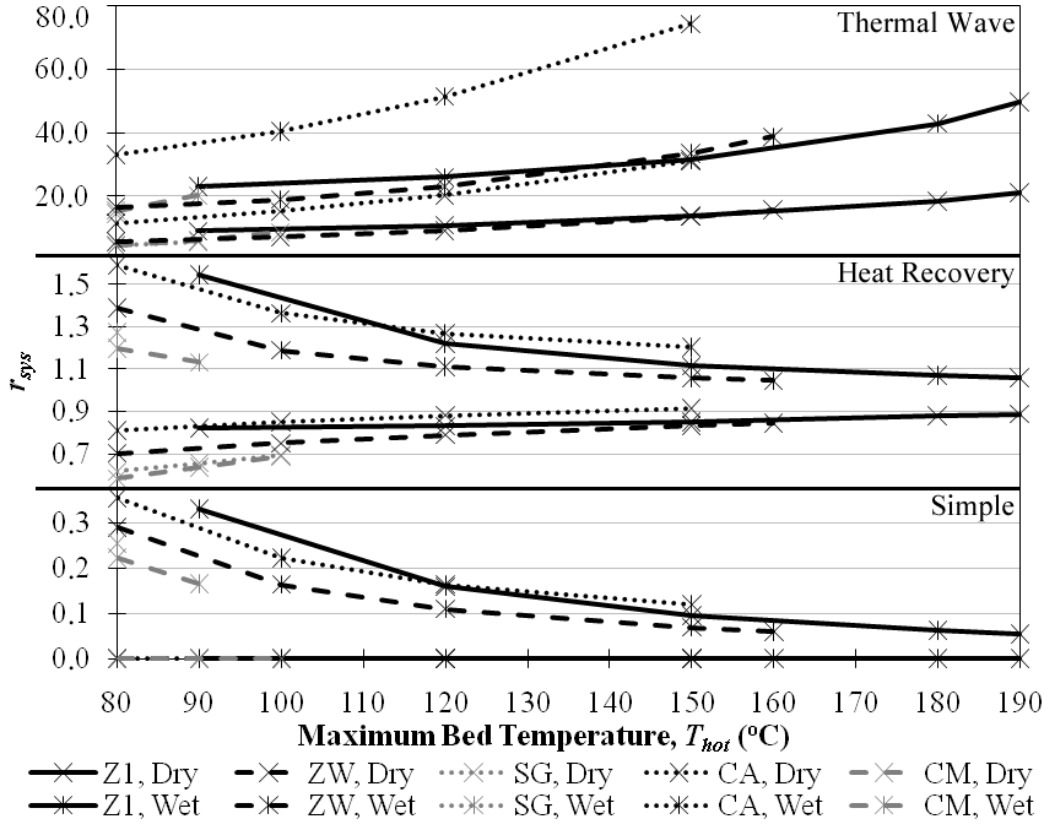

Figure 5.11. Cooling tower comparison for different adsorption cycle types, working pairs, T_{evap} = 10°C, R = 10 and ΔT_{excess} = 0°C (Legend shows working pair and condenser type).

5.3.3 Effects of Evaporation Temperature

Using steady simulations, effects of evaporation temperature (T_{evap}) on the performance of the adsorption cooling system (COP_{ads}) are analyzed, and representative results are given in Figure 5.12. As can be observed from Figure 5.12, as T_{evap} increases, COP_{ads} also increases for all the investigated cases. As with the effects of T_{cond} on COP_{ads} that are mentioned in Section 5.3.2, the differences between COP_{ads} curves of a particular case (i.e., adsorption cycle type, working pair, T_{cond}, ΔT_{excess} and R) due to changes in T_{evap} increase with increasing T_{hot}. Moreover, the increase in COP_{ads} as evaporation temperature increases from T_{evap} = 10°C to 15°C is larger than

the increase in COP_{ads} as evaporation temperature increases from T_{evap} = 5°C to 10°C for the investigated cases as can be seen in Figure 5.12.

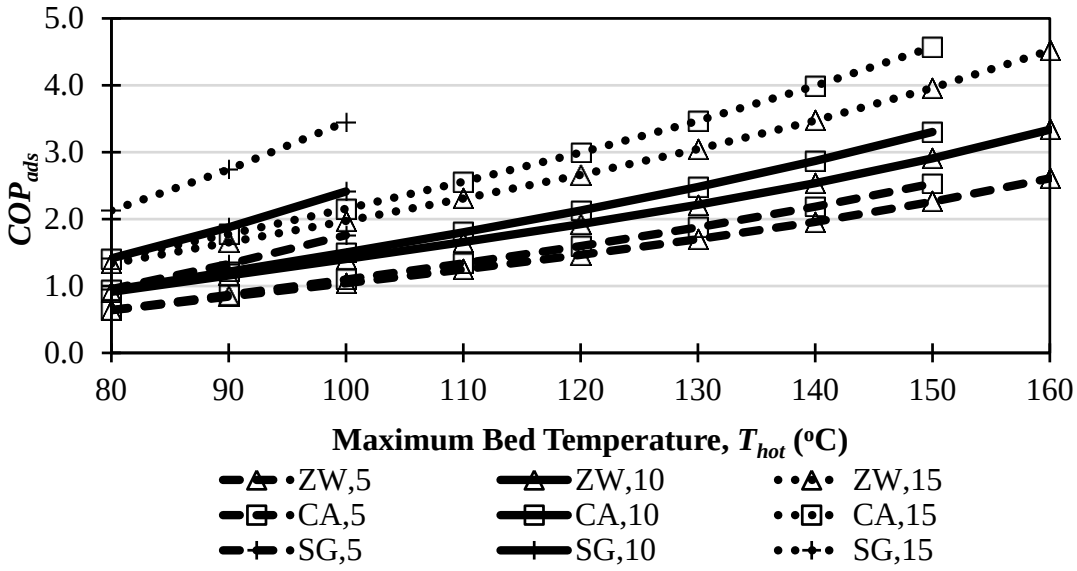

Figure 5.12. Evaporation temperature comparison for NMR, ZW, CA and SG pairs, T_{cond} = 30°C, R = 10 and ΔT_{excess} = 10°C (Legend shows working pair and T_{evap} (°C)).

Using seasonal-transient simulations, effects of T_{evap} on $COP_{sys,clg}$ are analyzed and shown in Figure 5.13 for a single set of working conditions, two different adsorption cooling cycle types and two different working pairs. As with the steady simulations, increasing T_{evap} increases the $COP_{sys,clg}$ values for the investigated cases given in Table 4.1. The differences between $COP_{sys,clg}$ curves become smaller for simple and heat recovery cycles as T_{hot} increases as can be seen in Figure 5.13. The differences between $COP_{sys,clg}$ curves as T_{evap} changes vary with the other operating conditions, adsorption cooling cycle type and working pairs.

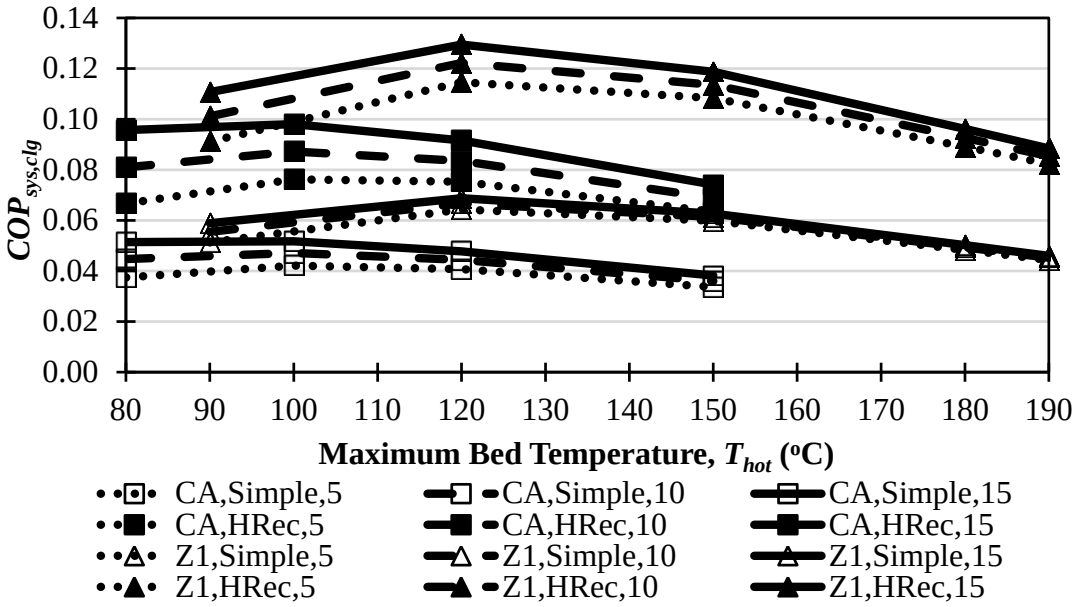

Figure 5.13. Evaporation temperature comparison for simple and heat recovery cycles, CA and Z1 pairs, T_{cond} = 30°C, R = 10 and ΔT_{excess} = 10°C (Legend shows the working pair, cycle type and T_{evap}(°C)).

General trends of r_{sys} as T_{evap} increases are almost same as changing from dry cooling tower to wet cooling tower. r_{sys} results from seasonal-transient simulations are given in Figure 5.14. With increasing T_{hot} and for all analyzed T_{evap} and working pairs, r_{sys} increase for the thermal wave cycles as shown in Figure 5.14 and r_{sys} values approach to zero for the simple cycle as in the T_{cond} cases. However, the trends for the heat recovery cycle are slightly different. r_{sys} for the heat recovery cycle with T_{evap} = 15°C reach a minimum value and then increase as T_{hot} increases, except for activated carbon – methanol (CM) pair. r_{sys} values for the heat recovery cycle with activated carbon – methanol (CM) pair and T_{evap} = 15°C increase as T_{hot} increases unlike other working pairs. Therefore, the general tendency of r_{sys} is increasing for the heat recovery cycle, but still the differences between r_{sys} values with different T_{evap} values decrease as T_{hot} increases. Ratios less than zero for the simple cycle show that those cases have COP_{sys} values less than COP_{sys} of the base case as can be inferred from Equation (4.4).

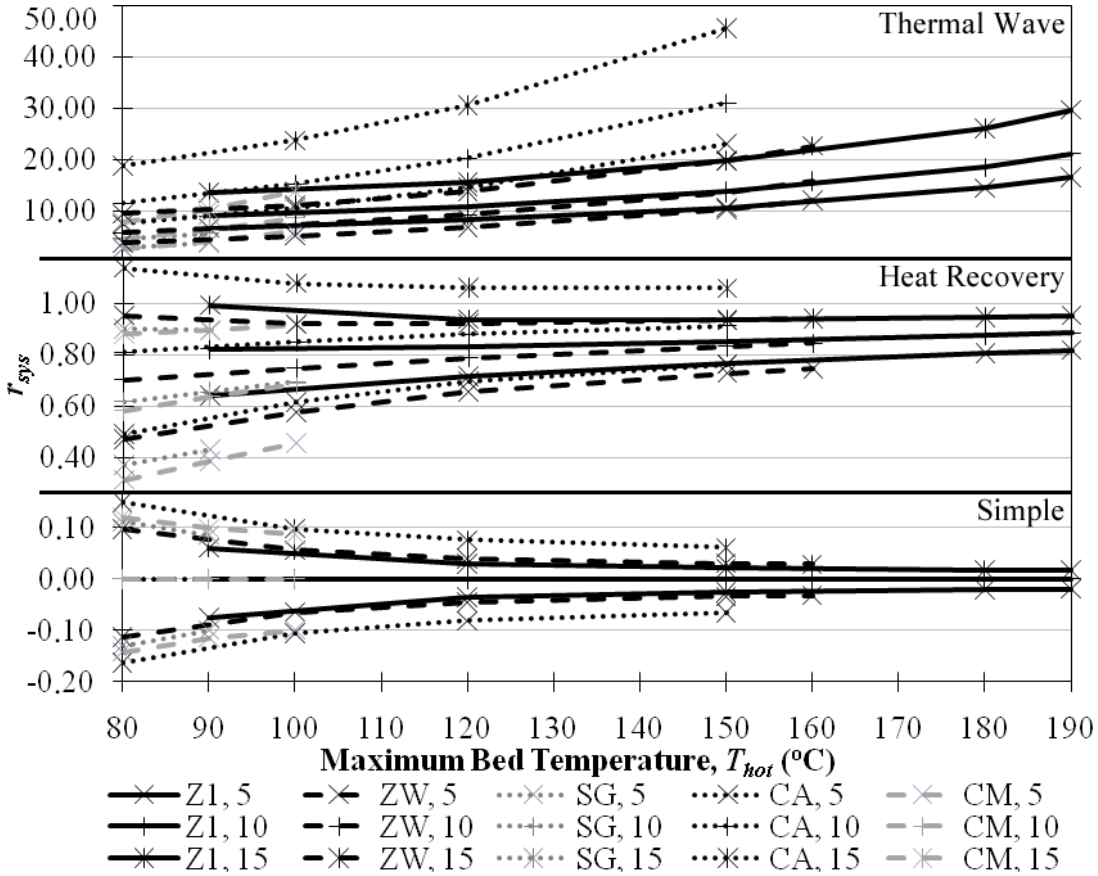

Figure 5.14. Evaporation temperature comparison for different adsorption cycle types and working pairs, T_{cond} = 30°C, R = 10 and ΔT_{excess} = 0°C (Legend shows working pair and T_{evap} (°C)).

5.3.4 Effects of Excess Bed Temperature

Effects of excess bed temperature (ΔT_{excess}) on adsorption cooling cycles are analyzed through a series of steady simulations, and representative results are given in Figure 5.15. As mentioned in Section 4.1, ΔT_{excess} is defined as the temperature difference between the minimum bed temperature (T_o) and the condensation temperature (T_{cond}). For all the investigated cases given in Table 4.1, increasing ΔT_{excess} shifts the COP_{ads} curve downwards on COP_{ads} vs. T_{hot} graph as shown in Figure 5.15. In other words, decreasing T_o to T_{cond} is advantageous in terms of COP_{ads}. Unlike the results for T_{cond} and T_{evap} in Sections 5.3.2 and 5.3.3, the differences between COP_{ads}

curves with only variations in ΔT_{excess} are almost constant. The differences between COP_{ads} values are also almost constant as T_{hot} varies.

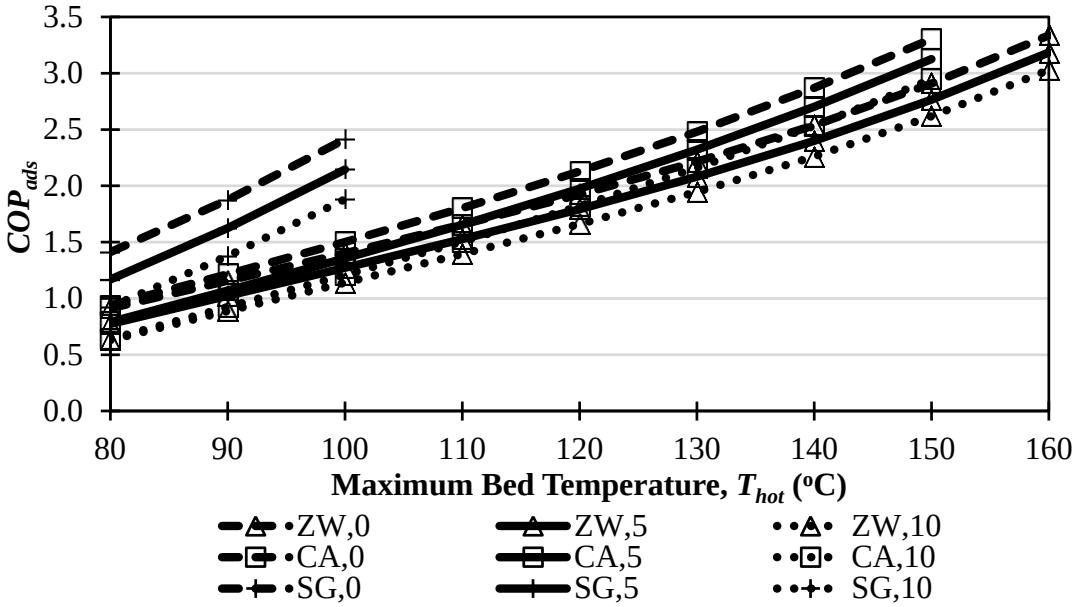

Figure 5.15. Excess bed temperature comparison for NMR and ZW, CA and SG pairs, T_{cond} = 30°C, T_{evap} = 10°C and R = 10 (Legend shows working pair and ΔT_{excess} (°C)).

For the steady simulations and simple or heat recovery cycles where $T_o = T_{cond} = T_{amb}$ (therefore ΔT_{excess} = 0°C), at lower T_{hot} values, low T_{cond} values give higher COP_{sys} while at higher T_{hot} values, high T_{cond} values give higher COP_{sys}. In another set of cases, a dry cooling tower is used (i.e., $T_{cond} = T_{amb}$) and excess bed temperature is either ΔT_{excess} = 10°C or 15°C. In these simulations, COP_{sys} increases with increasing ΔT_{excess} at low T_{hot} values (mostly in the region of T_{hot} < 120°C), but decreases with increasing T_{cond} as T_{hot} increases and at high T_{hot} values (for approximately T_{hot} > 120°C). For the final set of cases, T_{cond} and T_o are not equal to each other and ambient temperature is fixed at T_{amb} = 35°C. Results of these cases are similar to the results of the previous set of cases.

According to the results of seasonal-transient simulations, when the adsorbent bed is not cooled down to T_{cond} (i.e., $\Delta T_{excess} > 0$), $COP_{sys,clg}$ increases as shown in Figure 5.16. Additionally, as ΔT_{excess} increases, $COP_{sys,clg}$ increases except in one case. This exception is observed when using a dry cooling tower with T_{hot} = 90°C and R = 10 regardless of the collector type and adsorption cycle. In general, considering the investigated cases given in Table 4.1, the effect of ΔT_{excess} on $COP_{sys,clg}$ is small when compared to the effects of T_{cond} and T_{evap}.

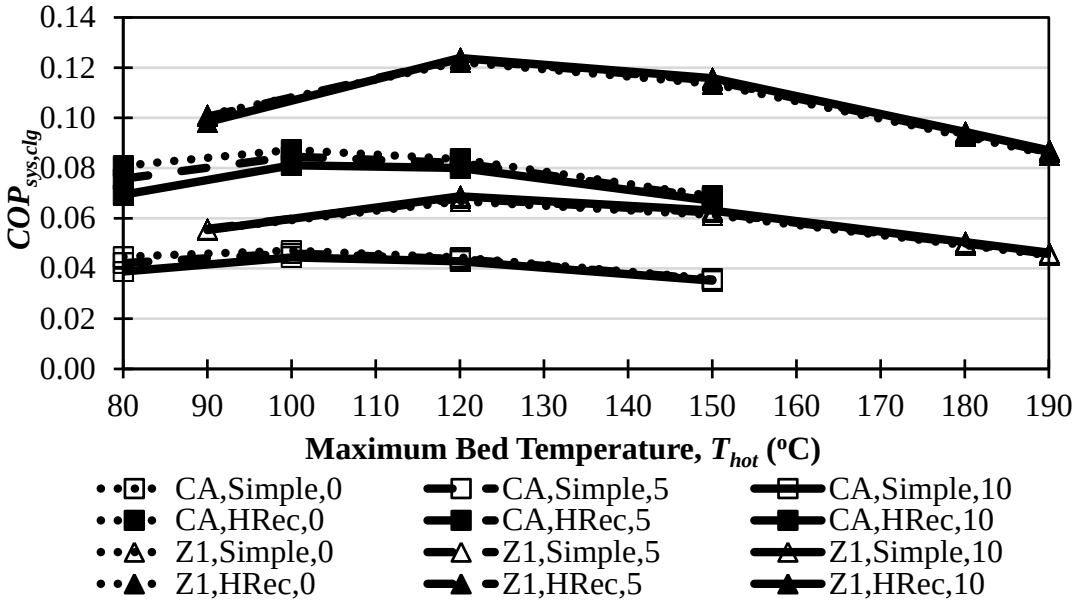

Figure 5.16. Excess bed temperature comparison for simple and heat recovery cycles, CA and Z1 pairs, T_{cond} = 30°C, T_{evap} = 10°C and R = 10 (Legend shows the working pair, cycle type and ΔT_{excess}(°C)).

Effects of ΔT_{excess} are also analyzed through r_{sys} that are obtained from seasonal-transient simulations. r_{sys} results are summarized in Figure 5.17. Increasing ΔT_{excess} for thermal wave cycle decreases r_{sys} for all working pairs. Additionally, as T_{hot} increases r_{sys} increases and the differences between ratios of different ΔT_{excess} values decrease slightly. The general r_{sys} trend for the simple and heat recovery cycles is similar to the trend for the thermal wave cycles, except r_{sys} values approach to some

specific values that depend on working pairs. r_{sys} of the simple and heat recovery cycles continuously increase and approach to those values as T_{hot} increases as can be seen in Figure 5.17. However, unlike other working pairs, r_{sys} of the simple cycle with zeolite NaX – water (Z1) pair approach their maximum values and then decrease. As shown in Figure 5.17, r_{sys} curves that correspond to different ΔT_{excess} values coincide around T_{hot} = 100-110°C for simple and heat recovery cycles with a zeolite NaX – water (Z1) pair.

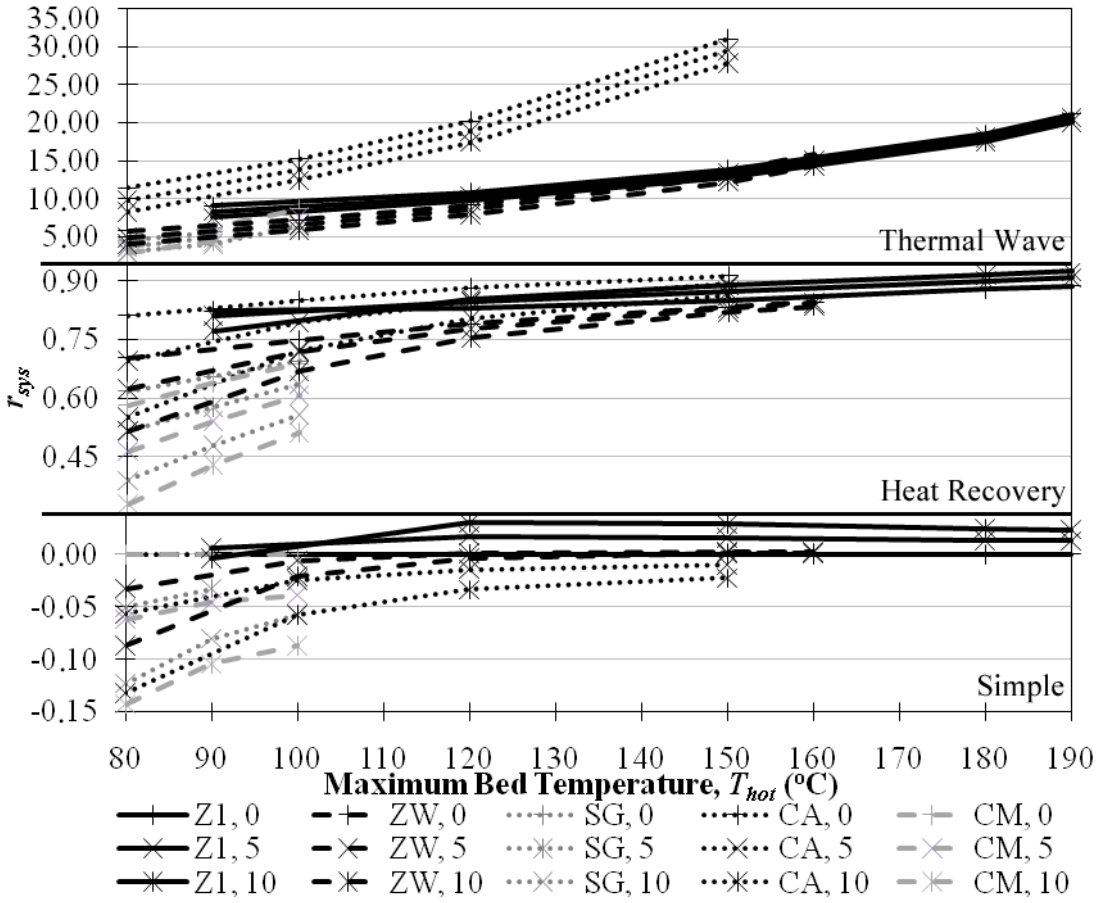

Figure 5.17. Excess bed temperature comparison for different adsorption cycle types and working pairs, T_{cond} = 30°C, T_{evap} = 10°C and R = 10 (Legend shows working pair and ΔT_{excess} (°C)).

5.3.5 Effects of Heat Capacity Ratio

Steady simulations are also performed to investigate the effects of the heat capacity ratio (R) values on COP_{ads}. Some of the results are given in Figure 5.18. As can be partially observed from Figure 5.18, increasing R decreases COP_{ads} of the simple and heat recovery cycles but increases COP_{ads} of the thermal wave cycles. For the investigated cases and similar to the effects of T_{cond} and T_{evap} given in Sections 5.3.2 and 5.3.3, the differences between COP_{ads} curves increases as R varies and T_{hot} increases. Additionally, in the steady cases for the zeolite NaX – water (Z1) pair, heat recovery cycle and evacuated tube collector, decreasing the heat capacity ratio from R = 10 to R = 0 while keeping all other variables constant causes COP_{sys} values to increase 2.7 – 6.5 times. Similar trends are obtained using flat plate collector, and these results are consistent with previous studies [90] as are the results for variations in COP_{sys} with variations in T_{hot}.

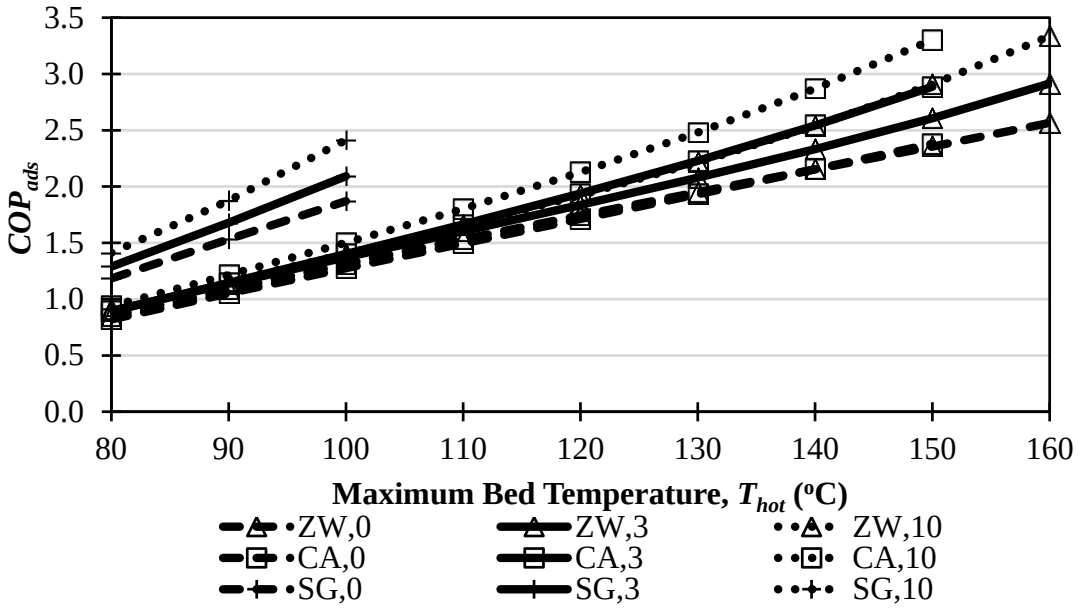

Figure 5.18. Heat capacity ratio comparison for NMR, ZW, CA and SG pairs, T_{cond} = 30°C, T_{evap} = 10°C and ΔT_{excess} = 0°C (Legend shows working pair and R).

Moreover, representative results of seasonal-transient simulation are given in Figure 5.19. From Figure 5.19, as R increases for the simple cycle, $COP_{sys,clg}$ decreases significantly in all cases, and adding heat recovery increases the $COP_{sys,clg}$ values around two times when compared with the simple cycle. However, increasing R increases $COP_{sys,clg}$ values for thermal wave cycles except for a few cases. These exceptions are observed when thermal wave cycles with zeolite NaX – water pair is used and when the maximum bed temperatures are below approximately (T_{hot} < ~150^{o}C). For these exceptional cases, increasing R decreases $COP_{sys,clg}$ as with the simple and heat recovery cycles.

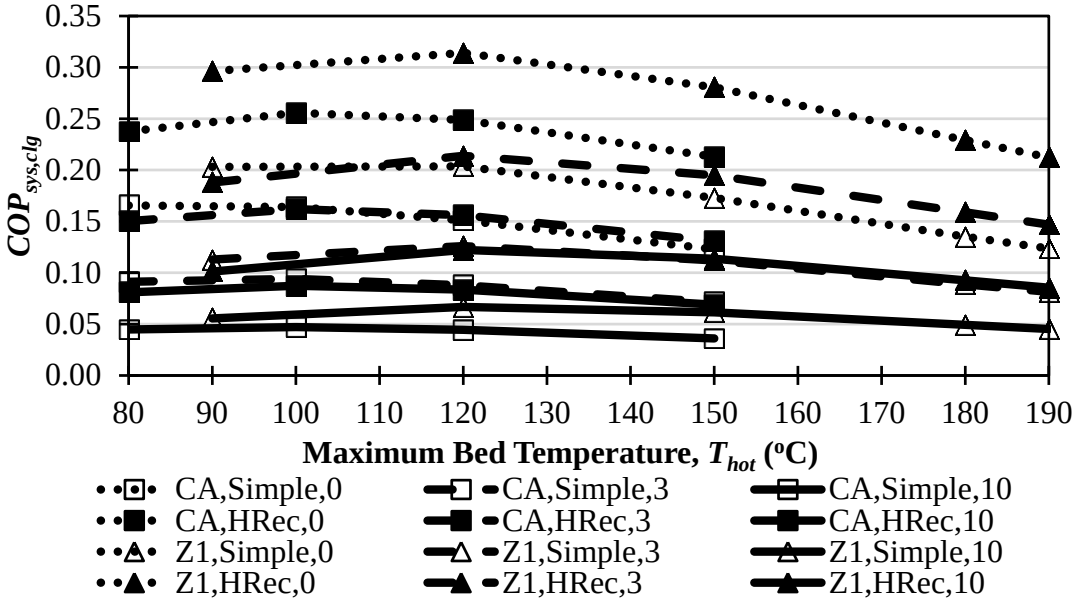

Figure 5.19. Heat capacity ratio comparison for simple and heat recovery cycles, CA and Z1 pairs, T_{cond} = 30^{o}C, T_{evap} = 10^{o}C and ΔT_{excess} = 10^{o}C (Legend shows the working pair, cycle type and R).

Although R does not have a strong effect on the COP_{sys} of the thermal wave cycles, it does have a strong effect on $COP_{sys,clg}$ ratios since R has a strong influence on the simple and heat recovery cycles [44]. r_{sys} values that correspond to different R values are given in Figure 5.20. For the investigated T_{hot} range and the thermal wave cycles,

$COP_{sys,clg}$ and r_{sys} increase and the differences between r_{sys} increase as T_{hot} increases for all working pairs, except for the zeolite NaX – water (Z1) pair. For the thermal wave cycles with zeolite NaX – water (Z1) pair, as with the $COP_{sys,clg}$ results, r_{sys} of different R values coincide at approximately T_{hot} = 150°C. Cases with zeolite NaX – water (Z1) pair and R = 0 have higher r_{sys} values for T_{hot} < 150°C while for T_{hot} > 150°C this case has lower r_{sys} values among the other cases with zeolite NaX – water (Z1) pair and various R values. The r_{sys} trends of working pairs with zeolite as adsorbent (zeolite NaX – water (Z1) and zeolite X13 – water (ZW) pairs) for simple and heat recovery cycles as R decreases are different than the other working pairs. As T_{hot} increases, r_{sys} curves of these pairs (Z1 and ZW) decrease and then increase after some T_{hot} values that depend on the working conditions and pair. However, the heat recovery cycle with silica gel – water (SG), activated carbon – ammonia (CA) and activated carbon – methanol (CM) pairs have continuously increasing trends as T_{hot} increases for all R values. For the simple cycles with various R values, the r_{sys} trends are similar to the heat recovery cycle's trends of zeolite NaX – water (Z1) and zeolite X13 – water (ZW) pairs. Nevertheless, as R increases, r_{sys} values decrease for all simple and heat recovery cycles.

5.3.6 Effects of Maximum Bed Temperature

From Figure 5.1 through Figure 5.20, all results are given based on maximum bed temperature (T_{hot}). As shown in these figures, T_{hot} has a direct effect on COP_{ads}, $COP_{sys,clg}$ and r_{sys}. As T_{hot} increases for steady simulations, COP_{ads} also increases for all the investigated cases including the different adsorption cycle types and working pair types. Seasonal-transient simulations show that $COP_{sys,clg}$ of the thermal wave cycles are approaching to $COP_{sys,clg}$ of the reversible cycle as T_{hot} increases for all working pairs as shown in Figure 5.5. Furthermore, $COP_{sys,clg}$ of the simple and heat recovery cycles increase until a maximum $COP_{sys,clg}$ value is reached, then decrease with increasing T_{hot}.

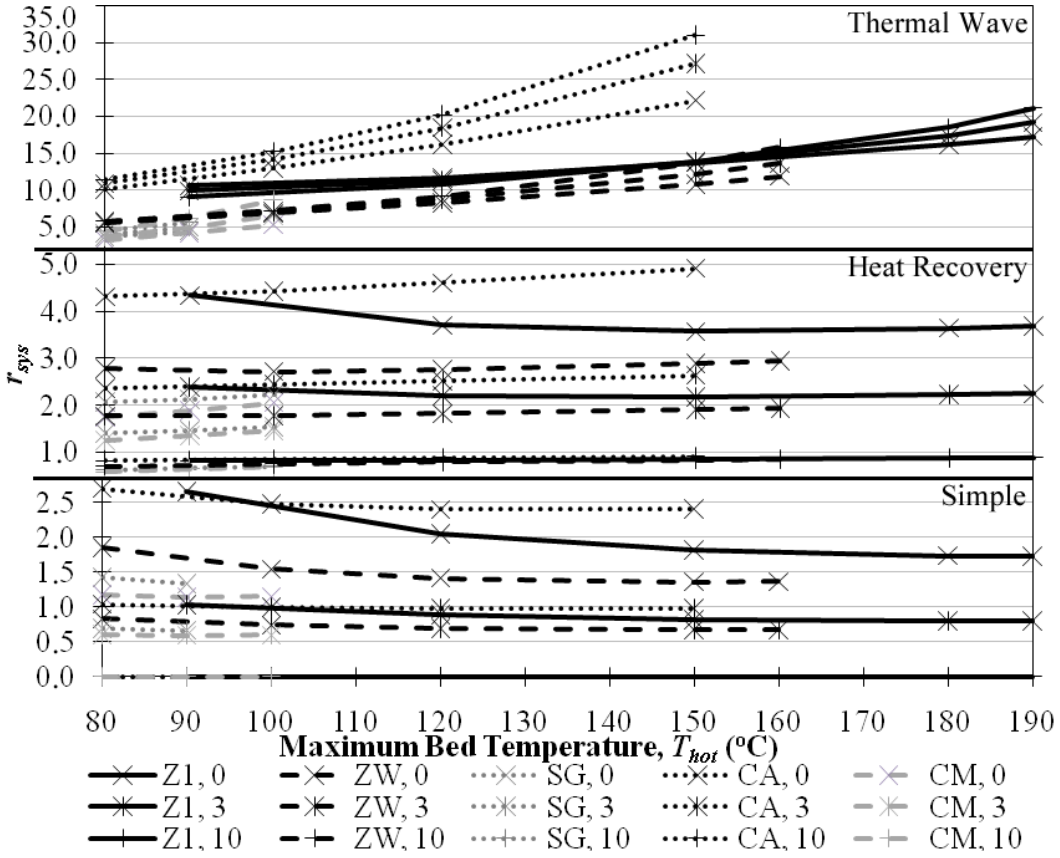

Figure 5.20. Heat capacity ratio comparison for different adsorption cycle types and working pairs, T_{cond} = 30°C, T_{evap} = 10°C and ΔT_{excess} = 0°C (Legend shows working pair and R).

5.3.7 Summary of Effects of Investigated Parameters

Results as different parameters, adsorption cycle types and working pairs vary are presented in terms of COP_{sys} for steady simulations and $COP_{sys,clg}$ and r_{sys} for transient simulations. Before concluding this subsection, it would be beneficial to present and compare the effects of investigated parameters representatively.

The results for the variation of the parameters given in Table 4.1 are shown in Figure 5.21 for IMR with by-pass line, with these results being typical of the other thermal wave cycles. As T_{hot} increases, COP_{ads} increases in all cases. Of investigated temperatures and for a fixed temperature change, T_{cond} has the largest effect on COP_{ads}

while T_{evap} has the second largest effect for the thermal wave cycles. COP_{ads} decreases with increasing T_{cond} but increases with increasing T_{evap}. Increasing ΔT_{excess} shifts the COP_{ads} curve downward in Figure 5.21. The effect of R on COP_{ads} is more complicated than the other parameters, since the effect of R depends on the adsorption cycle type. Increasing R decreases COP_{ads} for the simple and heat recovery cycles but increases COP_{ads} for the thermal wave cycles except for the zeolite NaX – water pair with maximum bed temperature, $T_{hot} < 150^{o}$C as shown in Figure 5.21. However, unlike for the simple and heat recovery cycles, variations in ΔT_{excess} and more importantly R do not affect the thermal wave cycles' COP_{ads} significantly.

The changes of COP_{ads} for the simple and heat recovery cycles in absolute values are not as large as the changes for the thermal wave cycles. Additionally, for the simple and heat recovery cycles, the investigated parameters have the same effects on the COP_{ads} values as for the thermal wave cycles. However, among all the investigated parameters, the effect of R on COP_{ads} for the simple and heat recovery cycles is the largest unlike the thermal wave cycles.

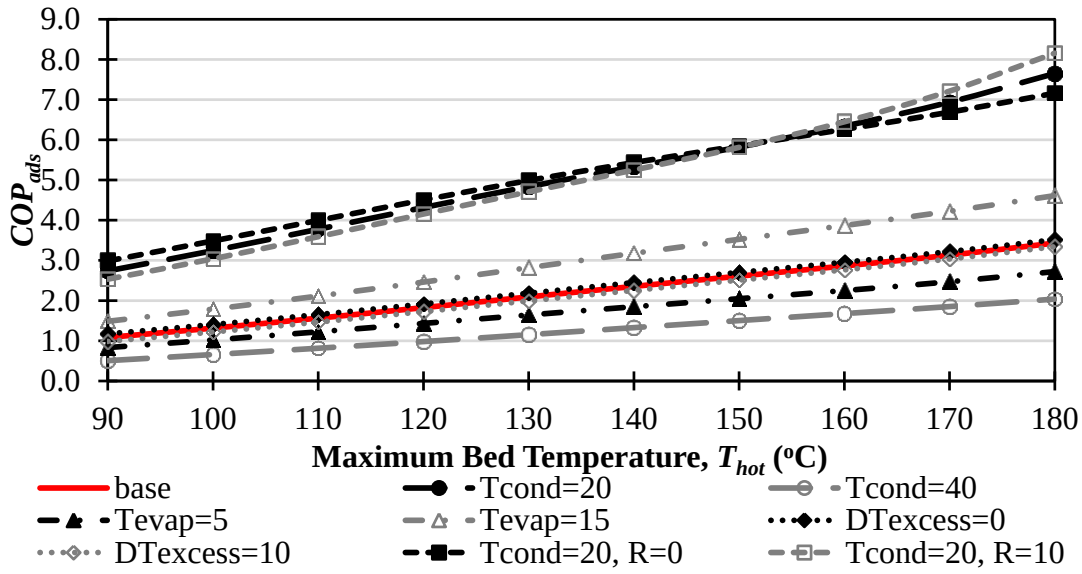

Figure 5.21. Effects of investigated parameters on COP_{ads} for IMR and Z1 pair (Legend shows deviations from the base case which is selected as T_{cond} = 30°C, T_{evap} = 10°C, R = 3 and ΔT_{excess} = 5°C).

In Figure 5.22, $COP_{sys,clg}$ values are given as investigated parameters and cycles vary for zeolite X13 – water (ZW) pair. The results of COP_{ads} are also applicable to the results of $COP_{sys,clg}$. The difference between the results of COP_{ads} and $COP_{ads,clg}$ is mainly due to the efficiency of the modeled solar thermal collectors as can be inferred from Equations (4.2) and (4.3). The general trend of $COP_{sys,clg}$ curves of the thermal wave cycles is to increase while the trend for the simple and heat recovery cycles are to increase, achieve a maximum value and then decrease with increasing T_{hot}. Additionally, the order of the parameters from the highest to lowest effect on $COP_{sys,clg}$ is the same as in COP_{ads} results.

5.4 Normalized Model Results

Seasonal-transient simulations using the normalized model are performed for the simple and heat recovery cycles but not for the thermal wave cycles, and effects of the normalized storage capacity ($q_{Storage,max}$), size of the system (S) and the other parameters listed in Table 4.1 on the solar (f) and loss (l) fractions, normalized collector area ($A_{coll,N}$) and normalized adsorbent mass ($m_{ads,N}$) are analyzed and results are given in this section.

The effects of $q_{Storage,max}$ on f and l are investigated for the simple and heat recovery cycles, and representative results for the user defined size of the cooling system, S = 1 are given in Figure 5.23 for f and in Figure 5.24 for l. Note if any net changes in storage between the start and end of a simulation are neglected, $1 - f$ is proportional to the required backup power. For $q_{Storage,max} > 10$ and $S = 1$, as T_{hot} increases l decreases and becomes zero at smaller $q_{Storage,max}$, and f also decreases but not significantly. Systems with evacuated tube collector result in higher f and l than systems with flat plate collector except when $T_{hot} = 90^{o}$C. When simple and heat recovery cycles are compared, f and l do not change significantly. Additionally, using a wet cooling tower increases f when compared to a dry cooling tower. The effect of cooling tower type on l is different for the flat plate and evacuated tube collectors. For wet cooling towers l is larger when flat plate collectors are used while for dry cooling

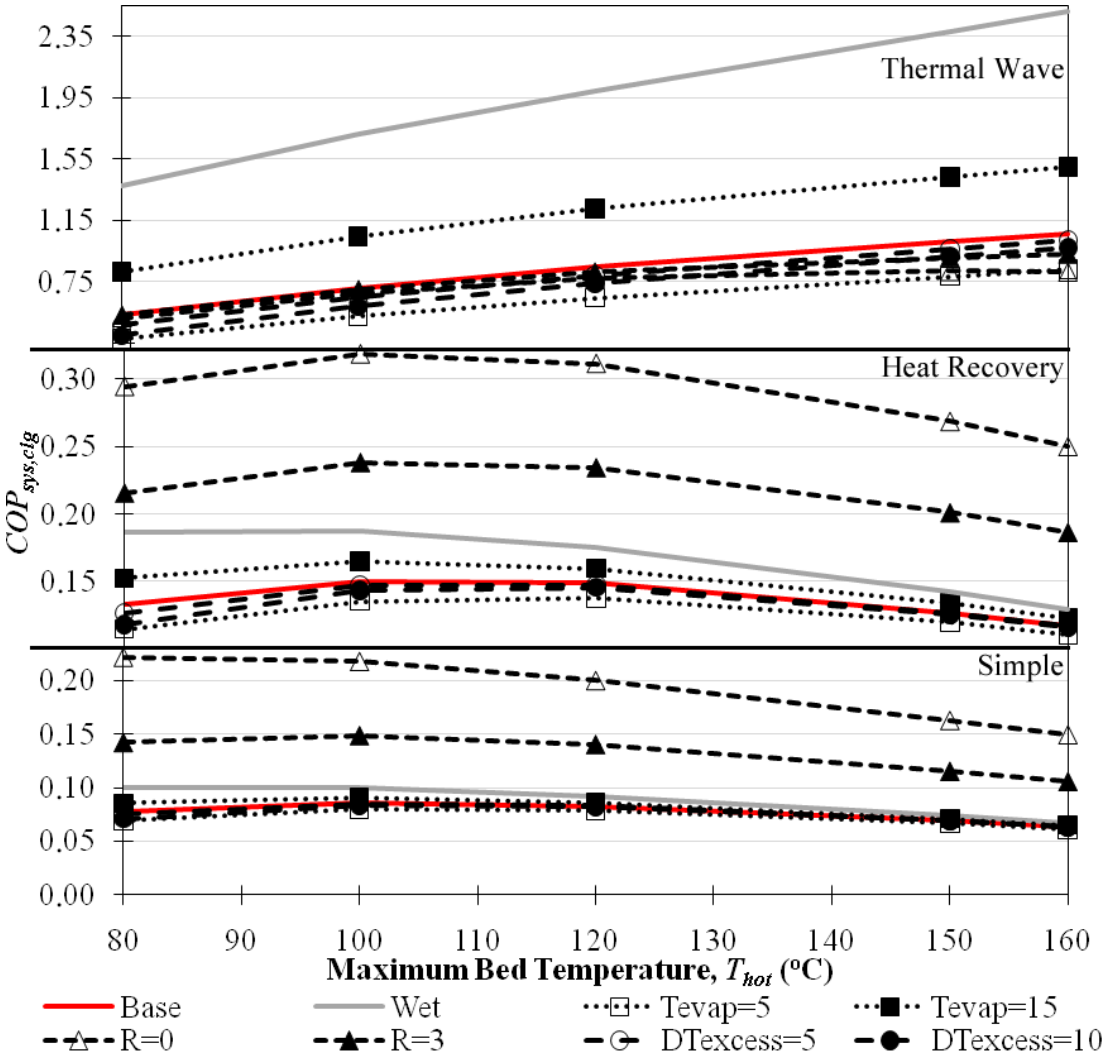

Figure 5.22. Effects of investigated parameters on $COP_{sys,clg}$ for different adsorption cycle types and ZW pair (Legend shows deviations from the base case which is selected as dry cooling tower, T_{evap} = 10°C, R = 10 and ΔT_{excess} = 0°C).

towers l is larger when evacuated tube collectors are used except when $q_{Storage,max}$ = 0. Reducing R increases f and reduces l. Moreover, as ΔT_{excess} increases, f decreases for all investigated $q_{Storage,max}$ and l increases for all investigated $q_{Storage,max} \geq 3$. Changes in f and l are more significant when the heat capacity ratio changes from R = 0 to R = 10 than when the excess bed temperature changes from ΔT_{excess} = 0°C to ΔT_{excess} = 10°C. It is worth noting that for the flat plate collector and maximum bed temperature at T_{hot} = 180°C, f and l are zero for all $q_{Storage,max}$ since the modeled flat plate col-

lector cannot achieve 180°C (i.e., stagnation temperatures are reached) and consequently $q_{clg,N} = 0$.

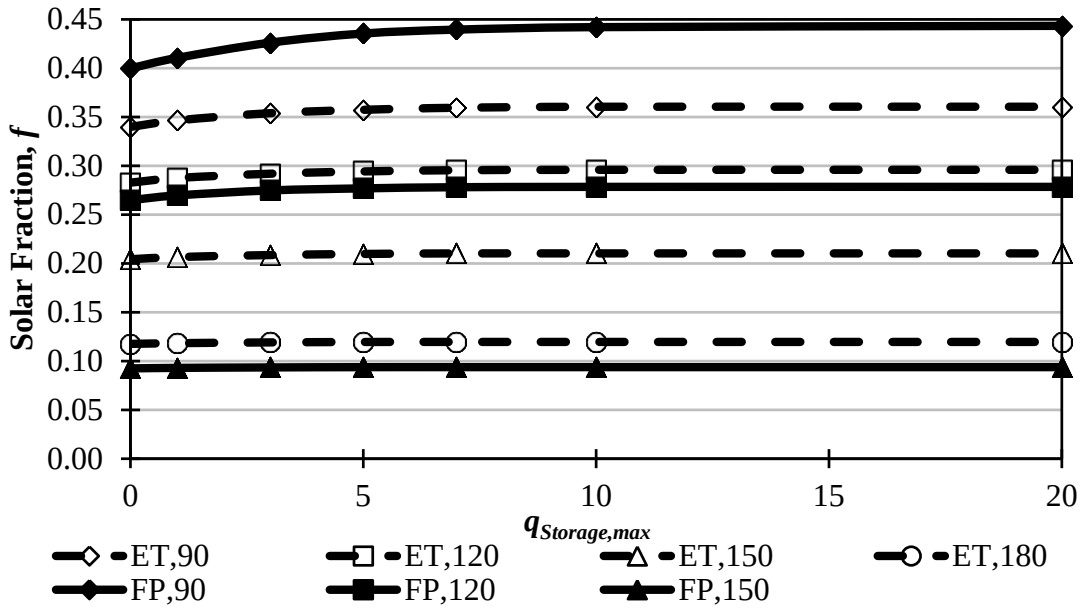

Figure 5.23. f vs. $q_{Storage,max}$ for various collector types and T_{hot}, S = 1, simple cycle, wet cooling tower, R = 10, ΔT_{excess} = 10°C (Legend: CC,HH where CC = collector type: FP = flat plate; ET = evacuated tube; HH=T_{hot} (°C)).

When the effects of S on f and l are compared, as S increases f increases and l decreases as seen representatively in Figure 5.25 for f and in Figure 5.26 for l. For S < 4, as S increases the change in f becomes less significant as $q_{Storage,max}$ increases. Conversely, as S increases changes in l become more significant as $q_{Storage,max}$ increases. Additionally, the benefit of increasing S by a fixed increment decays as S increases. As with the S = 1 cases, f and l of simple and heat recovery cycles do not differ significantly, and f and l decrease as the excess bed temperature increases from ΔT_{excess} = 0°C to 10°C. When cases with R = 0 are compared to cases with R = 10 while S is varying, f and l are lower for R = 10 cases. For those cases, the effects of R are more significant on the simple cycle than the heat recovery cycle.

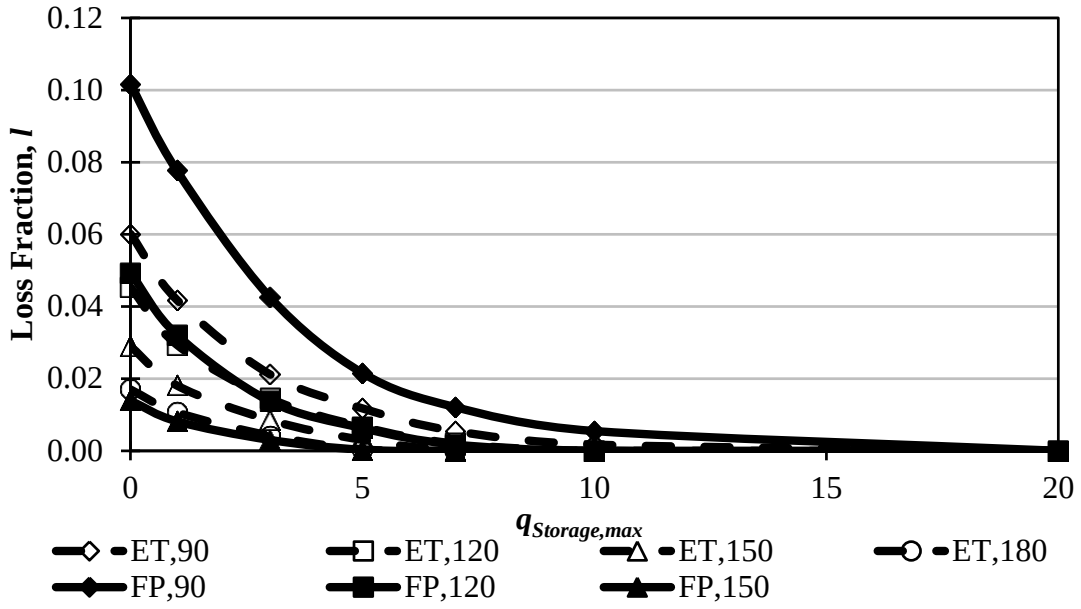

Figure 5.24. l vs. $q_{Storage,max}$ for various collector types and T_{hot}, S = 1, simple cycle, wet cooling tower, R = 10, ΔT_{excess} = 10°C (Legend: CC,HH where CC = collector type: FP = flat plate; ET = evacuated tube; HH=T_{hot} (°C)).

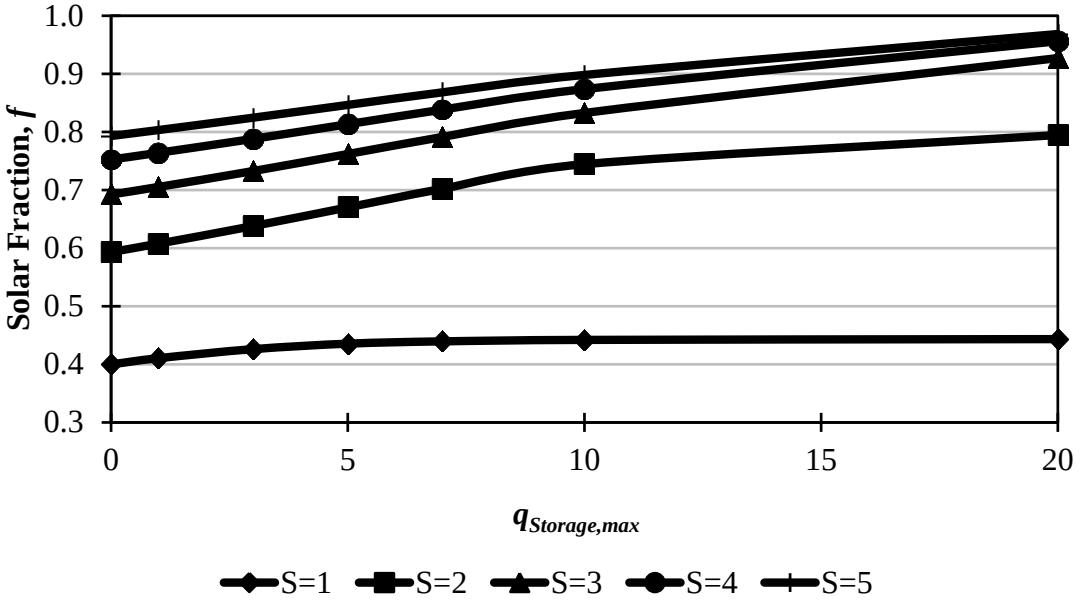

Figure 5.25. f vs. $q_{Storage,max}$ for various S values, flat plate collector, simple cycle, T_{hot} = 90°C, wet cooling tower, and R = 10.

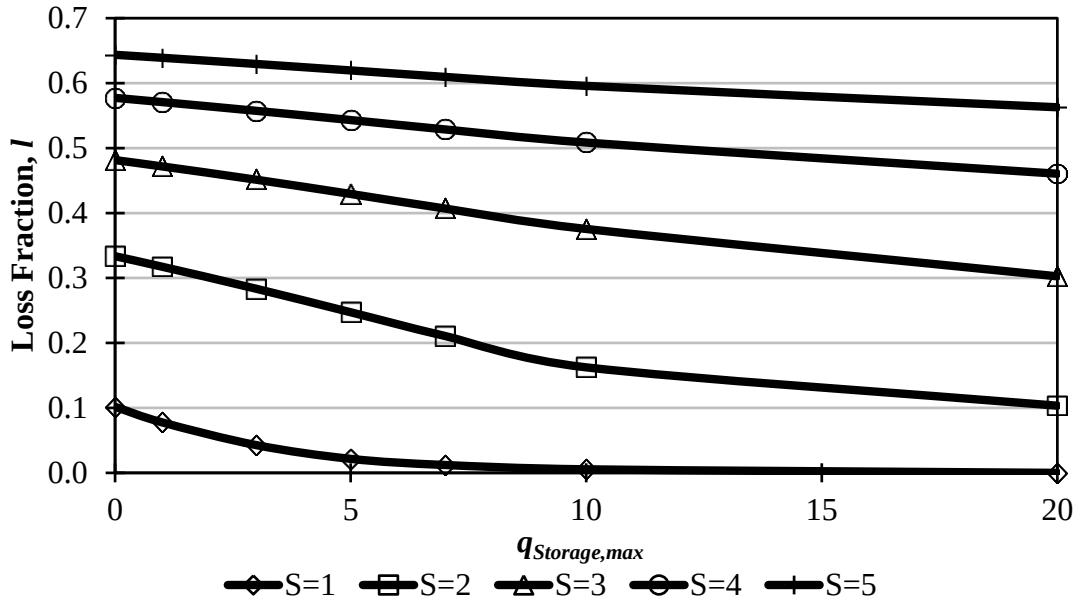

Figure 5.26. l vs. $q_{Storage,max}$ for various S values, flat plate collector, simple cycle, T_{hot} = 90°C, wet cooling tower, and R = 10.

Representative results for the normalized collector area ($A_{coll,N}$) are given in Figure 5.27. In all cases, $A_{coll,N}$ has a peak value around a maximum bed temperature of T_{hot} = 150°C, and it does not change significantly with ΔT_{excess}. For the range of investigated conditions, the parameters listed in order from the strongest to weakest effect on $A_{coll,N}$ are collector type, adsorption cycle type, cooling tower type and R. The required $A_{coll,N}$ is higher in systems with flat plate collector than systems with evacuated tube collector as seen in Figure 5.27. Additionally, it can be observed from Figure 5.27 that using the heat recovery cycle and/or a wet cooling tower results in smaller $A_{coll,N}$. Lastly, in contrast to COP_{sys} (or $COP_{sys,clg}$), $A_{coll,N}$ increases with increasing R.

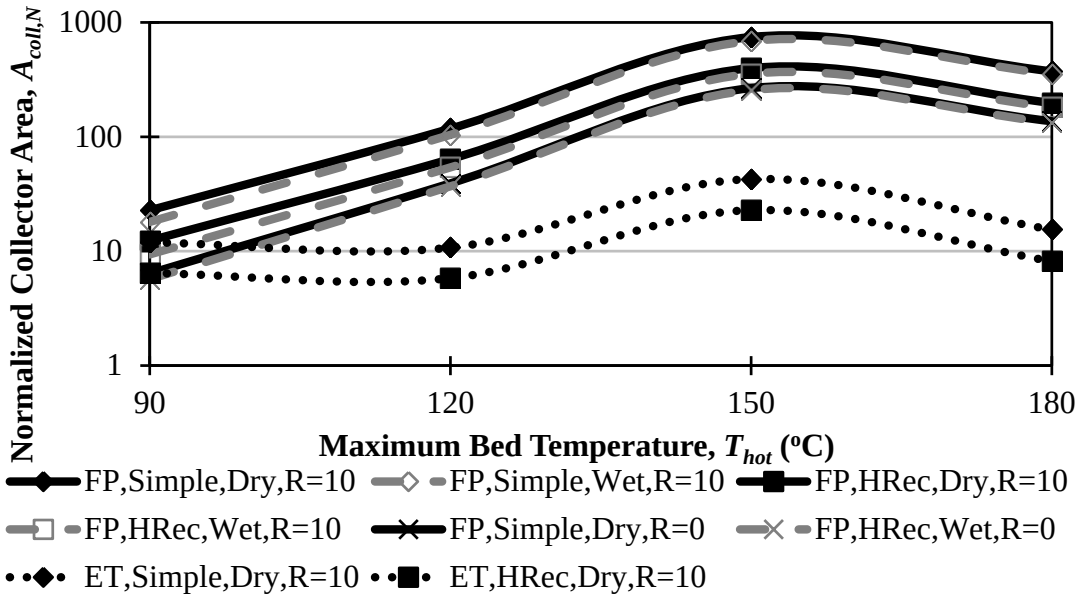

Figure 5.27. $A_{coll,N}$ vs. T_{hot} (°C) for different collector, adsorption cycle, cooling tower types and R and ΔT_{excess} = 0°C (Legend: CC,AAAA,DDD,R where CC=collector type: FP = flat plate; ET = evacuated tube; AAAA=cycle: HRec = heat recovery; Simple = simple; DDD=cooling tower type: Dry or Wet).

Normalized mass of adsorbent ($m_{ads,N}$) decreases as T_{hot} increases and this decrease is nearly linear for T_{hot} > 120°C as shown in Figure 5.28. Similar to $COP_{sys,clg}$ results, the required $m_{ads,N}$ increases with ΔT_{excess}, and systems with a wet cooling tower require smaller $m_{ads,N}$ than systems with a dry cooling tower. Although not shown in Figure 5.28, $m_{ads,N}$ is independent of the adsorption cycle type, collector type or R since $m_{ads,N}$ is only a function of the adsorption capacity change for a half cycle, $\Delta X = X_{max} - X_{min} = X(T_o,T_{evap}) - X(T_{hot},T_{cond})$.

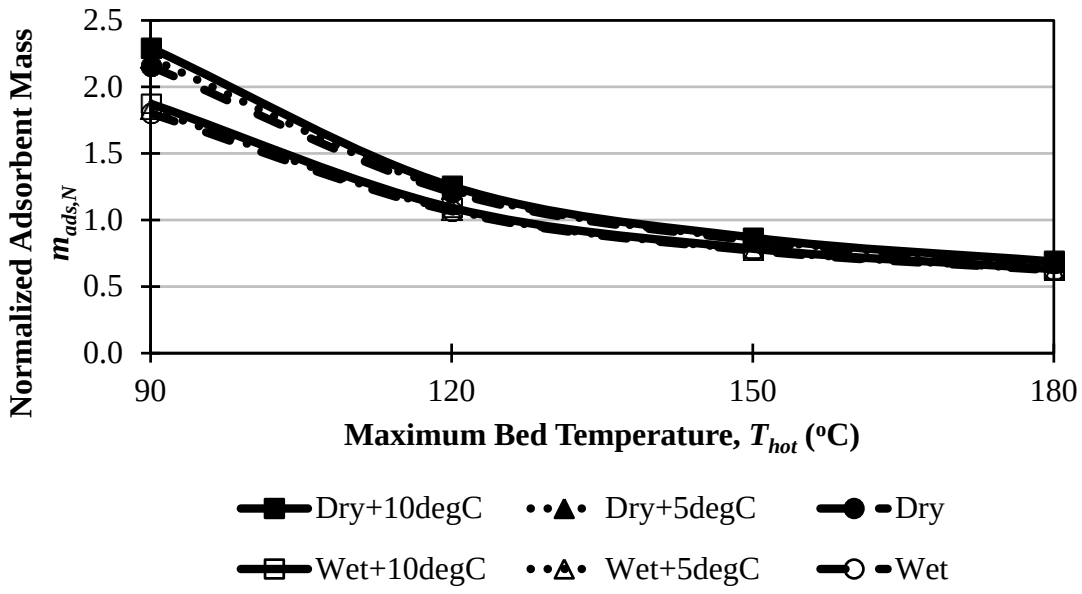

Figure 5.28. $m_{ads,N}$ vs. T_{hot} (°C) for evacuated tube collector, simple and heat recovery cycles, different cooling towers and T_o and R = 10 (Legend: Dry or Wet cooling tower + ΔT_{excess} (°C)).

CHAPTER 6

DISCUSSIONS

Stand alone and solar-thermal system integrated adsorption cooling cycles are analyzed as several operating conditions (T_{hot}, T_{cond}, T_{evap}, R and ΔT_{excess}), some design parameters (cooling tower and solar thermal collector types) and adsorbent – refrigerant (working) pairs (Z1, ZW, SG, CA and CM) are varied. Within this study, different ideal adsorption cycle types are thermodynamically modeled using MATLAB and these cycles are coupled with previously presented adsorbent – refrigerant pair models. The analyzed adsorption cycles include simple, heat recovery with two spatially isothermal beds, thermal wave cycle with no mass recovery, thermal wave cycle with adiabatic mass recovery and thermal wave cycle with isothermal mass recovery. The investigated thermal wave cycles are also divided into two types as thermal wave cycles with by-pass line and thermal wave cycles without by-pass line. All these adsorption cooling cycles are compared with a reversible cycle which is considered as the thermodynamically limiting case. Note that thermal wave adsorption cooling cycles with and without enhancements are presented. Two limiting mass recovery cases for the thermal wave cycles are considered: adiabatic mass recovery and isothermal mass recovery. The actual mass recovery process should be a process between adiabatic mass recovery and isothermal mass recovery.

The effects of conditions and parameters are analyzed through a series of simulations. These simulations can be categorized as steady and seasonal-transient simulations. All the simulations are run using TRNSYS software. In the seasonal-transient simulations, hourly weather data for the city of Antalya on Turkey's Mediterranean coast is used with 15-minute intervals for the summer period from June 1 to September 30. Water is selected as the heat transfer fluid for all the simulations.

The simulation results are obtained in terms of COP_{ads} and COP_{sys} for steady simulations and $COP_{sys,clg}$ and $COP_{sys,clg}$ ratios (r_{sys}) for seasonal-transient simulations. Among these results, r_{sys} show the opportunity to improve the selected base case of the simple adsorption cycle by introducing two spatially isothermal bed heat recovery or thermal wave cycles or by altering other operating conditions. Additionally, a normalized model is developed to investigate the modeled solar-powered adsorption cooling system in terms of solar and loss fractions, collector area and mass of adsorbent as the aforementioned parameters, maximum storage capacity and size of the system are varied. The normalized model is applied only to the simple and heat recovery cycles with zeolite NaX – water pair.

For all analyses, for simplicity, ideal systems are assumed to investigate (thermodynamic) limits to the energy performance, general trends and relative values. The models are used to make relative comparisons of different adsorption cycles, quantify limits to corresponding COP_{ads}, COP_{sys}, $COP_{sys,clg}$ and r_{sys} values, and provide directions for more detailed research. Therefore, absolute values should not be inferred from the results presented in this study.

Adsorbent – refrigerant (working) pairs are modeled using the formulations presented in the literature. However, these formulations do not generally include their corresponding limitations, i.e., the temperature or pressure range where the formulation is valid. Therefore, all the simulations are checked using the 2nd Law of Thermodynamics after applying the criteria mentioned in Section 4.1 and overall energy balance (the 1st Law of Thermodynamics) checks mentioned in Section 4.2. In fact, a small number of simulation results contradict with the 2nd Law of Thermodynamics. These contradictions are believed to originate from the adsorption capacity (X) models that are selected since the overall and component-based energy checks are satisfactory for the corresponding simulations.

In all investigated cases, the reversible cycle has the highest COP_{ads} (or COP_{sys} or $COP_{sys,clg}$) while the thermal wave cycles is second, the heat recovery is third and the simple cycle is the last as COP_{ads} (or COP_{sys} or $COP_{sys,clg}$) values are ranked from the

highest to the lowest. $COP_{sys,clg}$ values of the thermal wave cycles are approximately 36-93% of corresponding COP_{sys} values of the reversible cycles. Considering all working pairs, this proportion for the heat recovery cycle is around 3-42% and for the simple cycle 1.5-33.5% that of a reversible cycle. The deviation of the thermal wave cycle's COP_{ads} from the reversible case is directly related to the shift in the beds' outlet temperatures from the minimum bed temperature and maximum bed temperature caused by the sorption processes. Conversely, the irreversibility in the heat recovery cycle is mainly due to the heat transfer between the two beds at different temperatures.

Adding mass recovery to a thermal wave cycle increases both the total heating load and the total heat recovered. For the conditions considered, the increases in total heating load and heat recovery are similar resulting in little change in the cycle's COP_{ads}. The results showed that if the aim is to increase COP_{ads}, implementing mass recovery on thermal wave cycle is not essential when the complications of mass recovery process, like additional control instrumentation and physical connection of beds, are considered. However, adding mass recovery may be appropriate to meet other goals such as shortened cycle times and increased specific cooling power. For completeness of the effects of mass recovery, implementing isothermal mass recovery slightly increases COP_{ads} of the thermal wave cycle relative to the cycle with no mass recovery while the effects of implementing adiabatic mass recovery depend on the other operating conditions. Additionally, for the modeled thermal wave cycles, introducing a by-pass line also increases COP_{ads} slightly.

When adsorbent – refrigerant (working) pairs are compared, each pair has the highest $COP_{sys,clg}$ (or COP_{sys}) values for different maximum bed temperature range. If maximum bed temperature is around 80-100^{o}C where all working pair models are applicable, a system with silica gel – water pair has the highest $COP_{sys,clg}$ followed by activated carbon – methanol pair. For maximum bed temperature between 100^{o}C and 150^{o}C, a system with activated carbon – ammonia pair has the highest $COP_{sys,clg}$ for the thermal wave cycles and lowest $COP_{sys,clg}$ for the simple and heat recovery cycles in which systems with zeolite X13 – water pair achieve the highest $COP_{sys,clg}$ in the

same region for the simple and heat recovery cycles. For maximum bed temperature, $T_{hot} > 160^{o}$C, only the zeolite NaX – water model is applicable.

For the solar-powered adsorption cooling systems, systems with evacuated tube collector give higher COP_{sys} (or $COP_{sys,clg}$) than systems with flat plate collector as also stated by Çağlar et al. [114]. Additionally, as is obvious, an increasing solar radiation level increases the system performance (in terms of COP_{sys} or $COP_{sys,clg}$) as collector efficiencies increase and the amount of heat transfer that drives the adsorption cooling cycle increases. Among the investigated operating conditions, for thermal wave cycles the parameter that has the highest effect on COP_{sys} (or $COP_{sys,clg}$) is cooling tower type (or condensation temperature) while evaporation temperature has the second highest effect and the heat capacity ratio and excess bed temperature has little effect. For the simple and heat recovery cycles, the parameters that have the largest effect on COP_{sys} (or $COP_{sys,clg}$) are, in decreasing order, the heat capacity ratio, condensation temperature and evaporation temperature. These results are valid for all working pairs. In general, using a wet cooling tower instead of a dry cooling tower, increasing evaporation temperature and decreasing excess bed temperature increases COP_{ads} of all cycle types for all working pairs. In addition, increasing the heat capacity ratio decreases COP_{ads} of the simple and heat recovery cycles while it increases COP_{ads} of thermal wave cycle slightly regardless of working pair. All these effects of the parameters on COP_{ads} are consistent with previous studies [56, 63, 71, 73, 75]. However, the effect of maximum bed temperature on $COP_{sys,clg}$ contradicts with the presented results by Wang et al. [55] who only investigated a small portion of the maximum bed temperature range presented in this study. As indicated in Section 5.3.6, $COP_{sys,clg}$ increases, achieves a peak and then decreases as maximum bed temperature increases which is also consistent with results of Alam et al. [80].

According to the results of normalized model simulations, backup power is always necessary (i.e., $f < 1$) to meet the cooling demand in Antalya. On the other hand, the amount of the backup power can be reduced significantly by using an adsorption cycle with thermal regeneration (heat recovery adsorption cycle), evacuated tube collector and a larger storage unit (i.e., higher $q_{Storage,max}$).

Moreover, zeolite NaX – water pair requires a relatively high maximum bed temperature that cannot be reached easily using flat plate collectors due to their lower stagnation points. This result indicates the necessity of using evacuated tube collectors for the analyzed solar-thermal system integrated adsorption cooling system. To have the smallest collector area among the investigated cases, the system should be operated at a low maximum bed temperature (approximately 90^{o}C) which, in return, requires large adsorbent mass. In contrast, to have minimum adsorbent mass, the adsorption capacity swing of the half cycle should be high which corresponds to high maximum bed temperatures values since condensation temperature (or minimum bed temperature) is fixed by the weather data. Additionally, to have smaller backup power (and higher solar fraction), normalized collector area or mass of adsorbent (or to have higher $COP_{sys,clg}$), wet cooling towers are preferred over dry cooling towers if water consumption is not a problem.

CHAPTER 7

CONCLUSIONS

In this study, performance trends of a solar-thermal powered adsorption cooling system are presented using the thermodynamic models of ideal adsorption cooling cycles and explicitly modeled adsorbent – refrigerant (working) pairs and solar thermal system. These three models are integrated to form the investigated solar-thermal powered adsorption cooling system.

According to the obtained results of analyzed conditions, to have high performance in terms of coefficient of performance, the following configuration should be preferred,

- Evacuated tube collector should be chosen rather than flat plate collector since evacuated tube collector has higher thermal efficiency and stagnation temperature. Therefore, high maximum bed temperatures can be achieved.
- Wet cooling tower should be chosen rather than dry cooling tower as decreasing condensation temperature increases coefficient of performance of the cycle.
- High evaporation temperature should be preferred although it depends on the application area and cooling requirements.
- Adsorbent bed should be cooled down to condensation temperature as much as possible, i.e., excess bed temperature should be minimized.
- The simple and heat recovery cycles should be designed with a small dead mass (i.e., small heat capacity ratio) while dead mass is not so important for the thermal wave cycles.
- The modeled solar-thermal powered adsorption cooling system is simulated for Antalya, a city on the Mediterranean coast of Turkey where summers are

long and hot and backup power should be considered to meet the cooling demand unless very large collector areas are used.

- Adsorbent – refrigerant (working) pair choice depends strongly on the temperature of the available energy source and the designed/desired maximum bed temperature since each pair dominates different maximum bed temperature ranges.
- Although adding heat and mass recovery to the adsorption cooling cycle increases the coefficient of performance of the cycle, it also increases the complexity of the design of the cycle. Therefore, the choice of implementing heat and mass recovery to the adsorption cycles should be carefully chosen according to the needs and the desired operating conditions.

As a final remark, it is believed that this study forms a basis and shows the basic development guidelines for a very promising technology which is the solar-thermal powered adsorption cooling systems. In the future with appropriate and required developments and research, these systems will be commercially and commonly used and the cooling and refrigeration will almost be free of externally supplied electricity.

CHAPTER 8

SUGGESTIONS FOR FUTURE INVESTIGATIONS

This presented study should be considered a starting point for further studies. Although the current models present the general trends of the system performance in terms of coefficient of performance as the investigated parameters are varied, a number of improvements can be accomplished to improve the models and investigate the performance of the system in more detail. These improvements may include the following items,

- The current adsorption cycle models only include thermodynamic relations. These models can be improved by implementing heat and mass transfer and diffusion equations based on the specific thermal design of the adsorbent bed. As a result, some new important aspects, such as cycle time and specific cooling power, can be introduced.
- In order to enhance the current model and investigate the adsorption cycle in detail, two different approaches are suggested. One of them is to enhance the current thermodynamic model of the entire adsorption cooling cycle to include heat and mass transfer equations in MATLAB. The other approach is to use built-in TRNSYS components and model only the adsorption cycle including heat and mass transfer equations and consequently, to obtain a complete adsorption cooling cycle model in TRNSYS. The former approach may be more effective for steady analysis while the latter one is believed to be easier to implement for transient analysis. These further analyses can be done based on components rather than system. Therefore the effect of each component and their corresponding parameters on the system performance can be further distinguished.

- The current models which include only energy relations (the 1st Law of Thermodynamics) can be extended with the exergy (the 2nd Law of Thermodynamics) analysis to investigate the improvement areas on both system- and component-wise.
- The numerical models should be supported with experimental studies. Prototypes of the modeled cycles should be constructed and analyzed to further verify the results of numerical models. The emphasis in the design should be given to the design of adsorbent bed to assure the adsorption and heat transfer characteristics are as close as to the limiting cases provided in the present study.
- In the present study, the thermal wave cycles seem to be a promising technology to meet the cooling demands without introducing significant electrical loads, but in the present study only a square wave is considered for all thermal wave cycles which is a critical assumption. Therefore, some other kinds of waves (e.g., ramp wave) can be modeled to see the performance change according to the ideal square wave assumption.
- The results also suggest that in the thermal wave cycles, adsorbent beds with large dead mass can be used. For this reason, engineering effort should be put into designing the bed to approximate a square-thermal wave (which is the limiting case) or to minimize the width of the thermal wave, possibly at the expense of trying to minimize the bed's dead mass.
- New adsorption cycle models with heat and/or mass recovery can be modeled. The number of beds in these models can be varied from two to infinity and the effect of heat and mass recovery can be analyzed as the number of adsorbent beds is varied by defining new performance variables such as heat and/or mass recovery efficiencies.
- Further studies can also be directed to the availability of different adsorbent – refrigerant pairs to heat and mass recovery enhancements using steady simulations.

- New adsorbent – refrigerant pairs that are available in the literature can be added to the current models. These pairs may include some hybrid adsorbents such as SiO_2 / $CaCl_2$.

BIBLIOGRAPHY

[1] Conti, J. J., Sweetnam, G. E., and Doman, L. E., "International Energy Outlook 2009," Energy Information Administration, U.S. Department of Energy, Washington, 2009.

[2] Dhar, P. L., and Singh, S. K., "Studies on Solid Desiccant Based Hybrid Air-Conditioning Systems," *Applied Thermal Engineering*, vol. 21, no. 2, pp. 119-134, 2001.

[3] "Ongoing Research Relevant for Solar Assisted Air Conditioning Systems," International Energy Agency, Solar Heating and Cooling Programme, Freiburg, 2002.

[4] Calm, J. M., "Emissions and Environmental Impacts from Air-Conditioning and Refrigeration Systems," *International Journal of Refrigeration*, vol. 25, no. 3, pp. 293-305, 2002.

[5] McMullan, J. T., "Refrigeration and the Environment - Issues and Strategies for the Future," *International Journal of Refrigeration*, vol. 25, no. 1, pp. 89-99, 2002.

[6] Papadopoulos, A. M., Oxizidis, S., and Kyriakis, N., "Perspectives of Solar Cooling in View of the Developments in the Air-Conditioning Sector," *Renewable and Sustainable Energy Reviews*, vol. 7, no. 5, pp. 419-438, 2003.

[7] "Annual Development of Turkey's Gross Electricity Generation-Imports-Exports and Demand (1975-2008)," Turkish Electricity Transmission Co. (TEİAŞ), Ankara, 2008.

[8] "The Distribution of Gross Electricity Generation by Primary Energy Resources and the Electric Utilities in Turkey," Turkish Electricity Transmission Co. (TEİAŞ), Ankara, 2007.

[9] "Turkish Electrical Energy 10-Year Generation Capacity Projection," Turkish Electricity Transmission Co. (TEİAŞ), Ankara, 2009.

[10] Naukkarinen, P., "Solar Air Conditioning and Its Role in Alleviating the Energy Crisis of the Mediterranean Hotels," *International Journal of Sustainable Energy*, vol. 28, no. 1, pp. 93 - 100, 2009.

[11] Baş, K., *Antalya'da Yeni Enerji Yatırımlarına Ihtiyaç Duyuluyor*, Last accessed March 13, 2010, http://www.zaman.com.tr/haber.do?haberno=573763 *(in Turkish)*.

[12] Lewis, N. S., Crabtree, G., Nozik, A. J., Wasielewski, M. R., and Alivisatos, P., "Basic Research Needs for Solar Energy Utilization," U.S. Department of Energy, 2005.

[13] Weiss, W., Bergmann, I., and Faninger, G., "Solar Heat Worldwide: Markets and Contribution to the Energy Supply 2006," International Energy Agency - Solar Heating & Cooling Programme, Gleisdorf, 2008.

[14] Weiss, W., Bergmann, I., and Faninger, G., "Solar Heat Worldwide: Markets and Contribution to the Energy Supply 2007," International Energy Agency - Solar Heating & Cooling Programme, Gleisdorf, 2009.

[15] Abu Hamdeh, N. H., and Al-Muhtaseb, M. T. A., "Optimization of Solar Adsorption Refrigeration System Using Experimental and Statistical Techniques," Energy Conversion and Management: In Press, Corrected Proof, 2010.

[16] Bilgiç, M., Gırep, P., Türker, L., Yöntem, E., Aydınalp Köksal, M., Baker, D. K., and Erdil, E., "Modeling of Hourly Short and Long Term Electricity Demand at Load Distribution Regions," The Scientific and Technological Council of Turkey (TÜBİTAK) Project No: 108M001, Ankara, 2009.

[17] Sumathy, K., Yeung, K. H., and Yong, L., "Technology Development in the Solar Adsorption Refrigeration Systems," *Progress in Energy and Combustion Science*, vol. 29, no. 4, pp. 301-327, 2003.

[18] Wang, R., and Wang, L., "Adsorption Refrigeration-Green Cooling Driven by Low Grade Thermal Energy," *Chinese Science Bulletin*, vol. 50, no. 3, pp. 193-204, 2005.

[19] Ziegler, F., "State of the Art in Sorption Heat Pumping and Cooling Technologies," *International Journal of Refrigeration*, vol. 25, no. 4, pp. 450-459, 2002.

[20] Moran, M. J., and Shapiro, H. N., *Fundamentals of Engineering Thermodynamics*, Fifth Ed., Wiley, 2006.

[21] Sonntag, R. E., Borgnakke, C., and Van Wylen, G. J., *Fundamentals of Thermodynamics*, Sixth Ed., John Wiley & Sons, Inc., 2003.

[22] Sarı, O. G., "Exergy Analysis of a Solar Assisted Absorption Heat Pump for Floor Heating System," Master of Science, Department of Mechanical Engineering, Middle East Technical University, 2004.

[23] Trott, A. R., and Welch, T., *Refrigeration and Air-Conditioning*, Third Ed., Butterworth Heinemann, Boston, 2000.

[24] Wang, L. W., Wang, R. Z., and Oliveira, R. G., "A Review on Adsorption Working Pairs for Refrigeration," *Renewable and Sustainable Energy Reviews*, vol. 13, no. 3, pp. 518-534, 2009.

[25] Meunier, F., "Adsorptive Cooling: A Clean Technology," *Clean Technologies and Environmental Policy*, vol. 3, no. 1, pp. 8-20, 2001.

[26] Alefeld, G., and Radermacher, R., *Heat Conversion Systems*, CRC Press, Boca Raton, 1994.

[27] Herold, K. E., Radermacher, R., and Klein, S. A., *Absorption Chillers and Heat Pumps*, CRC Press, Boca Raton, 1996.

[28] Waugaman, D. G., Kini, A., and Kettleborough, C. F., "A Review of Desiccant Cooling Systems," *Journal of Energy Resources Technology*, vol. 115, no. 1, pp. 1-8, 1993.

[29] Henning, H. M., Erpenbeck, T., Hindenburg, C., and Santamaria, I. S., "The Potential of Solar Energy Use in Desiccant Cooling Cycles," *International Journal of Refrigeration*, vol. 24, no. 3, pp. 220-229, 2001.

[30] Daou, K., Wang, R. Z., and Xia, Z. Z., "Desiccant Cooling Air Conditioning: A Review," *Renewable and Sustainable Energy Reviews*, vol. 10, no. 2, pp. 55-77, 2006.

[31] ASHRAE, *Desiccant Cooling and Dehumidification*, American Society of Heating, Refrigerating and Air-Conditioning Engineers, Atlanta, 1992.

[32] Demir, H., Mobedi, M., and Ülkü, S., "A Review on Adsorption Heat Pump: Problems and Solutions," *Renewable and Sustainable Energy Reviews*, vol. 12, no. 9, pp. 2381-2403, 2008.

[33] Dieng, A. O., and Wang, R. Z., "Literature Review on Solar Adsorption Technologies for Ice-Making and Air-Conditioning Purposes and Recent Developments in Solar Technology," *Renewable and Sustainable Energy Reviews*, vol. 5, no. 4, pp. 313-342, 2001.

[34] Lambert, M. A., and Jones, B. J., "Review of Regenerative Adsorption Heat Pumps," *Journal of Thermophysics and Heat Transfer*, vol. 19, no. 4, pp. 471-485, 2005.

[35] Baker, D. K., and Kaftanoğlu, B., "Limits to the Thermodynamic Performance of a Thermal Wave Adsorption Cooling Cycle," *Proceedings of International Conference on Heat Transfer, Fluid Mechanics and Thermodynamics (HEFAT)*, pp. 6, Sun City, South Africa, 2007.

[36] Baker, D. K., and Kaftanoğlu, B., "Güneş Enerjisi Ile Çalışan Adsorplanma Soğutma Sisteminden Maksimum Teorik Başarım Sağlanması," *Proceedings of VI. Ulusal Temiz Enerji Sempozyumu (UTES)*, Isparta, Turkey, 2006.

[37] Qu, T. F., Wang, R. Z., and Wang, W., "Study on Heat and Mass Recovery in Adsorption Refrigeration Cycles," *Applied Thermal Engineering*, vol. 21, no. 4, pp. 439-452, 2001.

[38] Wang, R. Z., "Performance Improvement of Adsorption Cooling by Heat and Mass Recovery Operation," *International Journal of Refrigeration*, vol. 24, no. 7, pp. 602-611, 2001.

[39] Wang, X., and Chua, H. T., "A Comparative Evaluation of Two Different Heat-Recovery Schemes as Applied to a Two-Bed Adsorption Chiller," *International Journal of Heat and Mass Transfer*, vol. 50, no. 3-4, pp. 433-443, 2007.

[40] Akahira, A., Alam, K. C. A., Hamamoto, Y., Akisawa, A., and Kashiwagi, T., "Mass Recovery Adsorption Refrigeration Cycle - Improving Cooling Capacity," *International Journal of Refrigeration*, vol. 27, no. 3, pp. 225-234, 2004.

[41] Wang, W., Qu, T. F., and Wang, R. Z., "Influence of Degree of Mass Recovery and Heat Regeneration on Adsorption Refrigeration Cycles," *Energy Conversion and Management*, vol. 43, no. 5, pp. 733-741, 2002.

[42] Shelton, S. V., Wepfer, W. J., and Miles, D. J., "Ramp Wave Analysis of the Solid/Vapor Heat Pump," *Journal of Energy Resources Technology*, vol. 112, no. 1, pp. 69-78, 1990.

[43] Shelton, S. V., "Solid Adsorbent Heat Pump System," US Patent 4610148, USA, 1986.

[44] Taylan, O., Baker, D. K., and Kaftanoğlu, B., "COP Trends for Ideal Thermal Wave Adsorption Cooling Cycles with Enhancements," International Journal of Refrigeration: Under Review, 2009.

[45] Critoph, R. E., "Forced Convection Adsorption Cycles," *Applied Thermal Engineering*, vol. 18, no. 9-10, pp. 799-807, 1998.

[46] Sanborn, D. M., "Direct Heated Adsorbent Bed Heat Pump," US Patent 5505059, USA, 1996.

[47] Maier-Laxhuber, P., and Kaubek, F., "Continuously Acting Adsorption Devices and Process for Their Operation," US Patent 4660629, USA, 1987.

[48] Erickson, D. C., "Rotary Trisorption Heat Pump," US Patent 5279359, USA, 1994.

[49] Ebbeson, B., "Sorption Device," US Patent 5431716, USA, 1995.

[50] Llobet, J., and Goetz, V., "Rotary System for the Continuous Production of Cold by Solid-Gas Sorption: Modeling and Analysis of Energy Performance," *International Journal of Refrigeration*, vol. 23, no. 8, pp. 609-625, 2000.

[51] Chua, H. T., Ng, K. C., Malek, A., Kashiwagi, T., Akisawa, A., and Saha, B. B., "Multi-Bed Regenerative Adsorption Chiller - Improving the Utilization of Waste Heat and Reducing the Chilled Water Outlet Temperature Fluctuation," *International Journal of Refrigeration*, vol. 24, no. 2, pp. 124-136, 2001.

[52] Yong, L., and Sumathy, K., "Performance Analysis of a Continuous Multi-Bed Adsorption Rotary Cooling System," *Applied Thermal Engineering*, vol. 25, no. 2-3, pp. 393-407, 2005.

[53] De Boer, R., and Smeding, S. F., "Development and Testing of a Rotating System for a Continuous Solid-Sorption Process," *Proceedings of Heat Powered Cycles Conference*, Newcastle upon Tyne, 2006.

[54] Pons, M., and Guilleminot, J. J., "Design of an Experimental Solar-Powered, Solid-Adsorption Ice Maker," *Journal of Solar Energy Engineering*, vol. 108, no. 4, pp. 332-337, 1986.

[55] Wang, W., Wang, R. Z., Xu, Y. X., Wu, J. Y., and Gui, Y. B., "Investigation on Adsorption Refrigeration with a Single Adsorbent Bed," *International Journal of Energy Research*, vol. 22, no. 13, pp. 1157-1163, 1998.

[56] Pons, M., Meunier, F., Cacciola, G., Critoph, R. E., Groll, M., Puigjaner, L., Spinner, B., and Ziegler, F., "Thermodynamic Based Comparison of Sorption Systems for Cooling and Heat Pumping," *International Journal of Refrigeration*, vol. 22, pp. 5-17, 1999.

[57] Critoph, R., Tamainot-Telto, Z., and Davies, G., "A Prototype of a Fast Cycle Adsorption Refrigerator Utilizing a Novel Carbon - Aluminium Laminate," *Proceedings of the Institution of Mechanical Engineers, Part A: Journal of Power and Energy*, vol. 214, no. 5, pp. 439-448, 2000.

[58] Saha, B. B., Akisawa, A., and Kashiwagi, T., "Solar/Waste Heat Driven Two-Stage Adsorption Chiller: The Prototype," *Renewable Energy*, vol. 23, no. 1, pp. 93-101, 2001.

[59] Anyanwu, E. E., and Ezekwe, C. I., "Design, Construction and Test Run of a Solid Adsorption Solar Refrigerator Using Activated Carbon/Methanol, as Adsorbent/Adsorbate Pair," *Energy Conversion and Management*, vol. 44, no. 18, pp. 2879-2892, 2003.

[60] Wang, L. W., Wu, J. Y., Wang, R. Z., Xu, Y. X., and Wang, S. G., "Experimental Study of a Solidified Activated Carbon-Methanol Adsorption Ice Maker," *Applied Thermal Engineering*, vol. 23, no. 12, pp. 1453-1462, 2003.

[61] Wang, L. W., Wu, J. Y., Wang, R. Z., Xu, Y. X., Wang, S. G., and Li, X. R., "Study of the Performance of Activated Carbon-Methanol Adsorption Systems Concerning Heat and Mass Transfer," *Applied Thermal Engineering*, vol. 23, no. 13, pp. 1605-1617, 2003.

[62] Wang, S., and Zhu, D., "Adsorption Heat Pump Using an Innovative Coupling Refrigeration Cycle," *Adsorption*, vol. 10, no. 1, pp. 47-55, 2004.

[63] Chang, W. S., Wang, C. C., and Shieh, C. C., "Experimental Study of a Solid Adsorption Cooling System Using Flat-Tube Heat Exchangers as Adsorption Bed," *Applied Thermal Engineering*, vol. 27, no. 13, pp. 2195-2199, 2007.

[64] Zhai, X. Q., and Wang, R. Z., "Experimental Investigation and Theoretical Analysis of the Solar Adsorption Cooling System in a Green Building," *Applied Thermal Engineering*, vol. 29, no. 1, pp. 17-27, 2009.

[65] Banker, N. D., Prasad, M., Dutta, P., and Srinivasan, K., "Development and Transient Performance Results of a Single Stage Activated Carbon - HFC 134a Closed Cycle Adsorption Cooling System," Applied Thermal Engineering: In Press, Corrected Proof, 2010.

[66] Grisel, R. J. H., Smeding, S. F., and Boer, R. D., "Waste Heat Driven Silica Gel/Water Adsorption Cooling in Trigeneration," *Applied Thermal Engineering*, vol. 30, no. 8-9, pp. 1039-1046, 2010.

[67] Baker, D. K., and Kaftanoğlu, B., "Trends in COP for Adsorption Cooling Cycles with Thermal Regeneration and Finite Number of Beds," *Proceedings of Energy Sustainability 2008*, Jacksonville, Florida, USA, 2008.

[68] Myers, A. L., "Thermodynamics of Adsorption in Porous Materials," *AIChE Journal*, vol. 48, no. 1, pp. 145-160, 2002.

[69] Pons, M., and Kodama, A., "Entropic Analysis of Adsorption Open Cycles for Air Conditioning. Part 1: First and Second Law Analyses," *International Journal of Energy Research*, vol. 24, no. 3, pp. 251-262, 2000.

[70] Douss, N., Meunier, F. E., and Sun, L.-M., "Predictive Model and Experimental Results for a Two-Adsorber Solid Adsorption Heat Pump," *Industrial & Engineering Chemistry Research*, vol. 27, no. 2, 1988.

[71] Zheng, W., Worek, W. M., and Nowakowski, G., "Effect of Operating Conditions on the Performance of Two-Bed Closed-Cycle Solid-Sorption Heat Pump Systems," *Journal of Solar Energy Engineering*, vol. 117, no. 3, pp. 181-186, 1995.

[72] Zheng, W., Worek, W. M., and Nowakowski, G., "Effect of Design and Operating Parameters on the Performance of Two-Bed Sorption Heat Pump Systems," *Journal of Energy Resources Technology*, vol. 117, no. 1, pp. 67-74, 1995.

[73] Teng, Y., Wang, R. Z., and Wu, J. Y., "Study of the Fundamentals of Adsorption Systems," *Applied Thermal Engineering*, vol. 17, pp. 327-338, 1997.

[74] Sun, L. M., Feng, Y., and Pons, M., "Numerical Investigation of Adsorptive Heat Pump Systems with Thermal Wave Heat Regeneration under Uniform-Pressure Conditions," *International Journal of Heat and Mass Transfer*, vol. 40, no. 2, pp. 281-293, 1997.

[75] Pons, M., and Poyelle, F., "Adsorptive Machines with Advanced Cycles for Heat Pumping or Cooling Applications," *International Journal of Refrigeration*, vol. 22, no. 1, pp. 27-37, 1999.

[76] Sward, B. K., Levan, M. D., and Meunier, F., "Adsorption Heat Pump Modeling: The Thermal Wave Process with Local Equilibrium," *Applied Thermal Engineering*, vol. 20, no. 8, pp. 759-780, 2000.

[77] Wang, R. Z., Li, M., Xu, Y. X., and Wu, J. Y., "An Energy Efficient Hybrid System of Solar Powered Water Heater and Adsorption Ice Maker," *Solar Energy*, vol. 68, no. 2, pp. 189-195, 2000.

[78] Pons, M., and Szarzynski, S., "Accounting for the Real Properties of the Heat Transfer Fluid in Heat-Regenerative Adsorption Cycles for Refrigeration," *International Journal of Refrigeration*, vol. 23, no. 4, pp. 284-291, 2000.

[79] Saha, B. B., Koyama, S., Lee, J. B., Kuwahara, K., Alam, K. C. A., Hamamoto, Y., Akisawa, A., and Kashiwagi, T., "Performance Evaluation of a Low-Temperature Waste Heat Driven Multi-Bed Adsorption Chiller," *International Journal of Multiphase Flow*, vol. 29, no. 8, pp. 1249-1263, 2003.

[80] Alam, K. C. A., Saha, B., Akisawa, A., and Kashiwagi, T., "Influence of Design and Operating Conditions on the System Performance of a Two-Stage Adsorption Chiller," *Chemical Engineering Communications*, vol. 191, pp. 981-997, 2004.

[81] Wang, D. C., Xia, Z. Z., Wu, J. Y., Wang, R. Z., Zhai, H., and Dou, W. D., "Study of a Novel Silica Gel-Water Adsorption Chiller. Part I. Design and Performance Prediction," *International Journal of Refrigeration*, vol. 28, no. 7, pp. 1073-1083, 2005.

[82] Lambert, M. A., "Design of Solar Powered Adsorption Heat Pump with Ice Storage," *Applied Thermal Engineering*, vol. 27, no. 8-9, pp. 1612-1628, 2007.

[83] Liu, Y., and Leong, K. C., "Numerical Modeling of a Zeolite/Water Adsorption Cooling System with Non-Constant Condensing Pressure," *International Communications in Heat and Mass Transfer*, vol. 35, no. 5, pp. 618-622, 2008.

[84] Wang, D. C., and Zhang, J. P., "Design and Performance Prediction of an Adsorption Heat Pump with Multi-Cooling Tubes," *Energy Conversion and Management*, vol. 50, no. 5, pp. 1157-1162, 2009.

[85] Luo, H., Wang, R. Z., and Dai, Y. J., "Optimum Matching of Heat Source Temperature to a Solar Adsorption Air-Conditioning System for Maximum Solar Cooling Coefficient of Performance," *International Journal of Green Energy*, vol. 7, no. 1, pp. 91 - 102, 2010.

[86] Aristov, Y. I., "Novel Materials for Adsorptive Heat Pumping and Storage: Screening and Nanotailoring of Sorption Properties," *Journal of Chemical Engineering of Japan*, vol. 40, no. 13, pp. 1242-1251, 2007.

[87] Solmuş, İ., Yamalı, C., Kaftanoğlu, B., Baker, D. K., and Çağlar, A., "Adsorption Properties of a Natural Zeolite-Water Pair for Use in Adsorption Cooling Cycles," Applied Energy, In Press, Corrected Proof, 2009.

[88] Wang, R. Z., and Wang, Q. B., "Adsorption Mechanism and Improvements of the Adsorption Equation for Adsorption Refrigeration Pairs," *International Journal of Energy Research*, vol. 23, no. 10, pp. 887-898, 1999.

[89] Taylan, O., Baker, D. K., and Kaftanoğlu, B., "Adsorbent - Refrigerant Comparison for a Solar Powered Adsorption Cooling System Using Seasonal Simulations," *Proceedings of 10th REHVA World Congress*, Antalya, Turkey, 2010.

[90] Baker, D. K., "Thermodynamic Limits to Thermal Regeneration in Adsorption Cooling Cycles," *International Journal of Refrigeration*, vol. 31, no. 1, pp. 55-64, 2008.

[91] Lu, Y. Z., Wang, R. Z., Zhang, M., and Jiangzhou, S., "Adsorption Cold Storage System with Zeolite-Water Working Pair Used for Locomotive Air Conditioning," *Energy Conversion and Management*, vol. 44, no. 10, pp. 1733-1743, 2003.

[92] Daou, K., Wang, R. Z., Yang, G. Z., and Xia, Z. Z., "Theoretical Comparison of the Refrigerating Performances of a $CaCl_2$ Impregnated Composite Adsorbent to Those of the Host Silica Gel," *International Journal of Thermal Sciences*, vol. 47, no. 1, pp. 68-75, 2008.

[93] Wang, L. W., Wang, R. Z., Lu, Z. S., Chen, C. J., Wang, K., and Wu, J. Y., "The Performance of Two Adsorption Ice Making Test Units Using Activated Carbon and a Carbon Composite as Adsorbents," *Carbon*, vol. 44, no. 13, pp. 2671-2680, 2006.

[94] Ben Amar, N., Sun, L. M., and Meunier, F., "Numerical Analysis of Adsorptive Temperature Wave Regenerative Heat Pump " *Applied Thermal Engineering*, vol. 16, pp. 405-418, 1996.

[95] Saha, B. B., Habib, K., El-Sharkawy, I. I., and Koyama, S., "Adsorption Characteristics and Heat of Adsorption Measurements of R-134a on Activated Carbon," *International Journal of Refrigeration*, vol. 32, no. 7, pp. 1563-1569, 2009.

[96] Wang, R. Z., Jia, J. P., Zhu, Y. H., Teng, Y., Wu, J. Y., Cheng, J., and Wang, Q. B., "Study on a New Solid Adsorption Refrigeration Pair: Active Carbon Fiber-Methanol," *Journal of Solar Energy Engineering*, vol. 119, no. 3, pp. 214-218, 1997.

[97] Restuccia, G., Freni, A., Vasta, S., and Aristov, Y., "Selective Water Sorbent for Solid Sorption Chiller: Experimental Results and Modelling," *International Journal of Refrigeration*, vol. 27, no. 3, pp. 284-293, 2004.

[98] Wang, L. W., Wang, R. Z., Wu, J. Y., and Wang, K., "Compound Adsorbent for Adsorption Ice Maker on Fishing Boats," *International Journal of Refrigeration*, vol. 27, no. 4, pp. 401-408, 2004.

[99] Cui, Q., Tao, G., Chen, H., Guo, X., and Yao, H., "Environmentally Benign Working Pairs for Adsorption Refrigeration," *Energy*, vol. 30, no. 2-4, pp. 261-271, 2005.

[100] Hamamoto, Y., Alam, K. C. A., Saha, B. B., Koyama, S., Akisawa, A., and Kashiwagi, T., "Study on Adsorption Refrigeration Cycle Utilizing Activated Carbon Fibers. Part 2. Cycle Performance Evaluation," *International Journal of Refrigeration*, vol. 29, no. 2, pp. 315-327, 2006.

[101] Saha, B. B., El-Sharkawy, I. I., Chakraborty, A., Koyama, S., Banker, N. D., Dutta, P., Prasad, M., and Srinivasan, K., "Evaluation of Minimum Desorption Temperatures of Thermal Compressors in Adsorption Refrigeration Cycles," *International Journal of Refrigeration*, vol. 29, no. 7, pp. 1175-1181, 2006.

[102] El-Sharkawy, I. I., Saha, B. B., Koyama, S., He, J., Ng, K. C., and Yap, C., "Experimental Investigation on Activated Carbon-Ethanol Pair for Solar Powered Adsorption Cooling Applications," *International Journal of Refrigeration*, vol. 31, no. 8, pp. 1407-1413, 2008.

[103] Loh, W. S., El-Sharkawy, I. I., Ng, K. C., and Saha, B. B., "Adsorption Cooling Cycles for Alternative Adsorbent/Adsorbate Pairs Working at Partial Vacuum and Pressurized Conditions," *Applied Thermal Engineering*, vol. 29, no. 4, pp. 793-798, 2009.

[104] "TRNSYS," The University of Wisconsin-Madison Solar Energy Lab, Madison, 2007.

[105] *TRNSYS: The Transient Energy System Simulation Tool*, Last accessed March 16, 2010, http://www.trnsys.com/.

[106] *TRNSYS Overview*, Last accessed March 16, 2010, http://www.tess-inc.com/trnsys.

[107] *A Transient Systems Simulation Program*, Last accessed March 16, 2010, http://sel.me.wisc.edu/trnsys/default.htm.

[108] Taylan, O., Baker, D. K., and Kaftanoğlu, B., "Parametric Study and Seasonal Simulations of a Solar Powered Adsorption Cooling System," *Proceedings of 22nd International Conference on Efficiency, Cost, Optimization, Simulation and Environmental Impact of Energy Systems (ECOS)*, pp. 833 - 842, Foz do Iguaçu, Paraná, Brazil, 2009.

[109] "Methodology for Determining the Thermal Performance Rating for Solar Collectors," Solar Rating and Certification Corporation, Cocoa, 1994.

[110] Schmidt, P. S., Ezekoye, O., Howell, J. R., and Baker, D. K., *Thermodynamics: An Integrated Learning System*, Wiley, 2005.

[111] Kaftanoğlu, B., Yamalı, C., Baker, D. K., Solmuş, İ., Çağlar, A., and Taylan, O., "Solar Powered Zeolite Air-Conditioning System," The Scientific and Technological Council of Turkey (TÜBİTAK) Project No: 105M244, Ankara, 2009.

[112] Kalogirou, S. A., "Solar Thermal Collectors and Applications," *Progress in Energy and Combustion Science*, vol. 30, no. 3, pp. 231-295, 2004.

[113] Lin, G., and Yan, Z., "The Optimal Operating Temperature of the Collector of an Irreversible Solar-Driven Refrigerator," *Journal of Physics D: Applied Physics*, vol. 32, no. 2, pp. 94, 1999.

[114] Çağlar, A., Yamalı, C., Baker, D. K., and Kaftanoğlu, B., "Testing the Thermal Performances of Solar Collectors " *Proceedings of 7th International Conference on Heat Transfer, Fluid Mechanics and Thermodynamics (HEFAT 2010)*, Antalya, Turkey, 2010.

APPENDIX A

SAMPLE TRNSYS INPUT (DECK) FILE

```
VERSION 16.1
**********************************************************************
*** TRNSYS input file (deck) generated by TrnsysStudio
***
*** If you edit this file, use the File/Import TRNSYS Input File function in
*** TrnsysStudio to update the project.
***
*** If you have problems, questions or suggestions please contact your local
*** TRNSYS distributor or mailto:software@cstb.fr
***
**********************************************************************


**********************************************************************
*** Units
**********************************************************************


**********************************************************************
*** Control cards
**********************************************************************
* START, STOP and STEP
CONSTANTS 3
        START=3624
        STOP=6552
        STEP=0.25
```

```
* User defined CONSTANTS
        SIMULATION      START       STOP  STEP ! Start time    End   time
        Time step
        TOLERANCES 0.000001 0.000001                ! Integration    Conver-
    gence
        LIMITS 30 30 30             ! Max iterations Max warnings Trace limit
        DFQ 1                       ! TRNSYS numerical integration solver method
        WIDTH 80                    ! TRNSYS output file width, number of charac-
    ters
        LIST                        ! NOLIST statement
                                    ! MAP statement
        SOLVER 0 1 1                ! Solver statement Minimum relaxation factor
        Maximum relaxation factor
        NAN_CHECK 0                 ! Nan DEBUG statement
        OVERWRITE_CHECK 0           ! Overwrite DEBUG statement
        TIME_REPORT 0               ! disable time report
        EQSOLVER 0                  ! EQUATION SOLVER statement

* EQUATIONS "Equa"
*
EQUATIONS 6
     AdsNo = 1
     Tref = 21
     Tcold = 10
     Tadsmax = 90
     DTexcess = 0
     R = 10
     *$UNIT_NAME Equa
     *$LAYER Main
     *$POSITION 212 125
*-------------------------------------------------------------------------------
* Model "Type155" (Type 155)
```

```
*
        UNIT 11 TYPE 155    Type155
        *$UNIT_NAME Type155
        *$MODEL .\Utility\Calling External Programs\Matlab\Type155.tmf
        *$POSITION 105 479
        *$LAYER Main #
PARAMETERS 5
        0               ! 1 Mode
        7               ! 2 Number of inputs
        6               ! 3 Number of outputs
        0               ! 4 Calling Mode
        0               ! 5 Keep Matlab open after simulation
INPUTS 7
        16,1            ! Type92:Outlet fluid temperature ->input-1
        Tbedmin         ! Equa-2:Tbedmin ->input-2
        17,1            ! Type109-TMY2:Ambient temperature ->input-3
        Tcold           ! Equa:Tcold ->input-4
        R               ! Equa:R ->input-5
        AdsNo           ! Equa:AdsNo ->input-6
        14,1            ! Type2b:Output control function ->input-7
*** INITIAL INPUT VALUES
        90 30 30 10 0 2 0
LABELS 1
        " \..\..\..\..\sample.m"
*-------------------------------------------------------------------------------
* Model "Type25c" (Type 25)
*
        UNIT 9 TYPE 25      Type25c
        *$UNIT_NAME Type25c
        *$MODEL .\Output\Printer\Unformatted\No Units\Type25c.tmf
        *$POSITION 692 125
        *$LAYER Outputs #
```

```
PARAMETERS 10
        STEP            ! 1 Printing interval
        START           ! 2 Start time
        STOP            ! 3 Stop time
        35              ! 4 Logical unit
        0               ! 5 Units printing mode
        0               ! 6 Relative or absolute start time
        1               ! 7 Overwrite or Append
        -1              ! 8 Print header
        0               ! 9 Delimiter
        1               ! 10 Print labels
INPUTS 16
        hColl           ! Equa-2:hColl ->Input to be printed-1
        11,1            ! Type155:output-1 ->Input to be printed-2
        11,2            ! Type155:output-2 ->Input to be printed-3
        11,3            ! Type155:output-3 ->Input to be printed-4
        COPsys_rev      ! Equa-2:COPsys_rev ->Input to be printed-5
        COPsystww       ! Equa-2:COPsys_tw_w ->Input to be printed-6
        COPsystwwo      ! Equa-2:COPsys_tw_wo ->Input to be printed-7
        Qload           ! Equa-2:Qload ->Input to be printed-8
        19,3            ! Type71:Useful energy gain ->Input to be printed-9
        16,5            ! Type92:Rate of energy removed ->Input to be printed-10
        Qclg_rev        ! Equa-2:Qclg_rev ->Input to be printed-11
        Qclg_tw_w       ! Equa-2:Qclg_tw_w ->Input to be printed-12
        Qclg_tw_wo      ! Equa-2:Qclg_tw_wo ->Input to be printed-13
        DX_DXref        ! Equa-2:DX_DXref ->Input to be printed-14
        11,5            ! Type155:output-5 ->Input to be printed-15
        11,6            ! Type155:output-6 ->Input to be printed-16
*** INITIAL INPUT VALUES
        hColl COPrev COPw COPwo COPsys_rev COPsys_w COPsys_wo Qload
    Qcoll Qaux
        Qclg_rev Qclg_w Qclg_wo m_ads Errw Errwo
```

```
*** External files
        ASSIGN "Ad_Z1_90.out" 35
        *|? Output file for printed results |1000
*-------------------------------------------------------------------------
* Model "Type65d" (Type 65)
*
        UNIT 15 TYPE 65      Type65d
        *$UNIT_NAME Type65d
        *$MODEL .\Output\Online Plotter\Online Plotter Without File\Type65d.tmf
        *$POSITION 687 378
        *$LAYER Main #
PARAMETERS 12
        3               ! 1 Nb. of left-axis variables
        2               ! 2 Nb. of right-axis variables
        -2              ! 3 Left axis minimum
        2               ! 4 Left axis maximum
        0.0             ! 5 Right axis minimum
        250             ! 6 Right axis maximum
        1               ! 7 Number of plots per simulation
        12              ! 8 X-axis gridpoints
        0               ! 9 Shut off Online w/o removing
        -1              ! 10 Logical unit for output file
        0               ! 11 Output file units
        0               ! 12 Output file delimiter
INPUTS 5
        11,1            ! Type155:output-1 ->Left axis variable-1
        11,2            ! Type155:output-2 ->Left axis variable-2
        11,3            ! Type155:output-3 ->Left axis variable-3
        hColl           ! Equa-2:hColl ->Right axis variable-1
        16,1            ! Type92:Outlet fluid temperature ->Right axis variable-2
*** INITIAL INPUT VALUES
        COPrev COPnobypass COPbypass hColl Texit
```

```
        LABELS  3
        "Efficiencies"
        ""
        "Graph 1"
*-------------------------------------------------------------------------
* EQUATIONS "Equa-2"
*
EQUATIONS 10
        Tbedmin = [17,1]+DTexcess
        Qload = [17,1]-Tref
        hColl = [19,3]/1.62/([17,18]+1e-16)*gt([17,18],0)
        DX_DXref = [11,4]/0.125794687663051
        Qclg_rev = [16,5]*[11,1]
        Qclg_tw_w = [16,5]*[11,2]
        Qclg_tw_wo = [16,5]*[11,3]
        COPsys_rev = hColl*[11,1]
        COPsys_tw_w = hColl*[11,2]
        COPsys_tw_wo = hColl*[11,3]
        *$UNIT_NAME Equa-2
        *$LAYER Main
        *$POSITION 337 370
*-------------------------------------------------------------------------
* Model "Type2b" (Type 2)
*
        UNIT 14 TYPE 2        Type2b
        *$UNIT_NAME Type2b
        *$MODEL .\Controllers\Differential Controller w_ Hysteresis\for Tempera-
    tures\Solver 0 (Successive Substitution) Control Strategy\Type2b.tmf
        *$POSITION 467 498
        *$LAYER Controls #
        *$# NOTE: This control strategy can only be used with solver 0 (Successive
    substitution)
```

```
        *$#
PARAMETERS 2
        5               ! 1 No. of oscillations
        100.0           ! 2 High limit cut-out
INPUTS 6
        19,1            ! Type71:Outlet temperature ->Upper input temperature Th
        Tadsmax         ! Equa:Tadsmax ->Lower input temperature Tl
        0,0             ! [unconnected] Monitoring temperature Tin
        0,0             ! [unconnected] Input control function
        0,0             ! [unconnected] Upper dead band dT
        0,0             ! [unconnected] Lower dead band dT
*** INITIAL INPUT VALUES
        100 150 20.0 0 0 0
*-------------------------------------------------------------------------------
* Model "Type92" (Type 92)
*
        UNIT 16 TYPE 92      Type92
        *$UNIT_NAME Type92
        *$MODEL .\HVAC\Auxiliary Cooling Unit\Type92.tmf
        *$POSITION 646 294
        *$LAYER Water Loop #
        *$# This model is extremely similar to the TYPE6 Auxiliary Heater
PARAMETERS 4
        100000          ! 1 Maximum cooling rate
        4.19            ! 2 Specific heat of fluid
        0               ! 3 Overall loss coefficient
        1.0             ! 4 Cooling device efficiency
INPUTS 5
        19,1            ! Type71:Outlet temperature ->Inlet fluid temperature
        19,2            ! Type71:Outlet flowrate ->Fluid mass flow rate
        14,1            ! Type2b:Output control function ->Control Function
        Tadsmax         ! Equa:Tadsmax ->Set point temperature
```

```
        17,1            ! Type109-TMY2:Ambient temperature ->Temperature of sur-
    roundings
*** INITIAL INPUT VALUES
        20 100 1 150 20
*-------------------------------------------------------------------------
* Model "Type109-TMY2" (Type 109)
*
        UNIT 17 TYPE 109    Type109-TMY2
        *$UNIT_NAME Type109-TMY2
        *$MODEL .\Weather Data Reading and Processing\Standard For-
    mat\TMY2\Type109-TMY2.tmf
        *$POSITION 287 157
        *$LAYER Weather - Data Files #
PARAMETERS 4
        2               ! 1 Data Reader Mode
        41              ! 2 Logical unit
        4               ! 3 Sky model for diffuse radiation
        1               ! 4 Tracking mode
INPUTS 3
        0,0             ! [unconnected] Ground reflectance
        0,0             ! [unconnected] Slope of surface
        0,0             ! [unconnected] Azimuth of surface
*** INITIAL INPUT VALUES
        0.2 40 0.0
*** External files
        ASSIGN "\..\..\..\..\Antalya.tm2" 41
        *|? Weather data file |1000
*-------------------------------------------------------------------------
* Model "Type3d" (Type 3)
*
        UNIT 18 TYPE 3      Type3d
        *$UNIT_NAME Type3d
```

```
        *$MODEL .\Hydronics\Pumps\Single Speed - no Powercoeffi-
    cients\Type3d.tmf
        *$POSITION 53 402
        *$LAYER Main #
PARAMETERS 4
        100             ! 1 Maximum flow rate
        4.19            ! 2 Fluid specific heat
        60              ! 3 Maximum power
        0               ! 4 Conversion coefficient
INPUTS 3
        16,1            ! Type92:Outlet fluid temperature ->Inlet fluid temperature
        16,2            ! Type92:Outlet fluid flow rate ->Inlet mass flow rate
        0,0             ! [unconnected] Control signal
*** INITIAL INPUT VALUES
        20 100 1
*-------------------------------------------------------------------------------
* Model "Type71" (Type 71)
*
        UNIT 19 TYPE 71      Type71
        *$UNIT_NAME Type71
        *$MODEL .\Solar Thermal Collectors\Evacuated Tube Collector\Type71.tmf
        *$POSITION 287 294
        *$LAYER Main #
PARAMETERS 11
        1               ! 1 Number in series
        2               ! 2 Collector area
        4.19            ! 3 Fluid specific heat
        2               ! 4 Efficiency mode
        3.0             ! 5 Flow rate at test conditions
        0.825           ! 6 Intercept efficiency
        4.284           ! 7 Negative of first order efficiency coeficient
        0.0324          ! 8 Negative of second order efficiency coeficient
```

```
        42              ! 9 Logical unit of file containing biaxial IAM data
        10              ! 10 Number of longitudinal angles for which IAMs are pro-
    vided
        10              ! 11 Number of transverse angles for which IAMs are provid-
    ed
INPUTS 10
        18,1            ! Type3d:Outlet fluid temperature ->Inlet temperature
        18,2            ! Type3d:Outlet flow rate ->Inlet flowrate
        17,1            ! Type109-TMY2:Ambient temperature ->Ambient tempera-
    ture
        17,18           ! Type109-TMY2:total radiation on tilted surface ->Incident
    radiation
        17,20           ! Type109-TMY2:sky diffuse radiation on tilted surface -
    >Incident diffuse radiation
        17,22           ! Type109-TMY2:angle of incidence for tilted surface  ->Solar
    incidence angle
        17,10           ! Type109-TMY2:solar zenith angle ->Solar zenith angle
        17,11           ! Type109-TMY2:solar azimuth angle ->Solar azimuth angle
        17,23           ! Type109-TMY2:slope of tilted surface ->Collector slope
        0,0             ! [unconnected] Collector azimuth
*** INITIAL INPUT VALUES
        20 100 10 0 0 0.0 0.0 0.0 40 0.0
*** External files
       ASSIGN "..\..\..\Tess Models\SampleCatalogData\Bi-Axial IAMs\Iam_2d.dat"
    42
       *|? What file contains the 2D IAM data? |1000
*------------------------------------------------------------------------------
END
```

APPENDIX B

SAMPLE TRNSYS STUDIO REPORT

****

*** Control cards

****

TOLERANCES Integration 0.000001 Convergence 0.000001

LIMITS

  Max iterations: 30

  Max warnings: 30

  Trace limit: 30

TRNSYS numerical integration solver method: DFQ 1

TRNSYS output file width, number of characters:

WIDTH 80

NOLIST statement: LIST

MAP statement: none

Solver statement: SOLVER 0

START=3624

STOP=6552

STEP=0.25

Write TRNSED commands : OFF

* User defined CONSTANTS

****

*** Simulation order

****

1. Model: CONTROL CARD

2. Model: Equation Editor (Equa)

3. Model: MATLAB Caller (Type155)

4. Model: Output to File (Type25c)

5. Model: Output to Screen (Type65d)

6. Model: Equation Editor (Equa-2)

7. Macro: Solar Thermal System (Macro)

8. Model: Control Unit (Type2b)

9. Model: Heat Exchanger (Type92)

10. Model: Weather Data Reader (Type109-TMY2)

11. Model: Circulation Pump (Type3d)

12. Model: Evacuated Tube Collector (Type71)

****

*** Macro structure

****

Output to File (Type25c)

MATLAB Caller (Type155)

Equation Editor (Equa)

Output to Screen (Type65d)

Equation Editor (Equa-2)

Solar Thermal System (Macro)

  Control Unit (Type2b)

  Heat Exchanger (Type92)

  Weather Data Reader (Type109-TMY2)

  Circulation Pump (Type3d)

  Evacuated Tube Collector (Type71)

****

*** Unconnected inputs

****

CONTROL CARD (Unit 1, Type 0)

MATLAB Caller (Type155) (Unit 3, Type 155)

Output to File (Type25c) (Unit 4, Type 25)

Output to Screen (Type65d) (Unit 5, Type 65)

Control Unit (Type2b) (Unit 7, Type 2)

Monitoring temperature Tin - constant value is 20.0 [C]

Input control function - constant value is 0 [-]

Upper dead band dT - constant value is 0 [Temp. Difference]

Lower dead band dT - constant value is 0 [Temp. Difference]

Heat Exchanger (Type92) (Unit 8, Type 92)

Weather Data Reader (Type109-TMY2) (Unit 9, Type 109)

Ground reflectance - constant value is 0.2 [-]

Slope of surface - constant value is 40 [degrees]

Azimuth of surface - constant value is 0.0 [degrees]

Circulation Pump (Type3d) (Unit 10, Type 3)

Control signal - constant value is 1 [-]

Evacuated Tube Collector (Type71) (Unit 11, Type 71)

Collector azimuth - constant value is 0.0 [degrees]

****

*** All connections

****

CONTROL CARD (Unit 1, Type 0)

MATLAB Caller (Type155) (Unit 3, Type 155)

output-1 -> Left axis variable-1 (Output to Screen (Type65d))

output-1 -> COPrev (Equation Editor (Equa-2))

output-1 -> Input to be printed-2 (Output to File (Type25c))

output-2 -> Left axis variable-2 (Output to Screen (Type65d))

output-2 -> COPtw_w (Equation Editor (Equa-2))

output-2 -> Input to be printed-3 (Output to File (Type25c))

output-3 -> Left axis variable-3 (Output to Screen (Type65d))

output-3 -> COPtw_wo (Equation Editor (Equa-2))

output-3 -> Input to be printed-4 (Output to File (Type25c))

output-4 -> DX (Equation Editor (Equa-2))

output-5 -> Input to be printed-15 (Output to File (Type25c))

output-6 -> Input to be printed-16 (Output to File (Type25c))

Output to File (Type25c) (Unit 4, Type 25)

Output to Screen (Type65d) (Unit 5, Type 65)

Control Unit (Type2b) (Unit 7, Type 2)

Output control function -> Control Function (Heat Exchanger (Type92))

Output control function -> input-7 (MATLAB Caller (Type155))

Heat Exchanger (Type92) (Unit 8, Type 92)

Outlet fluid temperature -> Inlet fluid temperature (Circulation Pump (Type3d))

Outlet fluid temperature -> input-1 (MATLAB Caller (Type155))

Outlet fluid temperature -> Right axis variable-2 (Output to Screen (Type65d))

Outlet fluid flow rate -> Inlet mass flow rate (Circulation Pump (Type3d))

Rate of energy removed -> Qaux (Equation Editor (Equa-2))

Rate of energy removed -> Input to be printed-10 (Output to File (Type25c))

Weather Data Reader (Type109-TMY2) (Unit 9, Type 109)

Ambient temperature -> Temperature of surroundings (Heat Exchanger (Type92))

Ambient temperature -> Ambient temperature (Evacuated Tube Collector (Type71))

Ambient temperature -> Tamb (Equation Editor (Equa-2))

Ambient temperature -> input-3 (MATLAB Caller (Type155))

Ambient temperature -> Tcond (Equation Editor (Equa-2))

solar zenith angle -> Solar zenith angle (Evacuated Tube Collector (Type71))

solar azimuth angle -> Solar azimuth angle (Evacuated Tube Collector (Type71))

total radiation on tilted surface -> Incident radiation (Evacuated Tube Collector (Type71))

total radiation on tilted surface -> Radiation (Equation Editor (Equa-2))

sky diffuse radiation on tilted surface -> Incident diffuse radiation (Evacuated Tube Collector (Type71))

angle of incidence for tilted surface -> Solar incidence angle (Evacuated Tube Collector (Type71))

slope of tilted surface -> Collector slope (Evacuated Tube Collector (Type71))

Circulation Pump (Type3d) (Unit 10, Type 3)

Outlet fluid temperature -> Inlet temperature (Evacuated Tube Collector (Type71))

Outlet flow rate -> Inlet flowrate (Evacuated Tube Collector (Type71))

Evacuated Tube Collector (Type71) (Unit 11, Type 71)

Outlet temperature -> Upper input temperature Th (Control Unit (Type2b))

Outlet temperature -> Inlet fluid temperature (Heat Exchanger (Type92))

Outlet flowrate -> Fluid mass flow rate (Heat Exchanger (Type92))

Useful energy gain -> Qcoll (Equation Editor (Equa-2))

Useful energy gain -> Input to be printed-9 (Output to File (Type25c))

End of report.